Final Report
USC 53-4514-8152

UNIVERSITY OF SOUTHERN CALIFORNIA

SCHOOL OF ENGINEERING

MEASUREMENT OF DENSITY AND TEMPERATURE IN A HYPERSONIC TURBULENT BOUNDARY LAYER USING THE ELECTRON BEAM FLUORESCENCE TECHNIQUE

by
Angus D. McRonald

FINAL REPORT TO:

NATIONAL AERONAUTICS AND SPACE ADMINISTRATION

Grant NGR-05-018-140

For the period
October 1, 1969 to September 1, 1972

John Laufer
Principal Investigator

DEPARTMENT OF AEROSPACE ENGINEERING

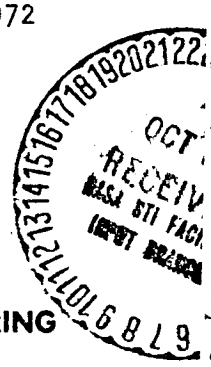

MEASUREMENT OF DENSITY AND TEMPERATURE IN A HYPERSONIC TURBULENT BOUNDARY LAYER USING THE ELECTRON BEAM FLUORESCENCE TECHNIQUE

by

Angus Duncan McRonald

A Dissertation Presented to the

FACULTY OF THE GRADUATE SCHOOL

UNIVERSITY OF SOUTHERN CALIFORNIA

In Partial Fulfillment of the

Requirements for the Degree

DOCTOR OF PHILOSOPHY

(Aerospace Engineering)

July 1975

ABSTRACT

Mean density and temperature fluctuations were measured across the turbulent, cooled-wall boundary layer in a continuous hypersonic (Mach 9.4) wind tunnel in air, using the nitrogen fluorescence excited by a 50 kV electron beam. Data were taken at three values of the tunnel stagnation pressure, the corresponding free stream densities being equivalent to 1.2, 4.0, and 7.4 torr at room temperature, and the boundary layer thicknesses about 4.0, 4.5, and 6.0 inches.

The mean temperature and density profiles were similar to those previously determined in the same facility by conventional probes (static and pitot pressure, total temperature). A static pressure variation of about 50% across the boundary layer was found, the shape of the variation changing somewhat for the three stagnation pressure levels. The quadrupole model for rotational temperature spectra gave closer agreement with the free stream isentropic level ($\sim$44 K) than the dipole model.

Depending on the location in the boundary layer and the stagnation pressure, the fluctuating light signal had

contributions from density and temperature fluctuations, and also from the integral of density fluctuations along the beam. Modal analysis of the signal gave peak density fluctuations of about 8% maximum, falling to about 3% in the free stream. The fluorescence technique can be used for quantitative gasdynamic measurement well into the collision quenched regime, with proper allowance for beam attenuation and temperature dependence.

TABLE OF CONTENTS

LIST OF FIGURES

LIST OF TABLES

NOMENCLATURE

Symbols

ℓ	path length in the gas
p	gas pressure
u	gas velocity
y	distance from the wall
I	integral of density along the beam
I'	integral of density fluctuation along the beam
L	light signal
M	Mach number
P_0	stagnation pressure
R	correlation coefficient
T	gas temperature
V	accelerating voltage
ρ	gas density

Subscripts

0	stagnation conditions
t	total conditions
w	conditions at the wall
e	at the edge of the boundary layer

∞	at free stream conditions
T	pertaining to temperature
ρ	pertaining to density
π	pertaining to the sound mode
σ	pertaining to the entropy mode
τ	pertaining to the vorticity mode

Superscripts

'	fluctuation of a quantity
"	rms fluctuation/ mean value of a quantity

Section I

PREFACE

Although it is not unusual for the author of a dissertation to seek to relate his work, or indeed to be required to relate his work to that of others, the present work bears an especially close relationship to prior work by others in the same flow facility. It is, in fact, one item of a set of measurements of both mean and fluctuating flow quantities having a common ultimate objective, that of detailed documentation of an established, turbulent hypersonic boundary layer. This program of measurement was conceived and set in motion several years ago by Professor John Laufer of the Department of Aerospace Engineering, University of Southern California, the present author's principal adviser in this dissertation work.

It therefore seems appropriate to begin with a brief account of the rationale for undertaking the set of measurements, and a description of the parts of the program already accomplished by others, before going on to describe the work of the dissertation proper.

Section II

INTRODUCTION

Practical interest in hypersonic boundary layers has been greatly stimulated in the last two decades or so by the considerable activity in the military and space fields, and this interest is likely to continue and grow as Earth satellite launch and re-entry activities increase and the Space Shuttle system develops.

The two main practical problems in hypersonic flight, namely, the prediction of aerodynamic drag and heat transfer on bodies, are not adequately solved, and are closely linked to a thorough understanding of the hypersonic boundary layer; in particular, the presence and nature of turbulence in the layer have a major effect on the drag and heating of a body in hypersonic flight.

Adiabatic nozzle wall studies by Kistler[1] in the Mach number 2-5 range, and by Rose[2] at Mach 4, and exploratory studies by Wallace[3] at Mach 8.8, by Fischer et al.[4] at Mach 20, and by Owen et al.[5] at even high Mach numbers, have revealed that density and temperature fluctuations

are increasingly present in the boundary layer as the speed of the gas stream increases. The prediction by Laufer[6] that pressure fluctuations are the main feature of boundary layer turbulence has been verified by Laderman and Demetriades[8] in studies in a cooled nozzle wall boundary layer at Mach 9.37. With the exception of Wallace's density measurements in a shock tunnel boundary layer using an electron beam, all the measurements have used the hot-wire technique.

It is well known that the hot-wire technique, which directly measures total temperature and mass flux fluctuations, is incapable of complete modal analysis when all turbulence modes - velocity, temperature and pressure are active. Various simplifying assumptions must be made, in order to separate the modes. In addition, the hot-wire technique has lower density and upper total temperature limits of application, so that its use in high Mach number flows, where such limits are typically exceeded, is restricted.

A technique such as the electron beam, which responds directly to density fluctuations, and operates best at low density, is therefore well suited to measurement of turbulence at high Mach number.

In regard to mean quantities, conventional methods of measurement (pitot and static pressure, total temperature) also find increasing difficulty at the low pressures and high recovery temperatures of high speed flow. Here again the electron beam method is capable of direct measurement of two mean flow static quantities, density and temperature.

The main purpose of the present work is to provide direct measurement of mean flow density and temperature and of density fluctuations, in a boundary layer already surveyed by conventional probes.

The prior work by others has taken the form of (a) exploratory measurements of velocity, temperature and pressure in the test section of the Hypersonic Wind Tunnel (HWT) at the Jet Propulsion Laboratory, Pasadena, California, by Laufer and A.Gupta of the University of Southern California (USC); and (b) detailed measurement of mean and fluctuating boundary layer quantities by A.J.Laderman and A.Demetriades.[7,8,9,10]

Laufer, Gupta and Ashkenas made surveys in the HWT test section of pitot pressure, static pressure and total temperature, at nominal Mach numbers of 9.5 and 6,

stagnation temperature of 1000 F, at a number of stations along the test section, and for three values of stagnation pressure at each Mach number. Their surveys confirmed that the flow in the HWT test section was sufficiently uniform and two-dimensional for the proposed detailed measurements to be meaningful. The Mach number of 9.5 was chosen for further measurement. Laderman and Demetriades conducted additional pitot pressure and total temperature measurements at the selected axial position, 160 in down from the nozzle throat, at the nominal Mach number of 9.5, stagnation temperature 1000 F, and stagnation pressures of 3200, 1700 and 500 cm Hg, for which the boundary layer thicknesses are about 4, 4.5 and 6 in, respectively. In their data reduction Reynolds-number-dependent corrections for the static pressure and the total temperature were applied, so that an iterative procedure was necessary to determine the best fit to the mean flow quantities. Their mean flow results are given in reference 7.

Laderman and Demetriades[8] also conducted hot-wire anemometer surveys of the same boundary layer at the same station and conditions, with particularly detailed measurements for the P_0 = 3200 case. Using the experimentally determined wire calibrations they found mass flux

and total temperature fluctuations peaking at about 12 and 2%, respectively, at two places: in the sublayer and in the central part of the boundary layer (about y = 1 to 3 in). These levels fell to about 3 and 0.5% at the edge of the layer.

They first analyzed the fluctuations under the no-sound ($p' = 0$) assumption, when the analytical modes (vorticity, entropy, sound) coincide with the flow modes (velocity, temperature, pressure), and the density and temperature fluctuations are equal, and found peak temperature fluctuations of about 12%. Then they analyzed the data with pressure fluctuations present and under various assumptions regarding mode variable and flow variable cross-correlations.

They found that physically meaningful solutions were obtained in both the free stream and the boundary layer only for the assumption: $R_{\sigma\pi} = R_{\pi\tau} = 0$, $R_{\tau\sigma} = -1$. In that case pressure fluctuations up to 18% and density fluctuations up to 14% of the corresponding mean local values were found. The crudeness of these assumptions and the lack of sufficient information points to the need for more direct measurements.

The present experiment seeks to supplement the prior work by measurements of static temperature and of mean and fluctuating density.

In its simplest form the experiment is this: a high-energy beam of electrons is injected into the HWT through the boundary layer and the resulting fluorescence light from nitrogen is scanned optically from outside the HWT; spectral resolution of a vibrational band will give static temperature, and quantitative examination of the light intensity and its fluctuations will give the mean and fluctuating density.

Section III

DESCRIPTION OF THE EXPERIMENT

1. General

An outline of the basic features of the experiment which constitutes the main part of this dissertation is given in Figure 1. A 1-mm diameter beam of 50 kV electrons generated in an electron beam welding gun is injected through the ceiling plate of the JPL HWT (20 in X 20 in working section) at a point approximately 160 in from the nozzle throat. The gas is air, the Mach number is nominally 9.5 and the boundary layer developing under the ceiling plate at this point is essentially two-dimensional, of thickness 4 to 6 in, depending on the stagnation pressure. The beam penetrates through the boundary layer, gradually attenuating and spreading, and is collected on a wedge-shaped Faraday cup located near the center of the HWT. The fluorescent light generated along the beam is viewed through a window in the side wall by a lens which images the beam on a slit used to admit a small vertical slice of the beam light, either to a spectrometer to resolve the fine rotational lines in a vibrational band and thus

measure static temperature, or to a photomultiplier measuring the total light from which one can deduce the gas mean and fluctuating density. The optical readout system is traversed vertically to perform a scan through the boundary layer.

The other main features include: differential pumping of the drift tube between the electron gun, which operates at relatively high vacuum, and the HWT, which operates at pressures around 1 torr; and a light output versus gas density calibration, performed on a subsidiary test stand outside the HWT, employing a still-air chamber to simulate the HWT.

2. The Electron Beam Fluorescence Technique

This technique, which has been fully reviewed by E.P.Muntz,[11] and recently by Butefisch and Vennemann,[20] has been applied extensively in air and other gases over the last 15 years or so.

Briefly, a well-collimated beam of electrons with electron energy of several tens of keV and a beam current of several hundred microamperes, and a beam diameter of about 1 mm, is directed into the test sample of gas, usually at a pressure in the range 0.01 to 0.1 torr; the beam usually traverses a length of about 5 to 20 cm before

being collected in a Faraday cup. Typically, the beam spreads out and attenuates due to collision with gas molecules, while the gas along the beam is excited and radiates light characteristic of the gas.

In general there are many competing processes of gas excitation and deexcitation. The experiments here are concerned with air, which has been investigated in detail by Bogden and McCaa.[12] The dominant fluorescence comes from nitrogen in two molecular band systems, the first negative and the second positive systems. Both systems exhibit a dependence of light emission on gas pressure typical of the electron beam fluorescence, i.e., an increase of light with increasing pressure until a saturation effect is reached. The first negative (1-) system gives emission increasing linearly with pressure up to several tenths of a torr before saturating, while the second positive (2+) system begins to emit appreciably above about 0.1 torr, increases as the square of the pressure for a certain range, and saturates at a pressure of several torr. The saturation results from collisional non-radiating deexcitation gradually overtaking radiative deexcitation as the pressure increases. The saturation process differs for different bands in the same system (see ref. 12), so that the saturation curves for the total light from one system, or for all the fluorescent light

are not well documented.

In nitrogen the 1- system is excited by primary high-energy electrons, while the 2+ system is excited by low-energy secondary electrons freed when ions are formed by inelastic collisions of the primary electrons with gas atoms and molecules. Both systems exhibit prompt radiative deexcitation, occurring in the order of microseconds, so that the drift distance in a flowing gas between the point of excitation and that of radiative deexcitation is very small, even at supersonic speeds. However, the range of the secondary electrons, and thus the distance from the primary beam over which the 2+ system can be excited, is on the order of 1 mm at a gas pressure of a few tenths of a torr. A compensating feature is that the 2+ emission only becomes appreciable when the gas pressure is relatively large, i.e., where the secondary electron range is relatively short.

A further feature of the high-energy electron beam is that there is a steady loss of primary electrons along the beam, due mainly to scattering. Although the scattering is predominantly through small angles, giving a small angle of divergence of the visible beam, eventually multiple scattering will cause the beam to diverge to a degree which precludes its use here as a measurement tool. Indeed, in some sense one objective of the present

experiment is to determine the useful range of application of the beam in the HWT boundary layer.

3. Application to the HWT Experiment

In the experiment described here the beam is to be injected through the flow channel wall (the ceiling) into a boundary layer known to be several inches thick and to have a steep increase in density (resulting mainly from a decrease of static temperature) quite close to the wall. Because the gas densities are in any case considerably above what is usual in the electron beam fluorescence technique, and the situation is compounded by the steep density gradient away from the wall, there was considerable uncertainty at the outset as to the distance into the boundary layer over which useful measurements would be possible.

Within the operating range of the HWT at the chosen Mach number of 9.5 the gas density at the wall varies from 0.3 to 1.3 torr (equivalent STP), based on the theoretical free stream pressure and the wall at room temperature. Since the prior measurements were mainly taken at the high end of this range, the electron beam must be used in conditions where beam spreading and attenuation will be severe.

The other possible limitation apparent ab initio was in the intensity of the useful beam current which could be delivered through the ceiling plate into the boundary layer. Calculations indicate that the wavelength resolution of the rotational spectra and the frequency resolution of the density fluctuations would require a beam current entering the HWT of about 1 mA. With good collection optics and reasonable spatial resolution (0.5 mm length of a 1 mm diameter beam) this current would give about 10^8 photons/sec at the detector. With a photomultiplier having a quantum efficiency of about 18% and a gain of about 10^6, the output current would be a few microamperes, yielding a voltage signal of up to a few volts, depending on the anode load resistance.

Adequate penetration of the beam through several inches of boundary layer whose density rises rapidly from the wall to a level equivalent to a few torr at room temperature requires that the beam voltage be about 40 to 50 kV. Assuming that 10% of the electrons generated in the gun can be focused to enter the HWT, the initial beam current is 10 mA, and the power to be dissipated is 500 W.

A further requirement is that the gun pressure should be below about 1 micron to insure long filament life, and a certain minimum path length is necessary for 50 kV electrical insulation at this pressure. The power and size

requirements of the gun, together with the limitations of access to the HWT working section from above, dictated that the gun be located about 20 in minimum above the beam entrance in the ceiling plate. The gun was joined to the ceiling plate via a cooled drift tube which included differential pumping stages and one or more focus coils to enable the maximum amount of the initial beam to pass through the beam entrance hole.

4. The Electron Beam Equipment

This equipment included a slightly modified commercial electron beam welding gun and high and low-voltage power supplies (manufactured by Brad Thompson Industries of Indio, California) and a drift tube module fabricated at USC and JPL whose function was to deliver the electron beam from the gun to the HWT.

The high-voltage supply, derived via a transformer and rectifiers from the 220 V (two-phase) mains, was adjustable up to 50 kV and had a measured 120 Hz ripple of about 3% peak-to-peak (measured with a resistor chain load at 10 kV and 3 mA). The equipment was provided with two servomechanisms which tended to maintain automatically the (manually) preset beam current: the gun filament current was adjusted electronically, and the high voltage was

adjusted by means of a motorized auto-transformer. The high voltage portions of the power supply were immersed in an oil bath.

In the early stages of the experiment difficulty with electrical breakdown was experienced: the problem was traced to faulty location of a high-voltage wire inside the oil bath; the fault was remedied and no further breakdown trouble was experienced.

The stainless steel gun was equipped with a quick-access door and a removable gun assembly (cathode, filament, anode) for ease of replacement of the filament or the high-voltage insulators. After some early difficulties with high-voltage breakdown and improper operating procedures, the gun and power supply behaved admirably, without even replacement of the filament during the final 12 months or so of their use in this work. In this period the equipment was operated for a total of several hundred hours and was moved several times from location in a test stand outside the HWT into the HWT and back again.

4.1 The Electron Beam Injection Module

The experimental arrangement (Figure 1) called for the electron beam (EB) to be injected through the HWT ceiling, to pass vertically downward through the boundary layer on the ceiling; the light generated along the beam would

then be viewed through the side window.

Thus, the beam package was to be installed in one of the three access wells above the HWT working section ordinarily available for model mounting and traverse assemblies. The well selected was roughly 12 in in diameter, and rose about 18 in from the ceiling hatch plate at its lower end before it emerged above the HWT. Above this point the required access for rotary mechanical pumps and an oil diffusion pump to be coupled to the drift tube was partially blocked in various ways by items like the hydraulic jacks for setting the HWT flexible top nozzle plate, and the sling mechanism used for removing the HWT side plate.

Nevertheless, a solution to these arrangement problems was found by coupling the oil diffusion pump to the EB gun via a vertical junction box about 2 ft long. The two stages of differential pumping and the diffusion pump back-up pump called for three mechanical pumps. Two pumps were positioned locally above the HWT and the third was remote, being in fact the HWT house vacuum system; all three were coupled to the EB package via flexible rubber hoses, of internal diameter 1 in for the differential pumps (which attached near the bottom of the well) and about 4 in for the diffusion pump back-up pump to which there was clear access. The pumps were located on ad hoc support brackets and platforms on top of the HWT. Figure 2 is a

photograph of the general layout showing these pumps.

The beam injection module was integrated with one of the standard ceiling hatch plates as its base plate, attached by three 1-in diameter exterior rods to a top bulkhead plate which mated with the gun (see photograph in Figure 3). Ancillaries such as cooling water lines and electrical leads to the focus coils and pressure monitoring gauges were integrated into the module, with plugs or disconnect fixtures on the top bulkhead. When arranged in this way the EB module could be installed and removed from the HWT, as was dictated at several times by the needs of other HWT users.

For calibration and shakedown purposes the beam module was set up on a still-air test stand where the HWT ceiling plate mated with a tank equipped with a viewing window and a vacuum pump.

The requirements of the HWT and of beam operation dictated the inclusion of several special features in the module or its environment, as follows:

(a) Flexible couplings: Two flexible (i.e., non-rigid) couplings were included (Figure 3a). One, a vertical sliding joint, allowing about 0.25 in of vertical travel between the gun and the HWT beam entrance hole, recognized that there were small movements in the drift tube section

resulting from evacuation and heating and cooling of the components. The second was a bellows coupling between the gun and the diffusion pump to accommodate relative motion, each being otherwise rigidly attached to different parts of the HWT; in particular, the gun was attached to the flexible nozzle plate, which was believed to move slightly as the HWT was evacuated and brought to the flow-on condition.

(b) Ceiling plate: This heavy steel plate about 10 in in diameter and 2 in thick, was provided with a 1 in diameter hole to receive the end of the drift tube, had an additional small hole about 1.5 in downstream and 1.5 in to one side, to equalize pressures and thus avoid flow through the beam entrance hole, and was equipped with a water-cooled coil of copper tubing, hard-soldered to its rear surface to remove HWT flow heating. When installed the ceiling plate was locked down and sealed by means of thin metal shims to ensure a near perfect flush fit into the HWT ceiling.

(c) Differential pumping: As has been noted, two stages of differential pumping were applied near the HWT end of the drift tube. Their primary purpose was to bridge the pressure jump from a level of 0.3 to 1.3 torr at the HWT wall (the operating range at Mach 9.4) to the much lower value, of the order of 10^{-4} torr, that will avoid oxidation

of the gun filament, electrical breakdown in the gun, and defocusing and scattering of the beam in the relatively long drift tube (about 26 in from gun exit to HWT entrance).

Each stage of differential pumping took the form of a side tube of 1 in diameter inserted between orifice plates in the drift tube, the central orifices having diameters of 4, 3, and 1 mm, respectively, proceeding from the gun to the HWT. In addition, a short balance chamber, about 0.5 in long, was formed by the addition of a fourth orifice plate with an orifice diameter of 1 mm, this one being the beam entrance hole into the HWT; the downstream bleed hole in the HWT ceiling plate communicated with the balance chamber via a short length of tubing. This technique reduced the flow out of the boundary layer into the drift tube at the site of the measurement.

(d) Beam steering technique: Some early experience with the beam operating into a vacuum system via a short drift tube indicated a problem in steering the beam through several orifices in succession. A remedy for this difficulty, and one which proved useful throughout the tests, was essentially to form a series of beam current collectors along the drift tube, by electrically insulating several parts of the tube, and returning these parts separately to electrical ground via small resistors (see Figure 4). A simple voltmeter could then be switched through the

resistors as the operator steered the beam by focus and deflection adjustments through the successive orifices until it emerged into the HWT or test chamber.

Since the orifice units were metal plates secured between flanged sections of the drift tube with neoprene 0-rings, it was a simple matter to choose 0-ring and groove sizes to prevent the metal parts quite coming together when assembled, and to add insulating bushings to avoid electrically short-circuiting by the metal locking screws. In all, five such separate electrical entities were provided; they served their purpose very well.

(e) Water cooling: Besides water cooling of the HWT ceiling plate (which was also the beam module baseplate) which was included into the high-pressure (100 psi) HWT water-cooling system for the entire nozzle section, separate low-pressure water cooling of most of the drift tube elements was provided. The gun as delivered had provision for water cooling of the high-voltage entry plug and the combined first focus and X and Y deflection coil immediately below the gun. A modest degree of water cooling was added for the orifice plates, which absorbed some portion of the beam during operation. Without this it was found, in particular, that the first two orifice plates of the differential pumping system would be heated enough to char the 0-rings and lose vacuum. Since the potential power

from the gun and its power supply was 1500 watts, the need for cooling is not surprising.

For these reasons the orifice plates were machined from substantial copper disks and equipped with generous water cooling by means of one or two turns of 0.25 in internal-diameter copper tubing wrapped around the disk and soldered to it with generous fillets of solder (Figure 5a). A similar technique was used on the two plates which formed the balance chamber; also, since this chamber is at HWT pressure, its length was kept short by having the upper orifice plate nested inside the lower one (Figure 5b); naturally, a long balance chamber in the beam direction at HWT pressure would attenuate the beam before it entered the HWT.

(f) Monitoring of drift tube and gun pressures: In order to understand and control the beam operation, provision was made for reading six pressures altogether (Figure 6), of which three were brought out from the beam module; two of these were electrical leads from thermocouple gauge heads tapped into the differential pumping lines near the drift tube; the third was a "Tygon" tube coming from a metal nipple on the balance chamber, to be read on a differential oil manometer.

The other three pressures included two more thermocouple

gauges, one on the junction pumping box, and one on the mechanical line backing the diffusion pump, and a filament-type ion gauge mounted in the gun housing (Figure 6).

(g) Vacuum valves: Three valves were included (Figure 6) to isolate the three pumping lines during start-up and shut-down of the HWT. Two were simple manually-operated clamps on the rubber hoses; the third was a manual quadrant-type "Globe" valve to isolate the gun rapidly if an emergency shut-down of the HWT supersonic flow occurred; it was operated remotely via a rotationally stiff flexible coupling.

(h) Beam focus and deflection: Two electromagnetic focus coils were included in the beam module, one immediately below the gun and combined with X and Y deflection coils, and a second located just above the differential pumping side tubes (Figure 3). Both were water cooled and came in a doughnut-shaped case as purchased. The combination unit was equipped with O-ring grooves and readily adapted to the vacuum system. The other came in a thin-walled casing which proved difficult to seal into the vacuum system. The final solution adopted was to use a separate internal stainless steel sleeve passing through the coil, and in fact constituting the vertical sliding joint alluded to above.

5. The Faraday Cup (Electron Collector)

Since the light output in the electron beam fluorescence technique varies directly with the beam current, the latter must be measured, or at least held constant, for any quantitative work.

In the present experiment the cup is necessarily located inside the HWT, which at once raises two problems: the cup must not block the flow or generate shock waves capable of perturbing the boundary layer at the site of measurement; and secondly, the cup will be heated by the gas stream, which has a stagnation temperature of 810 C and thus a recovery temperature of over 700 C.

The first difficulty was resolved by making the cup in the form of a flat-topped wedge as shown in Figure 7; if correctly aligned with the flow it will generate only a weak disturbance wave on the top side. The wedge was mounted on a sting in the HWT vertical traverse gear and could be moved; during these tests it was positioned about 9 in below the ceiling and with its leading edge about 2 in upstream of the plane of the electron beam, and centered in the lateral direction.

The second problem, the stagnation heating of the wedge, was compounded by the required electrical insulation of

the wedge used as a Faraday cup. Furthermore, the wedge support had to withstand the HWT starting and other transient loads.

After some deliberation it was decided not to cool the wedge; instead, several wedges were fabricated as replacements if the wedge were seriously damaged by the heating. The electrical insulation was provided by a short bushing of machinable high-temperature insulator. Several materials were tried, one of which seemed to be resistant to cracking at stress concentrations near tapped holes when the wedge was locked into position. As a safety measure the bushing was made captive inside an outer metal sleeve to guard against escape of fragments if the bushing were to split. A steel wire was led off through the hollow sting to the beam current meter.

Although attention was given initially to the possibility of extraneous light from secondary electrons ejected from the wedge by impact of primary electrons, early experience with the beam in the still-air calibration tank indicated that the spurious light from this source would be confined to the immediate vicinity of the wedge at the HWT pressures in question.

The wedges were made of copper, chosen for its good heat conduction property. A solid steel bar was silver-

soldered to the underside of the wedge, to mate with the sting via the insulating bushing.

In actual fact the wedge survived the tunnel runs very well, showing only superficial evidence of heating and electron bombardment. Since copper is known to oxidize and gradually spall off when heated above about 250 C in air, it is clear that there was good heat conduction through the insulator to the water-cooled sting-support system.

6. Wind Tunnel Window

A standard HWT window of quartz was used; this allowed the readout optics to traverse vertically in making a scan down the beam. The problem of viewing the beam entrance hole was solved by inclining the optical axis of the readout system slightly upward and upstream.

7. The Optical Readout System

The function of the optical readout system (Figure 9) was to collect a portion of the light emitted along the electron beam by means of the objective lens L1, to select a small horizontal "slice" of the image of the beam by means of the horizontal slit S1, and to scan along the beam (i.e., survey the boundary layer) by traversing the optical

system vertically.

The optical system actually comprised two subsystems, one for measurement of the mean gas density $\bar{\rho}$ and fluctuating density ρ', and a second subsystem for measurement of the mean static temperature $\bar{T}$; the objective and the traverse mechanism were common to both subsystems.

Since the largest item, required for resolution of rotational spectra in the measurement of $\bar{T}$, is the spectrometer, it seemed best to construct the optical systems around it. The objective lens was mounted on an optical bench clamped to the underside of the spectrometer, and both items were mounted on the long-axis slide of a two-axis lathe cross-slide whose feed screw was driven by a geared-down electric motor, to accomplish a vertical traverse of about 7 in in about 25 sec. An experimental check was made that this rate allowed the recording instruments for $\bar{\rho}$ and ρ' to follow the signal correctly. The cross slide also allowed lateral motion, which facilitated initial adjustment. The third fixed member of the cross slide was supported in either of two ways during the tests: it could be bolted to support brackets on the HWT below the window, or it could be mounted on a heavy-duty pedestal stand from the floor.

The $\bar{\rho}$ and ρ' subsystem comprised the objective L1, the

hinged mirror M1, the horizontal slit S1, and the photomultiplier P1. The spectrometer subsystem comprised the objective L1, the spectrometer SP, and the photomultiplier P2. The objective lens L1 was a good quality 5 in diameter biconvex lens of focal length 8.5 in, and was used in these tests at conditions close to unity magnification. Tests with a monochromatic (sodium) lamp source and a pinhole indicated that a very sharp image was formed of an object on the lens axis, i.e., in the conditions of use. Since the fluorescence from nitrogen lies mainly in a relatively narrow spectral range (the main bands of the $N_2^+(1-)$ system are the (0,0) at 3914 A and the (0,1) at 4278 A, and the main bands of the $N_2(2+)$ system are the (0,0) at 3371 A, the (0,1) at 3577 A, the (1,0) at 3160 A, and the (0,2) at 3805 A), the image-producing quality of the lens seemed to be satisfactory.

The function of the slit S1 is to admit a small portion of the image of the electron beam to the photomultiplier P1, thus giving the spatial resolution through the boundary layer during the scan, since light from portions of the beam above and below the portion imaged on the slit is intercepted. When the full 5 in of the lens was used and the total light was recorded in the measurement of mean density $\bar{\rho}$, the ratio of light signal to noise was large, and very fine resolution, on the order of 0.001 in, could be used; however, when the fluctuating density ρ' is

measured, the high frequencies of interest constitute only a small portion of the signal; also, such a fine slit setting would be inconsistent with the accuracy with which the traverse mechanism could be positioned and reset; a compromise figure of 0.017 in slit width was adopted.

The spectrometer used was a 0.5 meter Jarrell-Ash instrument with a reflection grating of 1100 lines/mm, blazed at 5000 A, and a motorized wavelength scan with ranges from 1 to 200 A/min. It had coupled precision entrance and exit slits about 2 cm in length, the slit length being defined by a sliding V-notch plate. Thus, the slit S1 was not necessary when the spectrometer was in use for temperature measurement; the movable mirror M1 was swung aside and the lens L1 formed an image of the beam directly on the spectrometer entrance slit. The vertical traverse was used to position the spectrometer axis at various points along the beam, at each of which a wavelength scan was performed. A scan was made at about 0.5 in intervals through the boundary layer.

Two different photomultiplier tubes were used: an EMI 9502 end-window tube with S11 response, and an RCA 1P28 side-window tube with S5 response. The 9502 has better signal-to-dark-current ratio, but is physically large and has a small (0.3 in diameter) photocathode; the 1P28 is quite small and has a large (0.75 X 0.5 in)

photocathode. The 9502 was used in a housing purchased from Products for Research, Inc., and included a dynode supply chain of resistors, with capacitor decoupling of the last two dynodes and Zener diode stabilization of the first stage (Figure 10a). The 1P28 tube was used in a housing fabricated at JPL, and included a dynode chain, decoupling capacitors on the last five stages, and HT input and signal output plugs (Figure 10b). A small short-focal-length relay lens was used ahead of each photomultiplier tube to converge the rays onto the photocathode.

8. The Data-Recording System

The data-recording arrangements for the three measurements (mean density, fluctuating density, static temperature) are shown in Figure 11, a, b, and c, respectively. The HP412A DC vacuum-tube voltmeter (0.001 to 1000 V full-scale deflection) was used to measure photomultiplier output directly, and also to amplify the signal and give a convenient low-impedance drive for a Moseley XY plotter (1 volt output at full scale, on all ranges of the VTVM). The HP412A was also used to measure the electron beam current, in terms of the voltage over resistors to ground, for all the electrically insulated portions of the drift tube and the wedge in the HWT.

In the measurement of fluctuating density ρ', AC amplification was provided by a model HP450 broad-band amplifier (10 Hz to 1 MHz, 20 db and 40 db gain settings), while filtering was provided by a Krohn-Hite model 310AB filter (independent selection of low and high ends of the pass band in the range 20 Hz to 200 kHz, 60 db per octave roll-off). The detector for the filtered and amplified AC signal was a thermocouple whose DC output was fed to an XY plotter.

Two other kinds of supplementary records were made: an HP310A wave analyzer (0 to 1.6 MHz, Δf = 200, 1000 or 3000 Hz) was used to measure the frequency spectrum of the fluctuating signal, and a multi-channel high-frequency magnetic tape-recorder was used to record segments of three signals - electron beam current, total light signal, and the high-frequency light signal, at a number of locations in the boundary layer.

Pressure readings on a differential oil manometer were taken of the pressure in the balance chamber compartment of the drift tube, and the pressure at a tap on the HWT sidewall about 15 in upstream of the beam station (the nearest available tap).

Other auxiliary parameters measured were the pressure in the drift tube and electron gun system, and the gun power

supply voltage.

9. Calibration and Set-Up Prior to the Air-On Tests

Besides the extensive work required to make the electron beam equipment reliably and continuously operational, particularly the work to remedy the vacuum and cooling problems and the work to assemble and check out the optical instrumentation and beam scan traverse mechanism, several other matters had to be dealt with prior to the air-on tests.

9.1. X-Ray hazard Following some brief early tests of the electron beam power supply and gun on the USC campus, the gun was incorporated into the drift tube module and set up at JPL to operate into a still-air tank for density calibration. At this point it was appropriate to check the x-ray emission.

Measurements of the unshielded equipment by means of an ion-chamber gauge indicated that certain items, particularly the orifice plates along the drift tube where electrons were intercepted, and the final beam collector in the calibration tank, emitted considerable amounts of soft x-ray radiation, when the gun operated at 50 kV and several milliamps of beam current. It was determined that lead shielding around the drift tube and shielding

with 0.060 in steel plates around the calibration tank reduced the radiation by factors of about 1000 to 10,000. The radiation levels in the vicinity of the equipment were then always well below the JPL limit (one tenth of the California State limit) of 0.2 mr/hr. Other provisions of the State code were also complied with, viz., that the equipment and operators be licensed, that the personnel wear film badges, and that hazard signs be displayed on the equipment and in the area.

The same question was later examined with the electron beam equipment installed in the HWT. In this case the massive bulk of the wind tunnel made special shielding unnecessary.

9.2. Light Intensity Calibration Because an accurate knowledge of the light intensity variation with air density calibration was fundamental to the electron beam method, a special calibration tank (Figure 12a) was fabricated. The tank was designed for use both on the still-air test stand (Figure 12b), where the calibration and equipment shakedown work could be done, and also in situ in the HWT (Figure 12c), where a final calibration in still air would include the possible effects of spectral absorption of the window. Photographs of the electron beam in the still-air tank at two different pressures are shown in Figure 12d.

Prior use of the electron beam fluorescence technique by others has been predicated on separate measurement of light output and collected beam current, with fixed beam voltage and optical geometry, so that one can derive a calibration curve of light per unit beam current as a function of gas density. This technique is well established at low pressures where there is little beam attenuation and scattering, and where the light versus density curve is almost linear.

However, early attempts by the present author to obtain a reproducible light versus density calibration curve in the calibration tank, expressed in terms of total light per unit collected beam current, were only partially successful: the data would become progressively more erratic as the pressure increased above a few tenths of a torr. It was noted that adjustments in beam focus, which were also observed to alter the beam current waveform, caused marked changes in the light per unit beam current.

The situation was not clarified until spectrally resolved light measurements were made, and provision was made for relatively fast recording of tank pressure changes by means of a strain-gauge pressure transducer whose output was registered on an XY plotter. Air could be bled into the tank to raise the pressure to a few torr in about one minute, and then the tank could be evacuated by means of

a mechanical vacuum pump working directly into the tank. This technique was combined with spectrally resolved light measurements at different locations along the beam, with simultaneous recording of collected beam current, and with the collector at different distances from the beam entrance, and with deliberate changes of the beam focus settings. Several problems were then identified and dealt with.

a) Spurious light The main reason for the initial difficulties in determining a light versus density calibration was the generation of secondary electrons from the sides of the beam entrance hole. Since both the light intensity produced by these electrons and their range are strong functions of the gas density, there is a source of 2+ system light whose intensity and spatial size vary greatly. The intensity of this source is up to ten times that of secondary electrons produced in the normal way along the beam, and the size of the source varies up to a few mm.

Figure 13 illustrates the total light intensity profile measured at various distances from the beam entrance orifice as a function of pressure. It can be seen that the light peaks at about 0.6 torr, falling off rapidly with both increase and decrease of pressure from this value, and that the light falls off quite rapidly with increasing distance from the entrance. Unfortunately, the expected range of gas density near the HWT wall for the conditions of the

tests is about 0.45 to 2.0 torr, so that one can expect trouble from this spurious peak. A possible way to avoid the peak would be to use only 1- system light for the scan near the wall (selected by means of an interference optical filter or a low-resolution spectrometer); the difficulties with this scheme are that one must use only one strong band, e.g., at 3914 A, and the 1- system is known to saturate at relatively low pressure, so that one would lose signal and sensitivity to density gradients. In actual fact the calibration was performed both in terms of total light and light transmitted by an interference filter admitting the strong 1- band at 4278 A.

b) Beam attenuation A second factor contributing to the calibration difficulties is that the collected beam current is a gradually decreasing fraction of the beam current entering the chamber, as the gas pressure increases and as the distance from the entrance to the collector increases. A significant point that emerges from the collector current measurements is that it would be impractical in the HWT tests to use the measured beam current collected in the Faraday cup wedge (located at the center of the tunnel, about 10 in from the ceiling) to evaluate the gas density profile from the measured light intensity distribution. The fact is that the density increases steeply through the boundary layer quite close to the ceiling, reaching its

free stream value some four to six inches from the ceiling and remaining at this high density level down to the wedge. This means that the collected current is perhaps only 10 to 20% of the electron current actually entering the HWT, and the actual density must be known before one can determine the ratio of the current collected to that entering. At best this would require an iterative procedure. Moreover, there is doubt that the collected current is free from errors due to ejection of secondary electrons at the collector.

For these reasons it is not appropriate to retain the collector current as a primary parameter in the light intensity versus density calibration. Instead, the calibration was obtained in terms of the light intensity relative to a particular point along the beam where the gas density is known. This procedure requires only that the beam current entering the tank or the HWT remains constant during the still-air calibration and during the HWT tests, and the performance of the equipment meets this criterion amply.

An obvious choice of location for the reference point is near the beam entrance, but far enough away to avoid the spurious light peak. The reference density chosen was 1 torr at room temperature (290 K) in the calibration tank. In the HWT case two possibilities present

themselves: the wall pressure and temperature are measured and hence the wall density is known; also the free stream value beyond the boundary layer is well established.

c) Internal reflections A third, relatively minor factor affecting the measurements was that minor irregularities in the light output along the beam arising from internal reflections inside the tank, from the window, etc.. A coating of matt black paint applied to the inside of the tank eliminated this problem, and the same treatment was given later to surfaces in the HWT.

d) Beam spreading A fourth factor to consider was the effect of beam spreading. The spreading was evident to the naked eye, and was confirmed by beam light profiles taken by translating the optical system laterally by means of the second element of the cross slide. The beam, of initial diameter about 1 mm (the entrance hole size), diverged to be 2 or 3 mm or more in diameter after traversing several inches of air at a (uniform) pressure of several torr. Fortunately, the first-order optical effect of the spreading is zero, i.e., no change in the amount of light reaching the photomultiplier photocathode, until the image began to spill over the photocathode. Care was taken to insure that the image remained smaller than the photocathode up to the largest calibration

pressure-distance integral used (the curve for both total light and filtered 4278 A band light seemed to saturate at about a path length of 5 in in air at pressure of about 3 torr, i.e., an integral of about 15 torr.in).

It would clearly be advantageous for reduction of the HWT measurements to have an analytical fit to the room temperature still-air calibration data of Figure 13. Inspection of Figure 13 suggests that two features, expected on theoretical grounds, and reported in the literature, are present:

(i) saturation or quenching of the light at high density, usually modeled as

$$L(\rho) = \frac{C_1 \rho}{1 + C_2 \rho} \qquad (1)$$

(ii) beam attenuation, increasing with distance from the entrance and with density, for which an appropriate model is:

$$L(\rho, y) = L_0 \exp\left\{ -C_4 \left[\int_0^y \rho \, dy - C_5 \right] \right\} \qquad (2)$$

where the C_5 factor accounts for the fact that the attenuation appears to have a threshold value.

In addition, there is theoretical and experimental evidence for two further factors in the model:

(iii) a ρ^2 term, significant in value at high density, reflecting the fact that the 2+ system light varies as the product of density and number of secondary electrons, which in turn varies as the density;

(iv) a temperature dependence of the quenching constant C_2.

Thus the full model is of the form:

$$L(\rho,y) = \frac{C_1\rho(1 + C_6\rho)}{1 + C_2\left[\frac{T}{T_0}\right]^{C_3}\rho} \exp\left\{-C_4\left[\int_0^y \rho dy - C_5\right]\right\} \qquad (3)$$

We note that the room temperature calibration offers no data on the value of C_3, for which values in the range 0,1 to 0,25 have been reported. Again, the value of C_2 cannot be fixed decisively from the calibration data.

However, it will be seen later that the values of C_2 and C_3 in this model are important for reduction of the mean density measurements in the HWT, where values of density up to 7 torr (room temperature equivalent) can occur, simultaneously with temperatures down to 45 K, at the boundary layer edge.

Many sets of constants C_1 to C_6 (with $C_3 = 0$) were fitted to the still-air calibration data, and were subsequently tested against the HWT results. The set finally adopted

was:

$$C_1 = 1.87,\ C_2 = 0.90,\ C_4 = 0.022,\ C_5 = 5,\ C_6 = 0.02,$$

and a value $C_3 = 0.2$ for the HWT data, where $L(\rho,y)$ of Equation (3) is normalized to 1 at $\rho = 1$ and $y = 0$, y is in inches and ρ is in 290 torr units (density of air at 1 torr and 290 K). Figure 14 shows the light intensity given by this model at room temperature, compared with the calibration measurements. It can be seen that the model fits the calibration data quite well, to within about 2 or 3% at all points.

9.3. Comments on the Light Calibration:

A certain amount of data on these constants has been published. Muntz[11] quotes quenching pressure values (pressure for which $C_2\rho = 1$ at room temperature) $p_q = 1.9$ torr (Camac,[13] for 100 kV electrons) and 1.1 torr (Brocklehurst[14]) for the (0,0) band of the nitrogen 1- system; these values compare quite well with the value $p_q = 1/0.9 = 1.1$ torr here, for total light over the whole spectrum.

Harvey and Hunter,[15] who used 28 kV electrons in nitrogen, recently reported a calibration of the form

$$L = \frac{C_1\rho(1 + C_6\rho)}{1 + C_2\rho}$$

where $C_2 = 0.765$ and $C_6 = 0.016$; these values compare reasonably well with the values $C_2 = 0.90$ and $C_6 = 0.02$ found here.

As regards the constants C_4 and C_5, Camac[13] gives an expression

$$I = I_0 \exp\left[\frac{-p\ell\ (\frac{300}{T})}{110\ V^2}\right]$$

with temperature T in deg K, beam voltage V in 10^5 volts, pressure p in torr, and path length ℓ in cm. Taking the attenuation to be the same for oxygen as for nitrogen, the equivalent value of C_4 for the present case (V = 0.48, T = 290) is 0.104, i.e., much larger than the present value. We note that the factor p/T is equivalent to ρ. Possible reasons for the apparent discrepancy are that Camac has no C_5 factor and that he measured the actual beam current collected in a cup of diameter 0.375 in at a distance of 6 in, in nitrogen at pressure up to 3 torr, at room temperature, with 100 kV electrons. However, in the present work the attenuation is measured in terms of the total spectrum light viewed with relatively wide-angle optics.

Some information on the value of the constant C_3 has been reported. Muntz[11] quotes a value from a Camac paper of $C_3 = 1/6$ for the (0,0) band of the 1- system, and

Camac[13] gives a preliminary value of 0.25 for the 1- system. Incidentally, a similar small positive value of C_3 was reported recently by Smith[16] for helium; he finds different values of C_3 for two different helium lines. Butefisch and Vennemann,[20] in reviewing the information on C_3 for air, report that the experimental uncertainties are too large for a conclusive result. It will be seen below that the interpretation of the HWT mean density measurements is very sensitive, at the higher test pressure conditions, to the values of C_3 and C_6. A value of $C_3 = 0.20$ was finally adopted.

We note in passing that the calibration of Equation (3) has implications for the measurement of density fluctuations, in that the light fluctuations will depend, in general, on fluctuations in T and $I = \int_0^y \rho dy$, in addition to the direct contribution from density fluctuations. This is analogous to the "separation of modes" problem encountered in hot wire measurements of turbulent fluctuations.

We also note in retrospect that a more precise determination of the constants C_4, C_5 (attenuation) and C_6 (ρ^2 term) would result if the still-air calibration had been extended to greater distance and higher density.

However, this would have called for increased pumping rate in the electron gun and drift tube vacuum system, which was designed for the HWT requirements, where the highest wall pressure was about 1.5 torr.

9.4. Development of an FET Preamplifier The field-effect transistor (FET) is known to have the attribute of high input resistance and low output resistance, and finds application where one wishes to drive a relatively low impedance device like a recorder from a relatively high output impedance device like a photomultiplier.

In the experiment described here the fluctuating signal was ample to drive the thermocouple detector (tens of millivolts), even from a relatively low photomultiplier anode load (tens of kilohms), and the cable length from photomultiplier to detector, or to a signal conditioning device such as a filter, was only a few feet. However, in the case of the magnetic tape-recorder used to record the signals as a back-up to the main experiment, the input signal required is 0.3 to 1.0 volt, and the closest point where the recorder could reasonably be placed was some 20 to 30 ft from the photomultiplier. It is presumed

that the fluctuating signal could have meaningful components up to 200 kHz, and a rough calculation indicates that 20 ft of Uniradio cable with 27 pF capacitance per foot, i.e., 540 x 10^{-12} F total, will attenuate by 6 db (and phase change by 45 deg) a 200 kHz sine wave from a source resistance of 14 kilohm.

The main technical difficulties in designing an FET stage are the need for a bias voltage of several volts between the "gate" and the "drain", the elimination of drift, and the arrangement of a single-ended output with one side grounded, to operate from a photomultiplier source which customarily has one end of the anode load grounded.

The type U1898 FET, which has high transconductance, was used in a balanced pair circuit to reduce drift, as shown in Figure 15. This circuit has adequately low drift (about 50 microvolts in 10 minutes), and delivers at least 4 volts of linear output, accurately following the input, with about 0.88 stage voltage gain (Figure 15a). The output resistance is about 180 Megohm, and the true input resistance of the FET is about 600 Megohm, although limited in the circuit shown to the values of the megohm bias network shown.

9.5. Calibration of the RMS Thermocouple Detector The mean square vacuum thermocouple detector was borrowed from Dr J.Kendall of JPL, who has used it extensively in the measurement of aerodynamic turbulent fluctuations. The frequency response was assumed to be linear over the range of interest here, but a calibration of DC output in terms of mean square input was performed, using a 1 kHz square wave generator as shown in Figure 16. The results, shown in Figure 16a, indicate that the DC output is proportional to mean square electrical input over a satisfactory range. A relation which fits the observed data in the arrangement used both in calibration and in taking the HWT data is

$$\text{mean square mV input} = 0.0137\ (\text{DC mV output} + 0.215)^2 \qquad (5)$$

9.6. Alignment of the Vertical Scan The procedure to align the vertical scan to follow the beam was checked on the still-air test stand. Since the lathe cross-feed mechanism was equipped with a manual lateral slide as well as the motorized vertical slide, it was very simple to use the lateral movement to find the maxima of the light signals near the top and bottom of the beam, and, by tilting the stand by means of its adjustable feet, to make the vertical traverse collinear with the beam center.

9.7. Definition of the Zero Position of the Vertical Scan

The hitherto undesired spurious light from secondary electrons near the beam entrance was useful in defining the zero or wall position of the vertical scan. In most circumstances the spurious light gave a small narrow peak superimposed on the true beam light signal, and the center of the peak could be located and taken to be the wall position. A steel rule readable to about 0.010 in, carried on the moving part and read against a ledge on the fixed part of the traverse was then used to determine the vertical position of the scan optics relative to the beam entrance hole.

It was also convenient to make the zero positions the same for the two alternative optical outputs (spectrometer and total light measurements), and this was done by adjustment of the set screw on which the movable mirror M1 came to rest when dropped into place and secured.

9.8. Definition of Operational Settings for the Spectrometer

A good deal of effort was expended on the determination of the best settings and arrangements for recording the rotational lines by means of the spectrometer, using the electron beam operating in the still-air chamber as source.

The spectrometer was first used with wide entrance slit to check the relativities of the vibrational bands in the nitrogen 1- and 2+ systems, in the pressure range 0.5 to 3 torr. It was found that the 1- band at 3914 A is always strong, even when quenched (saturated) at high density, and it has been chosen by several investigators (e.g., Ashkenas[17]) because it has many lines (22 at room temperature) in the R branch which can be resolved clear of other bands and lines.

Further work was done in order to improve the recorded spectrum, and a number of factors was explored: external optics, to improve the matching of the spectrometer to the external optical system, entrance slit width and length, first and second orders of the spectrum, rate of wavelength scan, type of photomultiplier tube, its voltage and anode load, amplification and recording of the output signal, possible rotation of the incoming light beam by means of a Dove prism, AC amplification of the light signal using the 120 Hz component of the basic beam current and therefore also of the light signal, mechanical chopping of the incoming light, and external modulation of the electron beam current via signals to the X and Y deflection coils.

Regrettably, these explorations did not discover any startling improvements, and the arrangement chosen was to use the second-order 3914 A band spectrum at 7828 A, DC

amplification of the total light signal using the HP312A VTVM to feed an XY plotter, a wavelength scan rate such as to take about 10 min for one spectrum, and a particular setting of slit width (265 on the micrometer slit scale, corresponding to about 0.002 in) which represented a compromise between signal strength and spectral resolution.

In addition, some gain in light entering the spectrometer could be achieved by stopping down the objective lens using black paper masks, and finding the best focus. The slit length used was about 2 mm, representing a compromise between spatial resolution along the beam and spectral signal amplitude.

Tests were made with a Dove prism and a mirror combination, but any gain seemed to be offset by problems of alignment with the optical axis. Turning the spectrometer would have entailed unacceptable delays for structural modifications in the traverse mechanism. The HWT tests were made with the slit vertical and without rotation of the image.

9.9. Electronic Frequency Spectrum of the Beam A frequency analysis of the total light signal from the electron beam in the still-air calibration chamber was

performed, using the HP310 wave analyzer. No component above 1 kHz was found; below this frequency there is a series of harmonics of the basic 110 Hz ripple waveform of electron beam current, probably arising from residual ripple on the gun accelerating voltage, in the 60 Hz gun filament heating, or in the two focus coils and the X and Y deflection coils.

10. Operational Procedures

The start-up began with the HWT at atmospheric pressure, and also the lower part of the drift tube, up to the closed manual isolating valve (MIV, Figure 6). On the top side of the MIV the gun system was always kept evacuated by means of the oil diffusion pump, backed by the mechanical pump MP3. When the test was about to commence, the rubber hoses linking the differential pumps MP1 and MP2 were closed by means of manually operated clamps, and the differential oil manometer was left in the "safe" position (vented across the U-tube), and pumps MP1 and MP2 were brought on, working into the closed tubing alone. At the same time the electronic items of the equipment were brought on, to allow warm-up and attainment of thermal equilibrium, particularly of the two focus coils and the beam X and Y deflection coils, and the cooling water to the drift tube orifices and coils was started.

Thereafter the HWT was evacuated, supersonic flow was established, and the process of bringing the tunnel up to the desired stagnation pressure and then to the desired stagnation temperature was begun, and continued for about 20 minutes before being complete. In the interim, as soon as supersonic flow was established, the electron beam could be brought on and also allowed to settle. To do this the hose clamps to MP1 and MP2 were released, the Televac thermocouple gauge channels were read to confirm that the lower part of the drift tube was at low pressure, the MIV was opened, and the beam was brought on, after confirming with the ion gauge that the gun pressure was low enough. First the 50 kV supply was brought on, and then the filament power; if the previous settings of the X and Y deflections and of the two focus coils were undisturbed, the beam could be picked up quite quickly by means of channels 1 to 6 of the beam current meter; at the same time the beam could be seen in the tunnel by eye (from the blue-violet fluorescence along the beam) if one pulled aside the blackout curtain.

Thereafter the beam current was brought up to the target value (usually about 8 mA from the supply was used, corresponding to about 1 mA beam current entering the HWT when conditions settled; the current collected by the wedge, located 9 to 10 in from the ceiling, was only a

small fraction of this, and varied with the HWT pressure), and cyclic adjustments were made of the focus and deflection settings in order to maximize the beam current in the HWT. Conditions for the first maximization could be found in a few minutes; thereafter the beam current would drift down to about half this value over a period of about 15 min, probably owing to the establishment of thermal balance in the electrically heated and water-cooled focus coils.

When the HWT reached settled conditions the electron beam controls were again adjusted for maximum current in the HWT; thereafter the drift in beam voltage and current was typically very little, and experience indicated that it was best not to make further adjustments, but to allow the system to drift gently around its natural equilibrium conditions. The question of stability is of course important, particularly for the spectral scans which required up to 10 min for one scan. The beam current was monitored and recorded frequently.

The procedure for planned shutdown of the HWT was essentially the reverse of that described for start-up, and will not be described in detail. The only major difference is that the beam was switched off by reducing the filament current, switching off the filament current, and then the 50 kV voltage, without altering the focus and deflection settings.

In the case of an emergency shutdown of the HWT, which occurred several times, as has been noted, the beam was immediately switched off, the MIV (Figure 6) was closed, the hoses to MP1 and MP2 were clamped, and the oil manometer returned to safe position if it were in use. This could be done in about 1 minute, and in any case, the HWT must continue to blow air for at least 5 to 10 minutes, to remove heat stored in the electrical heaters after the power to these has been cut, so that an emergency shutdown is in fact a shortened version of the normal shutdown. If the emergency arose from blowout of a cooling water hose, as was always the case in these tests, a great deal of cooling water was leaked around the working section during the shutdown and was something of a hazard.

As has been noted, the gun and drift tube behaved admirably over the last 12 months or so of use, a period which involved being twice installed and removed from the HWT. The gun filament remained intact, the vacuum system was not opened, and in fact the electron beam proved to be more durable in continuous operation than did the HWT.

Figure 17 shows photographs of the electron beam in the HWT and Figure 18 shows oscillograms of the beam current and light signal waveforms.

Section IV

RESULTS

1. Mean Static (Rotational) Temperature:

Scans of the rotational lines of the R branch of the (0,0) 3914 A band of the nitrogen 1- system were taken at approximately 0.5 in intervals, altogether at some 12 to 15 points, through the ceiling boundary layer in the HWT, for each of the three stagnation pressures, 500, 1700 and 3200 cm Hg. Near the wall (i.e., near room temperature) 22 lines were resolved, and out in the free stream about 10 lines could be resolved (the calculated free-stream static temperature at Mach 9.4 and stagnation temperature 1000 F is 44.4 K). A reasonable signal-to-noise ratio was achieved for all the conditions; sample records are shown in Figure 19.

The temperature data were first reduced in the conventional way (see refs 11, 17, and 18). A least squares fit is made of log (I/I_0) versus K(K+1), K being the ordinal number of the rotational line in the R branch, beginning at 1 and going towards shorter wavelengths, as is conventional. Actually, several variants of this method are in

vogue, employing different numbers of lines, for example. The data presented here are based on least squares fit to the first ten lines.

Secondly, the method recently proposed by Hickman et al.[19] was applied. Hickman takes exception to the unequal weighting of the various lines that is implicit in the previous logarithmic method. Briefly, his criticism is that the least squares process gives weight according to the distance of a data point (x,y) from the y and x axes, respectively, the result being that greatest weight is given to the least reliable data points where the measured signal is least. Hickman proposes a least squares fit of the linear measured signals to a theoretical curve which depends on temperature. The fit is a two-parameter one, one parameter being the scale factor between the measured profile and the standard one, the other being the temperature. Thus, the method gives weight to data points in strict proportion to the measured signal.

Actually, Hickman gives two theoretical curves, one the orthodox dipole theory, the other a quadrupole formulation. The outcome of the process, for which the present author wrote a computer program, is a dipole and a quadrupole temperature which best fit the measured rotational spectrum at each station in the boundary layer.

The results of the three procedures, the 10-point logarithmic, and linear dipole and quadrupole fits, are shown in Figure 20a,b,c for the three HWT stagnation pressures, respectively.

It is a reasonable assumption, for a long nozzle (160 inches from the throat) that under continuum conditions the mean rotational temperature measured is very close to the mean gasdynamic static temperature.

Figure 20a also shows the static temperature profiles for the 3200 cm Hg stagnation pressure case, as determined by Demetriades et al.[7] from their measured pitot pressure and total temperature profiles. The gasdynamic static temperature is seen to be in quite good agreement with the Hickman quadrupole determination of static temperature. The peak near the wall exhibited by the Demetriades data is not present in the spectrometer measurements.

Figures 20,a,b and c also show the measured wall temperatures (thermocouple, prior work) and the calculated isentropic free stream conditions.

Comparison of the three methods of data reduction (10-point, dipole and quadrupole) shows that all three

agree at the wall in the cases P_0 = 3200 and 1700, but in the 500 case the 10-point method gives a result much lower than the other two methods, which again agree. In the free stream the dipole method reads consistently above the quadrupole, while the 10-point method appears erratic; in two cases it gives the highest value, but in the P_0 = 500 case it is equal to the quadrupole reading. We note that the three methods share a common rotational spectrum, and differ only in the data treatment.

In regard to absolute values, the quadrupole agrees best in the free stream with the isentropic value and the value measured by Demetriades in the P_0 = 3200 case. The dipole method gives results about 10 and 15 degrees high, and the 10-point method is erratic and generally high, up to 30 degrees.

Near the wall there is considerable doubt as to the gas temperature that the spectrometer sees, for two reasons. First, Demetriades found a large gas static temperature excursion, from 300 K at the wall up to about 390 K and down again to 320 K in a distance of about 0.11 in (P_0 = 3200 case); since the spectrometer spatial resolution was about 2 mm, and the measurements were taken at

very few points along the beam, the spectrometer results represent a very crude spatial average (in this short region close to the wall). Secondly, near the wall the spectrometer views the gas actually within the beam entrance aperture. This gas is heated by secondary electrons ejected from the adjacent (copper) metal. Thus, the high temperature seen near the wall in the $P_0 = 500$ case may be real.

The coarse spectral resolution of the spectrometer could have been improved by positioning the electrom beam path normal to the spectrometer slit; but a much more rigid mount and traverse system would be needed to give the fine spatial resolution required to determine the gas temperature profile near the wall. Also, a great deal of test time would be necessary (about 10 minutes for the spectral scan at each point).

Figures 20a, b and c also show temperature profiles adopted for reduction of the HWT mean density measurements and for the calculation of the static pressure distributions. The profiles are the average of the quadrupole and dipole data near the wall, and asymptote to the isentropic free stream values at the edge of the boundary layer.

2. Wall Pressure:

In all cases oil manometer readings were taken of the HWT side wall pressure a short distance (about 15 in, nearest available tap) upstream of the beam station, and of the drift-tube balance-chamber pressure.

Figure 21 shows these pressures, expressed as a ratio to the theoretical free stream pressure. The scatter in measurement becomes increasingly large for the P_0 = 1700 and 500 cases. Also shown are Demetriades' values for the P_0 = 3200 and 1700 cases and Gupta's values for the P_0 = 3200, 1700 and 500 cases at the beam station (with the beam absent).

The balance-chamber pressure agrees with the upstream wall pressure for P_0 = 3200. For the P_0 = 1700 and 500 cases both pressures rise, and the wall pressure rises to more than twice the free stream value. The points given by Demetriades also show a rise from P_0 = 3200 to 1700, but are high relative to the present pressures (23% at 3200 and 14% at 1700). Gupta's values are also high relative to the present work at P_0 = 3200 and 1700 (12% and 7%, respectively) but low at P_0 = 500 (11% low).

The measured and calculated wall and free stream conditions (temperature, pressure, density) are shown in

Table 1. It is clear that there is considerable uncertainty in the gas density (calculated from pressure and temperature) in the electron beam near the wall. The range of ρ_w is 0.391 to 0.506, 0.936 to 0.963, and 1.389 to 1.557 290 torr, for the P_0 = 500, 1700 and 3200 cases, respectively. These figures represent a range of 29, 3 and 12%, respectively.

Table 1

CALCULATED AND MEASURED WALL AND FREE STREAM CONDITIONS

		Stagnation pressure, cm Hg			Units
		500	1700	3200	
measured Mach number	M_∞	9.155	9.33	9.375	
calculated (isentropic expansion)	p_∞	0.2117	0.6350	1.158	torr
	ρ_∞	1.344	4.179	7.690	290 torr
	T_∞	45.70	44.06	43.66	deg K
measured (present)	p_w	0.427	0.876	1.343	torr
measured (prior, Gupta)	p_w	0.386	0.940	1.505	torr
measured (thermocouple)	T_w	294	297	300	deg K
calculated (from p and T)					
present	ρ_w	0.506	0.936	1.389	290 torr
prior, Gupta	ρ_w	0.391	0.963	1.557	290 torr
measured (electron beam)	ρ_w	0.38	0.93	1.50	290 torr

3. Mean Density:

The basic measured light profiles were first reduced to light/light at the wall, and corrected, where necessary, for the spurious light peak near the beam entrance. All three profiles showed light increasing from the wall: in the P_0 = 1700 and 3200 cases a maximum was reached at the boundary layer edge (y = 4.6 and 4.1 in, respectively), followed by a fall due to beam attenuation. In the P_0 = 500 case the light profile became flat in the region y = 5 to 6 in.

At the maximum the ratios light/light at the wall were 2.73, 2.13 and 1.87, respectively. Reference to the light calibrations of Figures 14, 14a and 14b and the wall densities in Table 1 indicates that such large light ratios are incompatible with $C_3 = 0$ in Equation (3). This is confirmed by attempts to derive the density from the light profiles.

Briefly, the calculation diverges if one approaches saturation. Thus, the determination for density profiles for the three P_0 cases is essentially a determination of C_3; since the temperature structure through the boundary layer should exhibit some similarity for the three cases, we seek a single value of C_3 to give a reasonable fit at the known densities at the wall and in the free stream.

It has been noted that the wall density (i.e., in the electron beam near the entrance) is uncertain to some extent. However, the free stream value is known more precisely from the wind tunnel calibrations.

To derive the density profile from the light profile one assumes a wall value of density and values of the calibration constants C_1 to C_6. It was noted above that a number of such sets gave a reasonable fit to the still-air calibration data, and all of these were investigated with respect to the HWT data. From the analytical model one evaluates L_w, the light intensity at the wall, and proceeds to the next point, where L_{w+} = measured light ratio x L_w; hence ρ_{w+} is evaluated, allowing for the local temperature; the fact that beam attenuation depends on $\int_0^y \rho dy$ means that some iteration is necessary.

This analysis was performed for various assumed values of C_3 and sets of calibration constants. The criterion for success was that the resulting density profiles should reach the known free stream value at the boundary layer edge, for all three cases of P_0. It turned out that many sets of constants fitting the calibration data did not yield satisfactory results with the HWT data; for the sets that came close, there was to some extent a trade-off between the constants C_3 and C_6; C_3 was varied in the

range 0 to 0.25 and C_6 in the range 0 to 0.08. Values of $C_3 = 0.2$ and $C_6 = 0.02$ were finally adopted for giving the most consistent density distributions. The resulting mean density profiles are shown in Figure 22a, b, and c for the cases $P_0 = 3200$, 1700 and 500, respectively. The values of the constants are

C_1	C_2	C_3	C_4	C_5	C_6
1.87	0.90	0.2	0.022	5	0.02

It can be seen in Figures 22a and b that the calculated ρ profiles do not level off as they should at the boundary layer edge. The cause is believed to be the fact that the light-density calibration model and the constants are not quite correct; for example, a value of $C_4 \sim 0.007$ in the free stream (at T = 45 K) would give a level profile of ρ, whereas the value to fit the still-air calibration (at T = 290 K) was 0.022. However, the inclusion of such a temperature dependence of C_4 is beyond the scope of the present work.

Figures 22a, b and c also show the ratio ρ/ρ_∞, and in the $P_0 = 3200$ case Figure 22a shows ρ/ρ_∞ as calculated by Demetriades (from measured static and pitot pressures and total temperature). The sharp maximum near the wall (resulting from the sharp peak of T near the wall) found by Demetriades is not present in the electron beam

measurements. The measured ρ profiles are approximately "logarithmic" (straight line on log-linear graph) in all three P_0 cases, with a slight curvature near the wall in the $P_0 = 3200$ case, however.

From the measured temperature and density profiles the static pressure profiles can be calculated as shown in Figure 23a, b and c for the cases $P_0 = 3200$, 1700 and 500, respectively. The figures also show the available Demetriades and Gupta uncorrected and corrected profiles.

The electron beam pressure profiles all show an elevated pressure at the wall and a monotonic fall towards free stream level in going out through the boundary layer. The percentage excess pressure at the wall increases from the 3200 to the 500 cases, and there is a simultaneous increase in the distance from the wall at which the free stream level is reached: the excess pressures and the distances are: 30% and 0.7 in for $P_0 = 3200$, 48% and 3.1 in for $P_0 = 1700$, and 82% and 4.8 in for $P_0 = 500$. In the 3200 and 1700 cases the calculated points diverge sharply above the free stream level in the free stream; as mentioned above, this is attributed to inaccuracy in the attenuation factor in the calibration model at high ρ and low temperature. In all three P_0 cases the pressure falls steeply for about 1 inch near the wall; in the

P_0 = 1700 and 500 cases there is another fall further out in the boundary layer.

The uncorrected, directly measured static pressure profiles of Demetriades and Gupta lie well above the isentropic free stream level everywhere; all have a slight minimum in the region y = 1 to 2 in (at 32, 55 and 142% above the isentropic level, for the 3200, 1700 and 500 cases, respectively), and rise to a maximum in the free stream. The correction, which is zero at the wall, gives a profile which is flat for about 3 in near the wall, thereafter falling steeply towards the free stream.

We note, in comparing the directly measured and electron beam pressure profiles, that the electron beam profiles indicate a sharp fall in pressure near the wall, with a possible further decrease towards the free stream. In contrast, the static pressure probe measurements indicate pressure levels from 50 to 200% above the isentropic free stream level, and can only be brought to the free stream level near the boundary layer edge by application of a very considerable correction for viscous interaction.

The electron beam pressure profiles can be used to determine the new Mach number profiles, in conjunction with the prior (Gupta) pitot profiles. Then the Mach number profiles can be combined with the measured static

temperature profiles to give total temperature profiles. These Mach number and total temperature profiles are shown in Figure 24a, b and c for the cases P_0 = 3200, 1700 and 500, respectively. The available Gupta and Demetriades profiles are also shown.

In general, the electron beam Mach number profiles differ from the prior work where the static pressures differ, since the same pitot pressures are used. In the P_0 = 3200 case the electron beam profile of T_t/T_{te} differs appreciably from the Demetriades profile; we recall that his total temperature probe measurements were corrected according to a Reynolds number dependent correction.

The apparent "bump" in total temperature in the P_0 = 500 case near the free stream is probably not real, but due to the thermal boundary layer adopted differing from the viscous one near the free stream.

Figure 25a, b and c shows a plot of total temperature through the boundary layer in terms of the quantity $T^* = (T_t - T_w)/(T_{te} - T_w)$ as a function of u/u_e, for the cases P_0 = 3200, 1700 and 500, respectively. The figures also show the Crocco relation $T^* = u/u_e$ and the parabolic relation $T^* = (u/u_e)^2$. The prior measurements of Demetriades and Gupta are also shown.

In all three cases the electron beam data fall close to the quadratic curve near the boundary layer edge. In the P_0 = 500 and 1700 cases the data indicate a shift towards the linear curve, at $u/u_e \sim 0.8$ and 0.7, respectively, but this trend is not apparent in the 3200 case. However, since $u/u_e \sim 0.6$ corresponds to about y = 0.5 in, and the pitot pressures become small and difficult to measure near the wall, the data at low u/u_e in Figure 25 are not reliable.

4. Density Fluctuations:

The first step in reducing the fluctuation data was to select a low-frequency cut-off that would exclude harmonics of the mains frequency known to be present in the electron beam current waveform. Examination of the thermocouple signal at the boundary layer edge (where the aerodynamic turbulence is low) indicated that almost all of the beam-borne fluctuation was removed at a filter setting of 1 kHz. Data with this filter setting were accordingly used for the analysis. Boundary layer profiles for many other values of the low cut-off frequency were recorded for the P_0 = 1700 case; above 1 kHz these formed a self-consistent set of typical boundary layer shape; below 1 kHz the boundary layer was progressively swamped by the beam-borne fluctuations.

The wide band (>1 kHz) net thermocouple signal was then coverted to rms value by means of the thermocouple calibration. The analysis of Appendix A shows that the total fluctuating signal is made up, in general, of six terms, three primary contributions from ρ, T and I, plus three cross-correlation terms. It is instructive to explore the possible relative magnitudes of the terms. We note that the cross term coefficients are related to those of the primary terms, which means that no cross term is significant unless at least one of its associated primary terms is significant, and we consider the sum of the primary squared terms:

$$L''^2 = L_\rho{}^2 \rho''^2 + L_T{}^2 T''^2 + L_I{}^2 I''^2 \qquad (6)$$

where

$$L_\rho = 1/X; \quad X = C_1 \rho/L; \quad L_T = C_3(X-1)/X;$$

$$L_I = C_4 I; \quad I = \int_0^y \rho dy; \quad I' = \int_0^y \rho' dy$$

We note that Equation (6) is valid only if one of the terms dominates, but it is useful for computing regions where this may occur.

We know X = X(y) and I = I(y) through the boundary layer, from the mean measurements, and we have the values

$C_3 = 0.2$, $C_4 = 0.022$.

The procedure in the data reduction was as follows. First, the profile of ρ'' was determined, assuming $T'' = I'' = 0$. Then a first estimate of I'' could be made, and the process continued iteratively. Finally, a crude estimate that $T'' = \rho''$, based on the data of Demetriades, was made.

The results of this exploration are shown in Figure 26,a b and c, for the cases $P_0 = 3200$, 1700 and 500, respectively. It can be seen that the contributions of T'' and I'' fluctuations to the total light signal, i.e., L''_T and L''_I. increase in going from $P_0 = 500$, 1700 and 3200; that of L''_T is never dominant (it peaks at a location where $L''\rho$ is large), while that of L''_I becomes dominant towards or in the free stream for the 1700 and 3200 cases. Thus, we conclude that accurate knowledge of C_3 is not important for determination of ρ'' per se, and also that the estimates of ρ'' are valid for the inner parts of the boundary layer, up to the edge for $P_0 = 500$, and to about $y = 3.1$ and 1.6 in, respectively, for the 1700 and 3200 cases (the criterion being that the ρ'' mean square signal should be 90% or more of the total).

Also shown in Figure 26 are the asymptotic free stream levels of ρ'' expected at the appropriate values of M_∞ and Re/inch, on the basis of the p'' measurements

of Laufer,[22] assuming that the free stream fluctuations form a pure sound field in which the isentropic relations (Laufer[23]) hold: $p'' = \gamma\rho'' = [\gamma/(\gamma-1)]T''$.

In regard to the outer boundary layer region, the case $P_0 = 500$ is the only one of the three for which ρ'' can be determined from the L'' measurements; in this case the asymptotic value of ρ'' is 2.8% and would be reached about one boundary layer thickness (about 5 in here) into the free stream. The measured ρ'' profile appears to be consistent with this picture.

Figure 27 shows a comparison of the ρ'' fluctuations for the three values of P_0, as well as the range of the Demetriades hot wire results (his solution with $R_{\sigma\pi} = R_{\pi\tau} = 0$, $R_{\tau\sigma} = -1$) for the $P_0 = 3200$ case. We note that the shapes of the electron beam ρ'' profiles are quite similar; each has a fairly flat peak region (about 6 to 8%) over the central part of the boundary layer (about 15 to 80%). The 1700 and 3200 cases show a progressively more specific sub-peak at about y = 2.5 and 2.0 in, respectively, possibly where the signal ascribed entirely to ρ'' has a contribution from T'', which is a maximum there.

Section V

CONCLUSIONS

1. Technique

The electron beam has been shown to be a useful quantitative tool as applied here to boundary layer studies in a continuous hypersonic air wind tunnel. Besides being of fast response, non-perturbing, and capable of excellent spatial resolution, the equipment used in this work has met and overcome several challenges. In spite of the seriously restricted access the beam was delivered successfully into the boundary layer and gave stable, long-term operation. The usefulness of the beam steering method based on insulating segments of the drift tube was demonstrated.

The work has shown that a 50 kV electron beam can be used quantitatively in air out to a range (integral of gas density over path length) of at least 15 torr-inch room temperature equivalent before beam spreading seriously impairs the measurement. The technique of using beam

current essentially as a measure of beam constancy, and obtaining absolute gas density from circumstantial evidence appears valid.

A light output correlation for 50 kV electrons in air has been found, and depends on local temperature and beam attenuation as well as local gas density. For flow fluctuations the output light contains contributions from local temperature fluctuations and integrated beam attenuation fluctuations, in addition to that from local gas density fluctuations.

The temperature dependence of some of the coefficients of the light-density calibration could not be defined in the present study as well as one would wish, and the question warrants further study in a flexible calibration facility where a range of known densities and temperatures could be set up.

In this example of the simultaneous use of conventional probes (total temperature, pitot and static pressure, hot wire anemometer) and the electron beam technique, the latter has shown itself capable of quantitative operation at relatively high density levels which are marginally low for the conventional methods.

2. Flow Parameters

Boundary layer profiles of mean gas temperature and density and of rms wideband density fluctuations have been determined at three values of HWT stagnation pressure, within the limitations of the electron beam technique and the facility related constraints and limitations.

The mean temperature determined from a quadrupole model of rotational spectral intensity gives better agreement in the free stream with isentropic flow theory than when a dipole theory is used.

Density profiles were obtained for all three values of the HWT stagnation pressure, although difficulties were experienced with light-density calibration at the high density and low temperature near the free stream, particularly for the highest HWT stagnation pressure.

Pressures inferred from the mean density and temperature show a variation through the boundary layer of about 50%, and the shape is different for the three values of stagnation pressure. The pressure profiles differ substantially from those derived from static probe measurements. The Mach number and total temperature profiles calculated from the electron beam derived

pressure and temperature profiles are typical of supersonic wind tunnel nozzles. The total enthalpy ratio T^* follows a quadratic dependence on velocity ratio u/u_e near the outer edge of the boundary layer.

The wideband gas density fluctuations were measured out to at least several inches from the wall, for all three stagnation pressures. The rms fluctuations reach a peak of from 6 to 8% of the mean density in the central part of the boundary layer, and fall to about 3% at the edge; the trend in the free stream is consistent with the sound field measurements of Laufer.

The peak density fluctuations are approximately one half of the level found for the P_0 = 3200 case by Demetriades. In addition, in the 3200 and 1700 cases the density fluctuation profile from the electron beam measurements differs from that of Demetriades in having only a single sub-peak at somewhat smaller y than his outer peak, and the electron beam profiles do not show his inner peak near the wall. A possible explanation for the difference is the simplified assumptions which he makes in his analysis concerning the correlation coefficients for the flow parameters.

REFERENCES

1. Kistler, A.L. "Fluctuation Measurements in a Supersonic Turbulent Boundary Layer." The Physics of Fluids, Vol.2, No.3, pp. 290-296 (May-June, 1959).
2. Rose, W.C. "Turbulence Measurements in a Compressible Boundary Layer." AIAA Journal, Vol.12, No.8, pp. 1060-1064 (August, 1974).
3. Wallace, J.E. "Hypersonic Turbulent Boundary Layer Measurements Using an Electron Beam." Cornell Aeronautical Laboratory Report CAL AN-2112-Y-1 (August, 1968).
4. Fischer, M.C., D.V.Maddalon, L.M.Weinstein, and R.D.Wagner, Jr. "Boundary Layer Pitot and Hot-Wire Surveys at M = 20." AIAA Journal, Vol.9, No.5, pp. 826-834 (May, 1971).
5. Owen, F.K. and C.C.Horstman. "On the Structure of Hypersonic Turbulent Boundary Layers." Journal of Fluid Mechanics, Vol.53, Pt.4, pp. 611-636 (June, 1972).
6. Laufer, J. "Thoughts on Compressible Turbulent Boundary Layers." NASA SP-216, pp. 1-13 (December, 1968).

7. Laderman, A.J. and A.Demetriades. "Mean Flow Measurements in a Hypersonic Turbulent Boundary Layer." Philco-Ford Corporation Publication No.U-4950, Newport Beach, California (August, 1971).

8. Laderman, A.J. and A.Demetriades. "Turbulent Measurements in the Hypersonic Boundary Layer over a Cooled Wall." Philco-Ford Corporation Publication No.U-5079, Newport Beach, California (September, 1972).

9. Laderman, A.J. and A.Demetriades. "Hot-Wire Measurements of Hypersonic Boundary Layer Turbulence." The Physics of Fluids, Vol.16, No.2, pp. 179-188 (February, 1973).

10. Laderman, A.J. and A.Demetriades. "Mean and Fluctuating Flow Measurements in the Hypersonic Boundary Layer over a Cooled Wall." Journal of Fluid Mechanics, Vol.63, Part 1, pp. 121-144 (January, 1974).

11. Muntz, E.P. "The Electron Beam Fluorescence Technique." NATO Agardograph 132 (December, 1968).

12. Bogdan, L. and D.J.McCaa. "Experimental Study of Electron-Excited Emission in Air and Nitrogen up to 8 Torr." Cornell Aeronautical Laboratory Report CAL AG-2679-Y-1 (May, 1970).

13. Camac, M. "Boundary Layer Measurements with an Electron Beam." AVCO Everett Research Report 275 (July, 1967).

14. Brocklehurst, B. "Luminescence of Gases Excited by High-Energy Radiation: Part 1 - Collisional Deactivation in Nitrogen." Transactions of the Faraday Society, Vol.60, pp. 2151-2157 (July, 1964).

15. Harvey, W.D. and W.W.Hunter. "Experimental Study of a Free Turbulent Shear Flow at M = 19 with Electron Beam and Conventional Probes." Private Communication (Proposed NASA Technical Note, March 1975).

16. Driscoll, J.F. and J.A.Smith. "The Electron Beam Fluorescence Technique for Measurements in Hypersonic Turbulent Flows." Private Communication (Gas Dynamics Laboratory, Princeton University: submitted for publication in the Journal of Fluid Mechanics, March 1975).

17. Ashkenas, H. "Rotational Temperature Measurements in Electron Beam Excited Nitrogen." The Physics of Fluids, Vol.10, No.12, pp. 2509-2520 (December, 1967).

18. Robben, F. and L.Talbot. "Measurements of Rotational Temperatures in a Low Density Wind Tunnel." The Physics of Fluids, Vol.9, No.4, pp. 644-652 (April, 1966).

19. Kassem, A.E. and R.S.Hickman. "On the Determination of Rotational Temperature in Nitrogen Using Electron Beam Induced Fluorescence." Private Communication; Paper submitted to Physics of Fluids, May 1974.

20. Butefisch, K.A. and D.Vennemann. "The Electron Beam Technique in Hypersonic Rarefied Gas Dynamics." Progress in Aerospace Sciences Vol.15, ed.D.Kuchemann, Pergamon Press, 1974, pp. 217-256.

21. Horstman, C.C. and F.K.Owen. "Turbulent Properties of a Compressible Boundary Layer." AIAA Journal, Vol.10, No.11, pp. 1418-1424 (November, 1972).

22. Laufer, J. "Some Statistical Properties of the Pressure Field Radiated by a Turbulent Boundary Layer." The Physics of Fluids, Vol.7, No.8, pp. 1191-1197 (August, 1964).

23. Laufer, J. "Aerodynamic Noise in Supersonic Wind Tunnels." Journal of the Aerospace Sciences, Vol.28, No.9, pp. 685-692 (September, 1961).

Appendix A

MODAL DECOMPOSITION OF THE ELECTRON BEAM FLUCTUATING LIGHT SIGNAL

The relative light from a point along the beam, distant y in from the entrance, with ambient gas density ρ and static temperature T is

$$L = \frac{C_1 \rho (1 + C_6 \rho)}{\left[1 + C_2 \rho \left(\frac{T}{T_0}\right)\right]^{C_3}} \exp\left[-C_4 \left(\int_0^y \rho dy - C_5 \right)\right]$$

where the values of the constants, from the room-temperature still-air calibration, are $C_1 = 1.87$, $C_2 = 0.90$, $C_4 = 0.022$, $C_5 = 5.0$, $T_0 = 290$ K, ρ is in 290 K torr equivalent, y is in inches, and C_3 is estimated to be ~ 0.20. The variation ΔL arising from variations $\Delta\rho$, etc., can be written as

$$\frac{\Delta L}{L} = \left(\frac{\frac{\partial L}{\partial \rho}}{\frac{L}{\rho}}\right)\left(\frac{\Delta \rho}{\rho}\right) + \left(\frac{\frac{\partial L}{\partial T}}{\frac{L}{T}}\right)\left(\frac{\Delta T}{T}\right) + \left(\frac{\frac{\partial L}{\partial I}}{\frac{L}{I}}\right)\left(\frac{\Delta I}{I}\right), \text{ where } I = \int_0^y \rho dy$$

$$= \frac{1}{X}\left(\frac{\Delta \rho}{\rho}\right) - C_3 \frac{(X-1)}{X}\left(\frac{\Delta T}{T}\right) - C_4 I \left(\frac{\Delta I}{I}\right), \text{ where } X = \frac{C_1 \rho}{L}$$

Squaring and taking time averages, we have

$$L''^2 = \frac{1}{X^2}\rho''^2 - C_3\frac{(X-1)^2}{X}T''^2 + (C_4 I)^2 I''^2$$

$$- \frac{2(X-1)}{X^2} C_3 \rho''T''R_{\rho T} + 2C_3 \frac{(X-1)}{X^2} C_4 I T''I''R_{TI}$$

$$- 2C_4 \frac{I}{X} \rho''I''R_{\rho I} \qquad (5)$$

where L'' denotes $\frac{L_{rms}}{\bar{L}}$, etc., and $R_{\rho T}$ is the correlation coefficient for ρ and T fluctuations, etc..

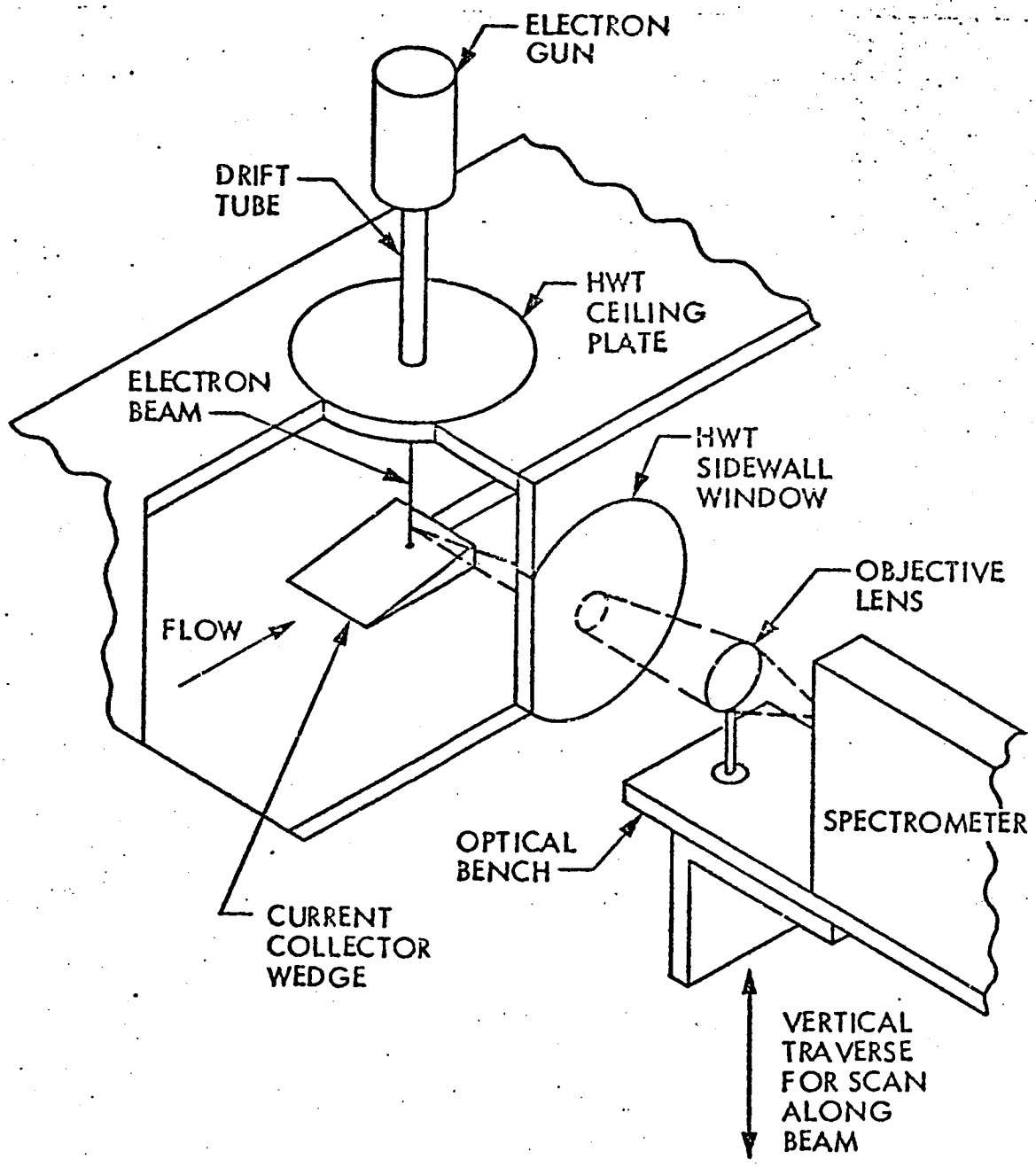

Fig. 1. Arrangement of electron beam, current collector wedge, and optical readout system for the HWT boundary layer studies

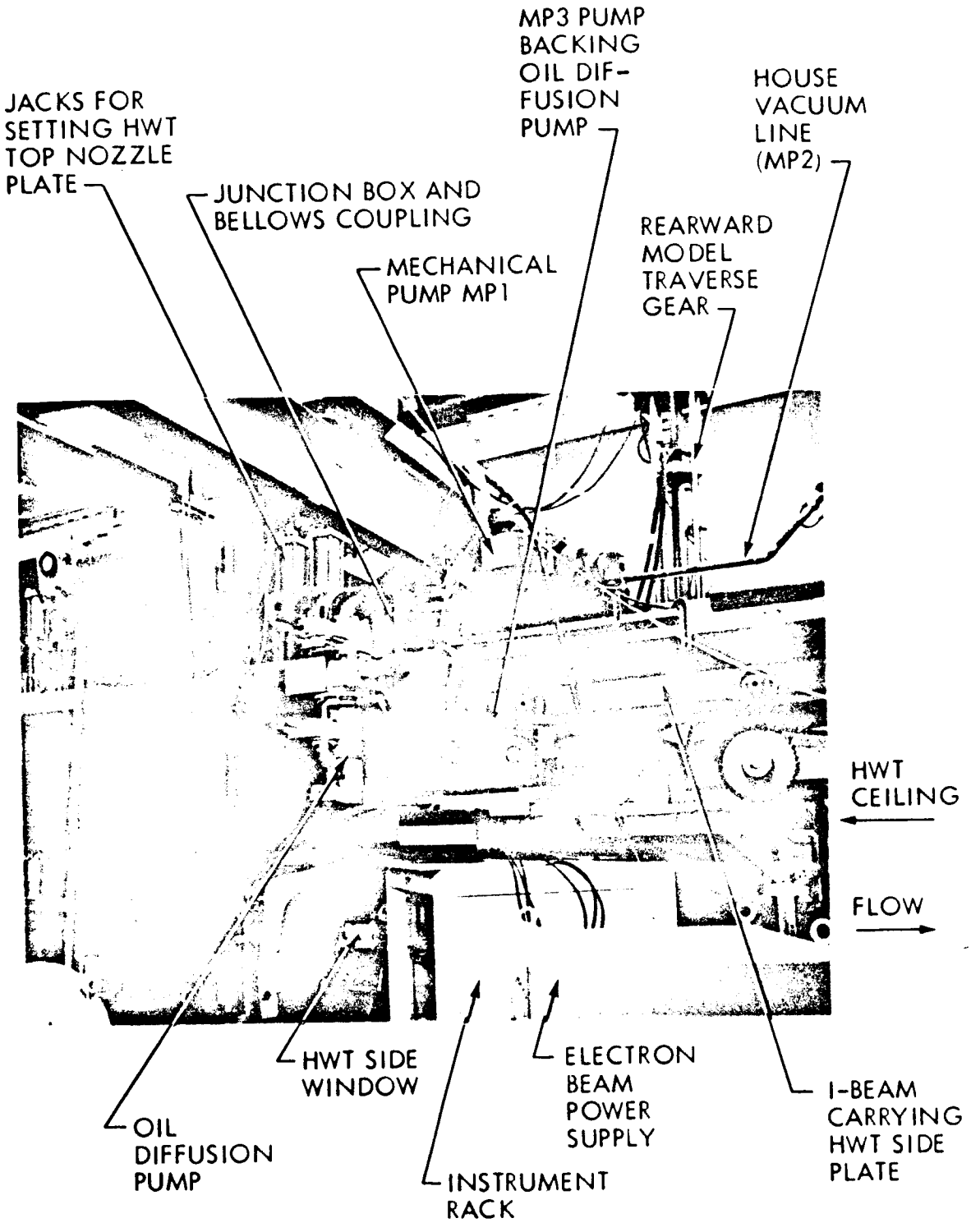

Fig. 2. General view of arrangement of electron beam pumps above the HWT working section

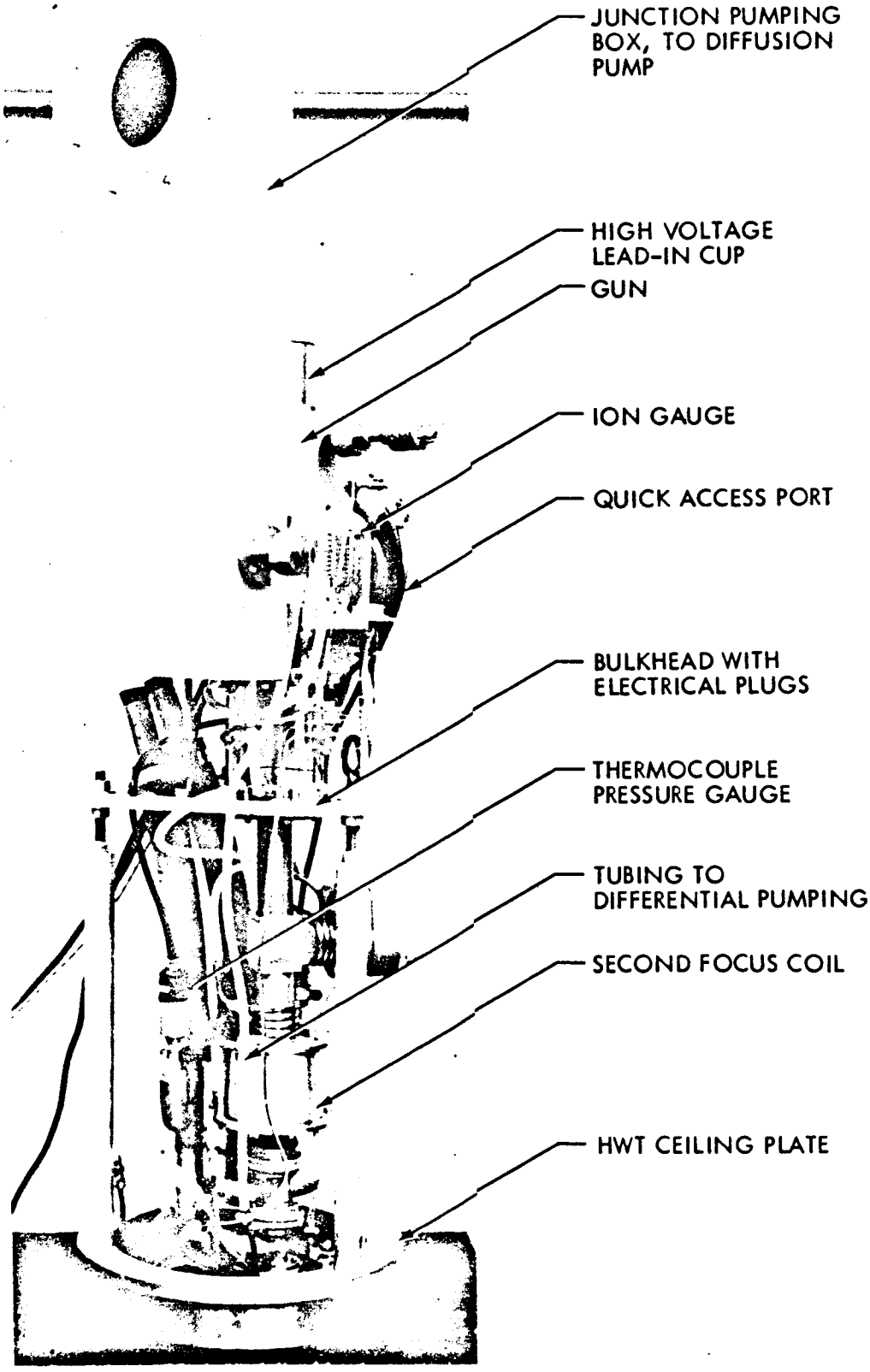

Fig. 3. Beam injection module

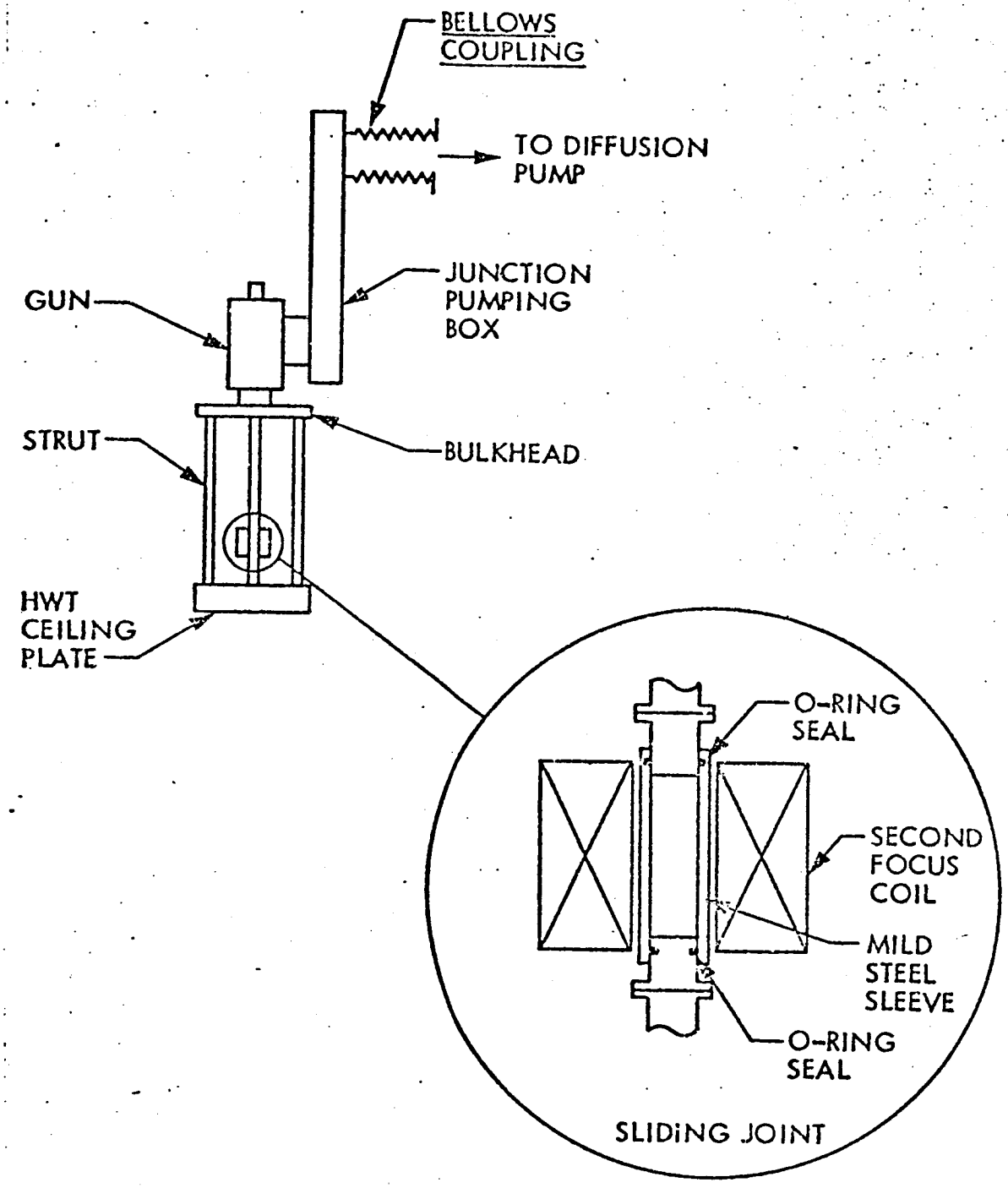

Fig. 3a. Details of flexible joints

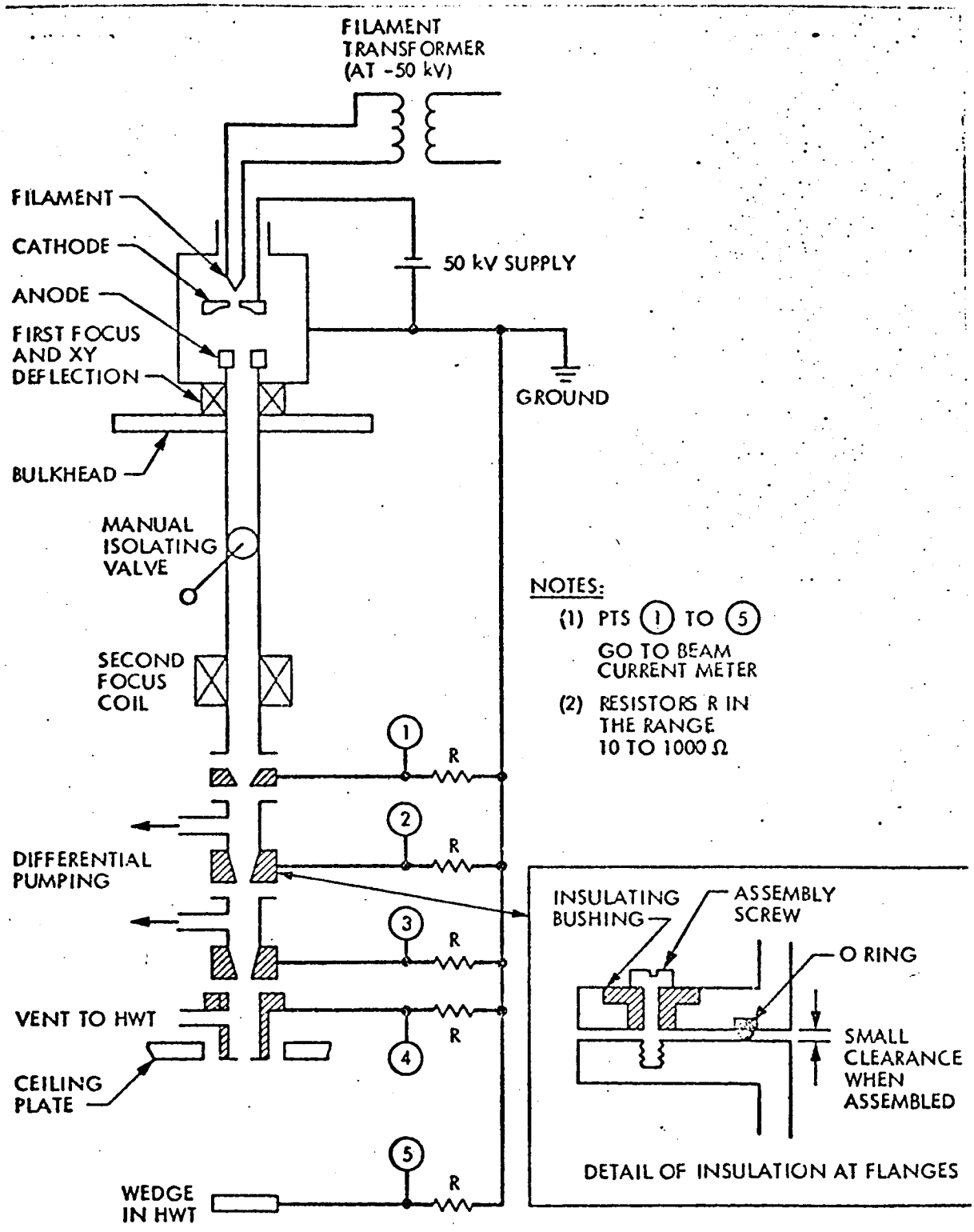

Fig. 4. Schematic diagram of beam steering technique

C-2

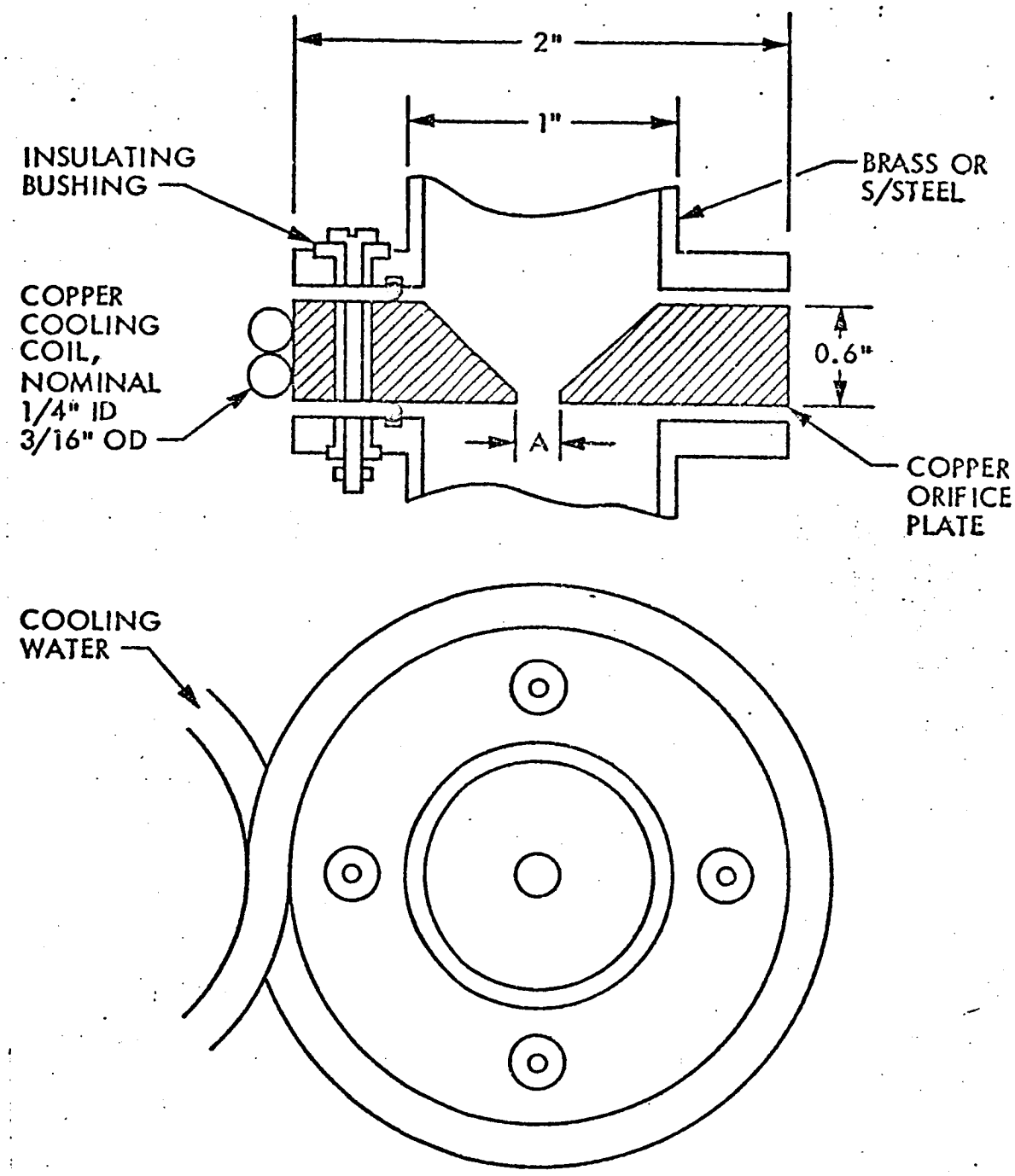

NOTE: DIAMETER A HAD VALUES 4, 3, 1 AND 1 mm FOR THE FOUR ORIFICES FROM THE SECOND FOCUS COIL TO THE HWT BOUNDARY LAYER.

Fig. 5a. Construction and cooling of orifice plates

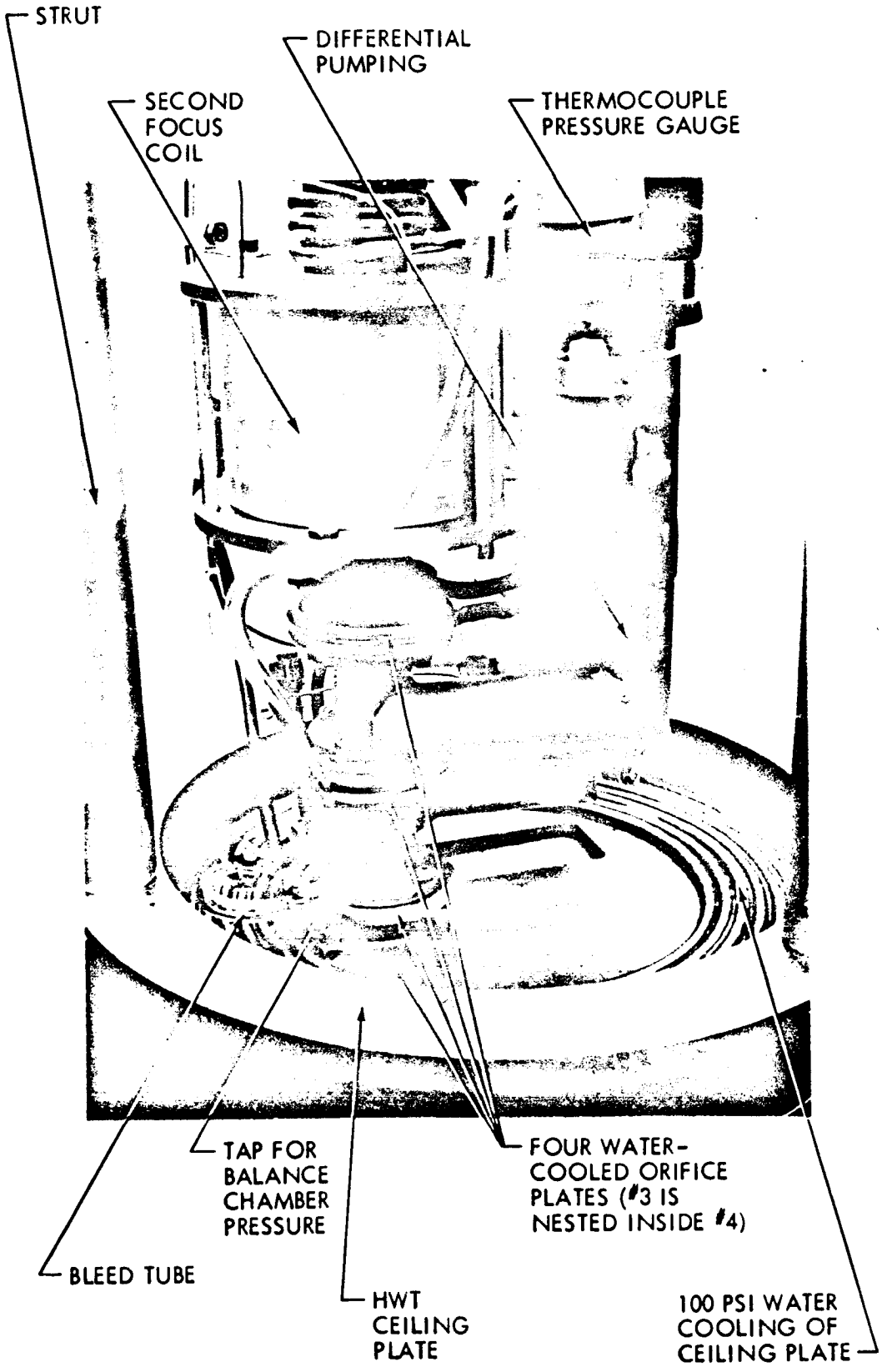

Fig. 5b. Photograph of orifice plate assembly

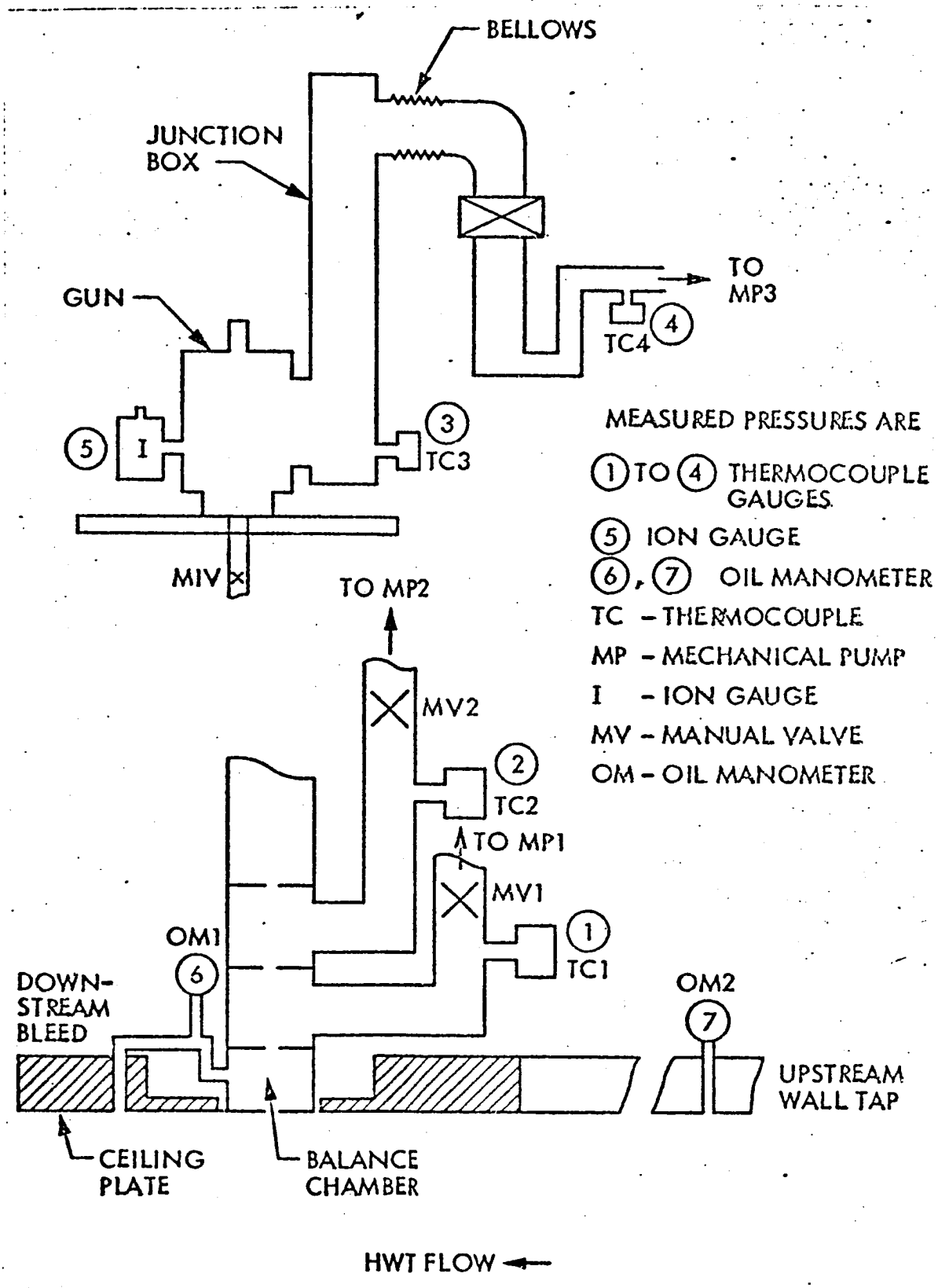

Fig. 6. Location of pressures measured or monitored

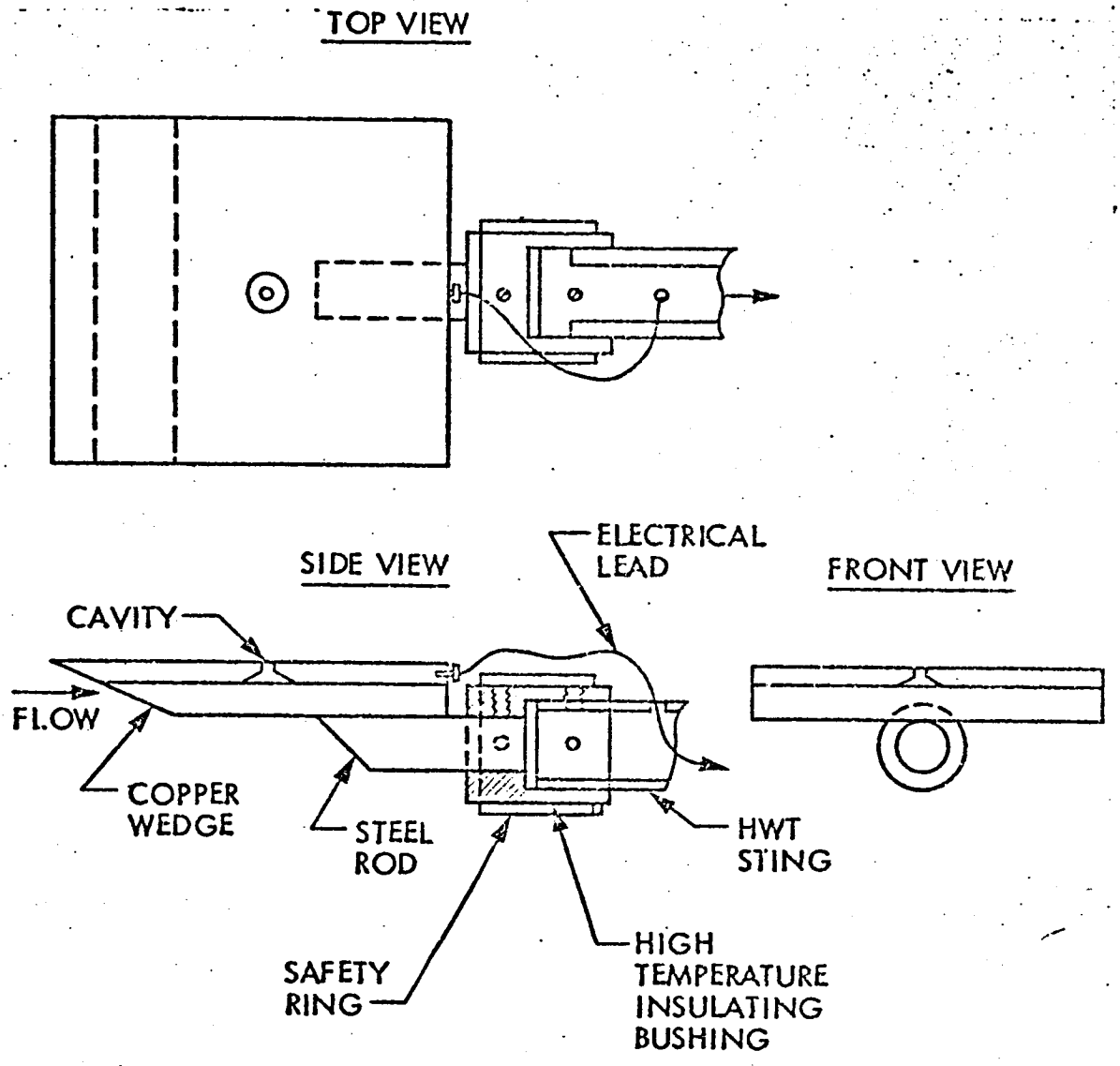

Fig. 7. Wedge for collecting beam current in the HWT

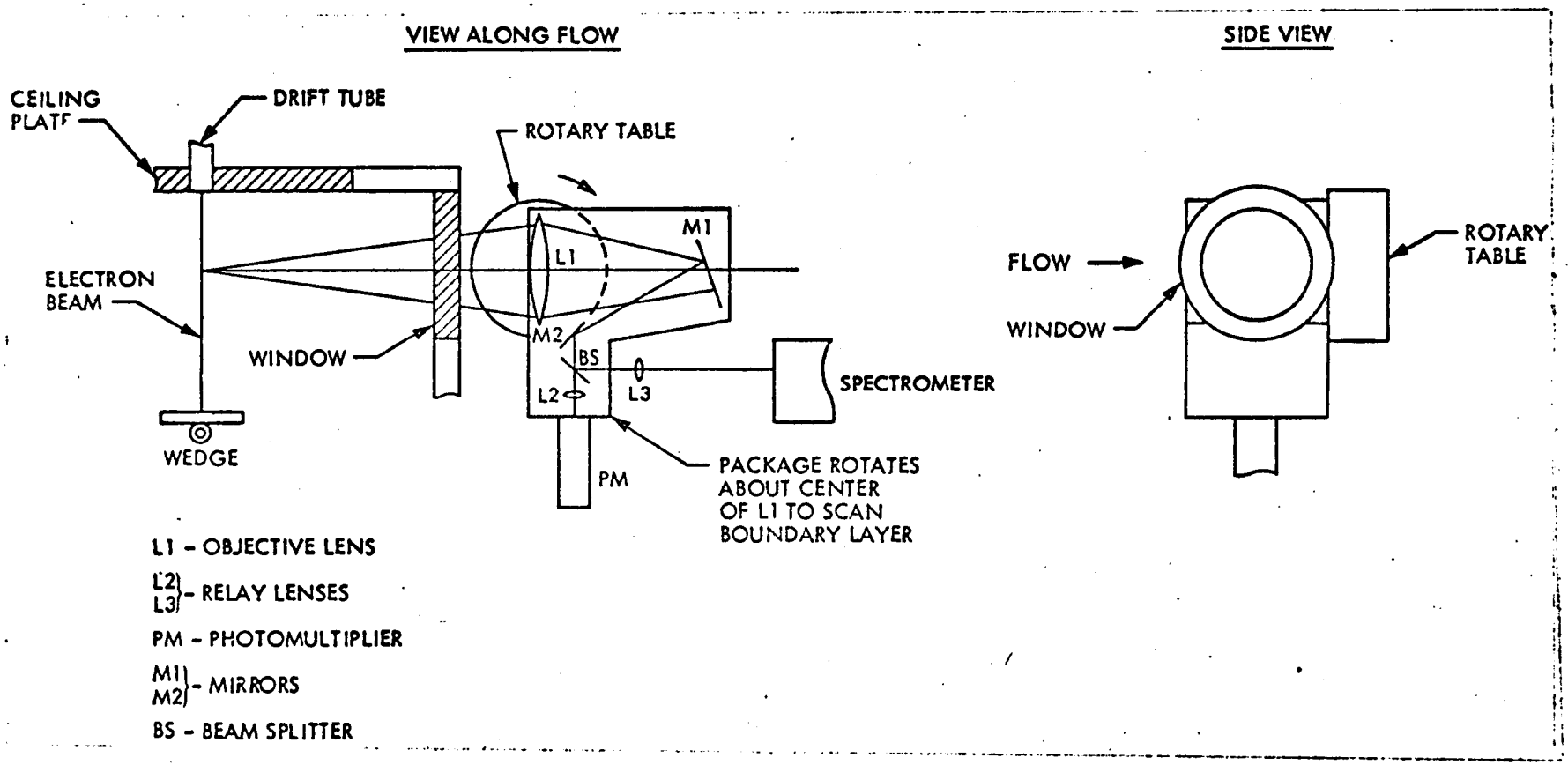

Fig. 8. Rotary form of optical readout system

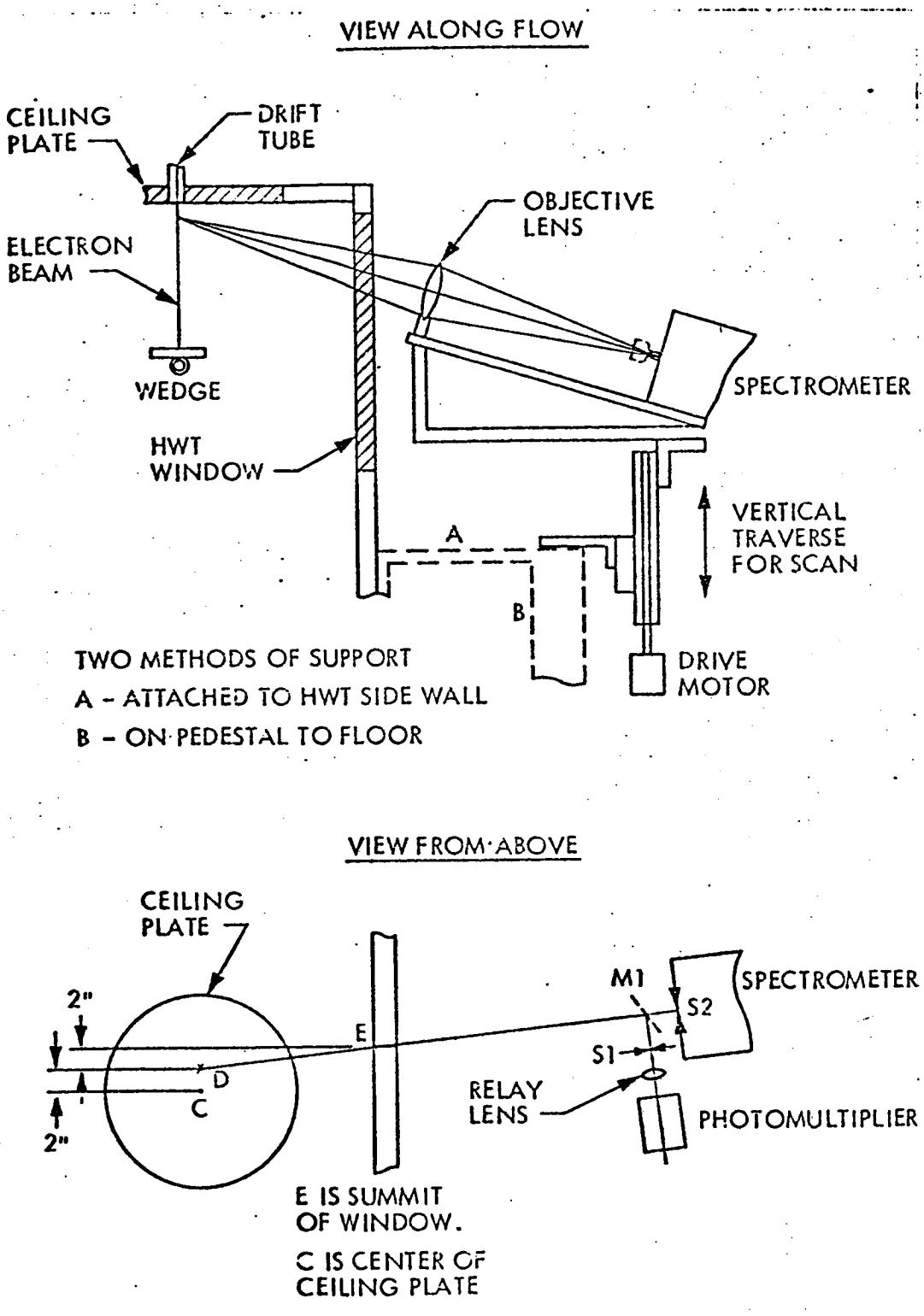

Fig. 9. Optical readout system: final form

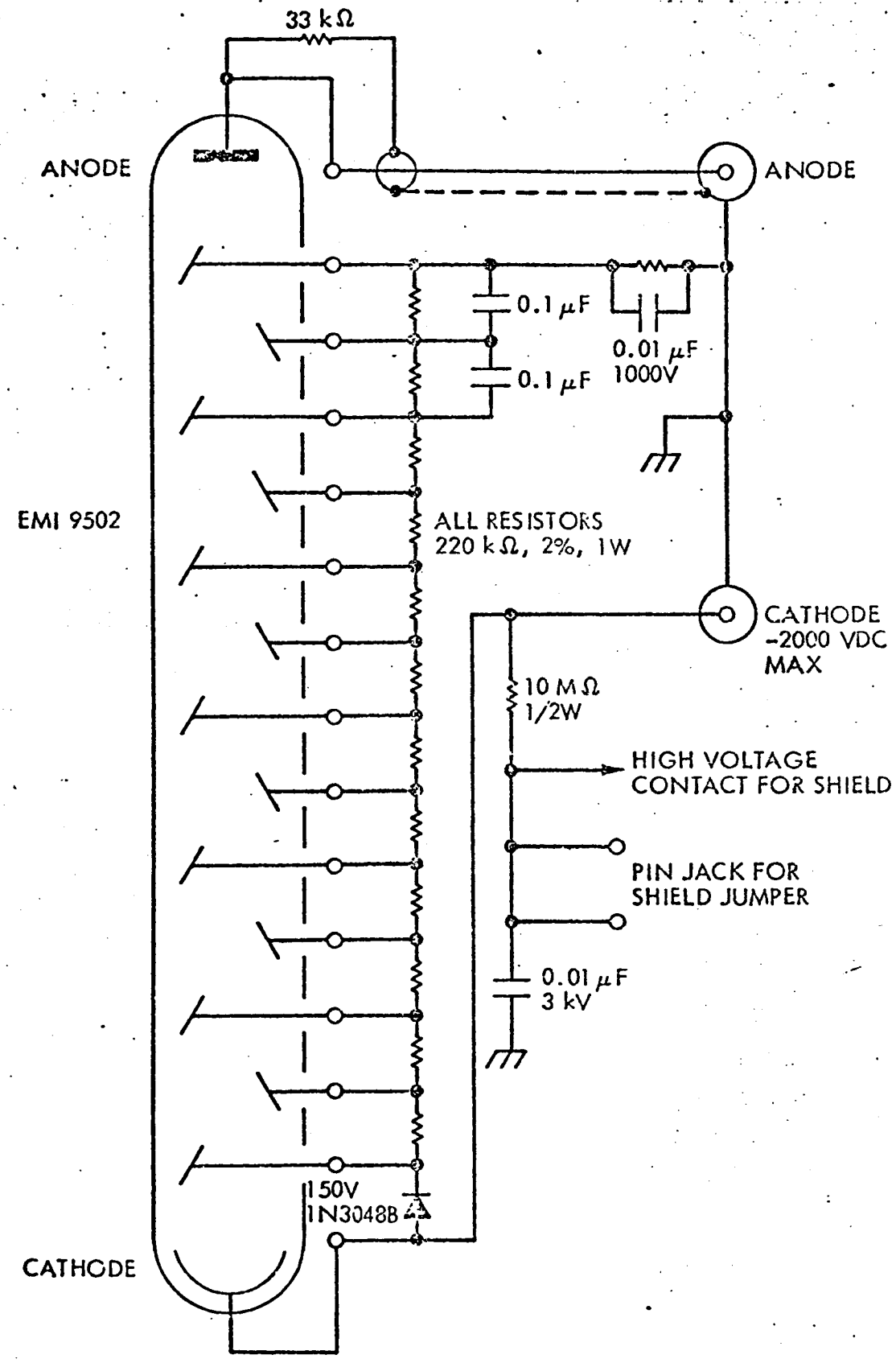

Fig. 10a. Photomultiplier circuit, 9502 tube

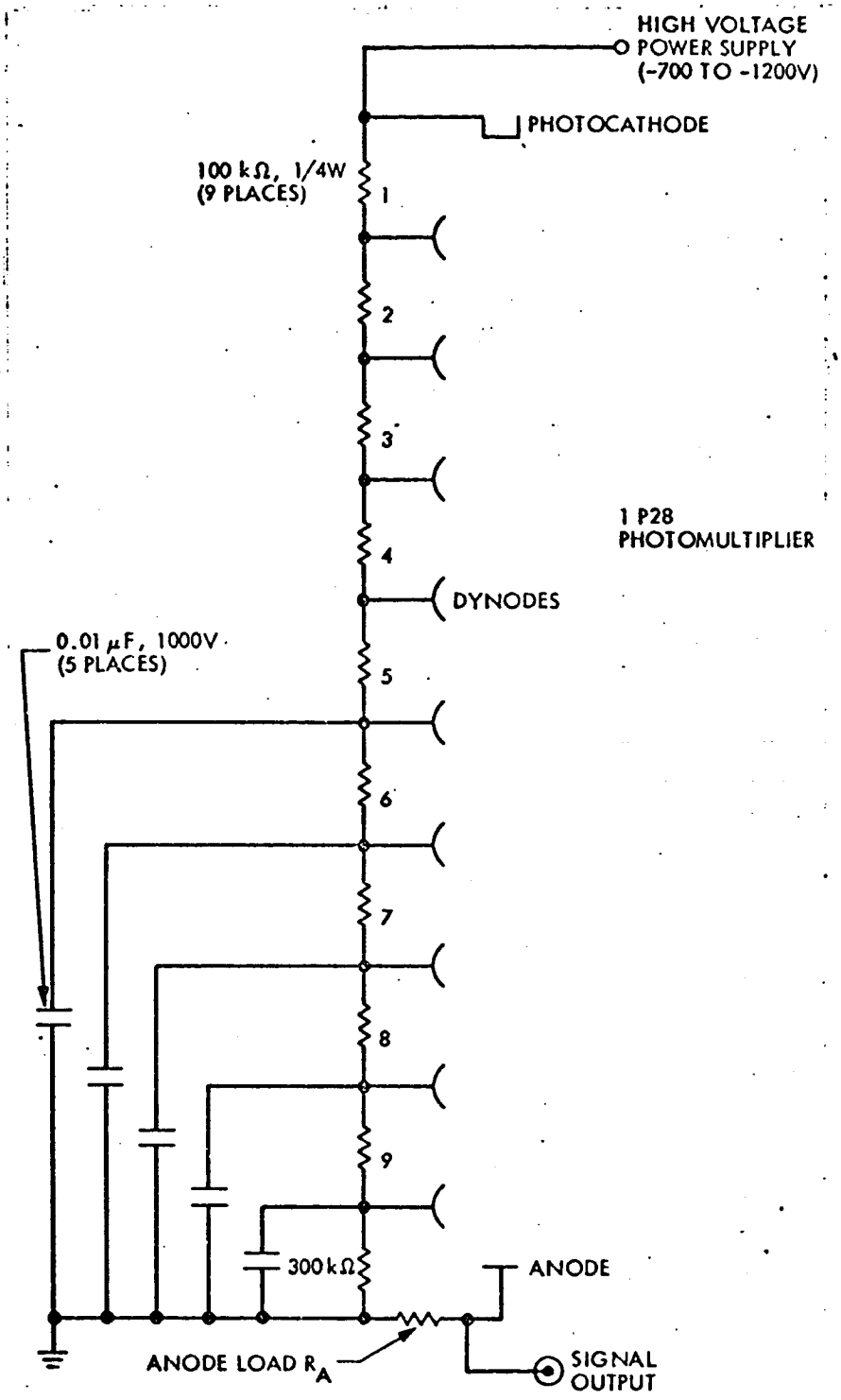

R_A = (1) 100 kΩ DIRECT TO XY RECORDER
(2) 1 MΩ TO HP412A DC MILLIVOLTMETER
(3) 36 kΩ FOR DIRECT ρ' FLUCTUATIONS, KRONHITE FILTER
(4) ~ 1 MΩ (INPUT BIAS RESISTORS) WITH FET

Fig. 10b. Photomultiplier circuit, 1P28 tube

(a) MEASUREMENT OF $\bar{\rho}$

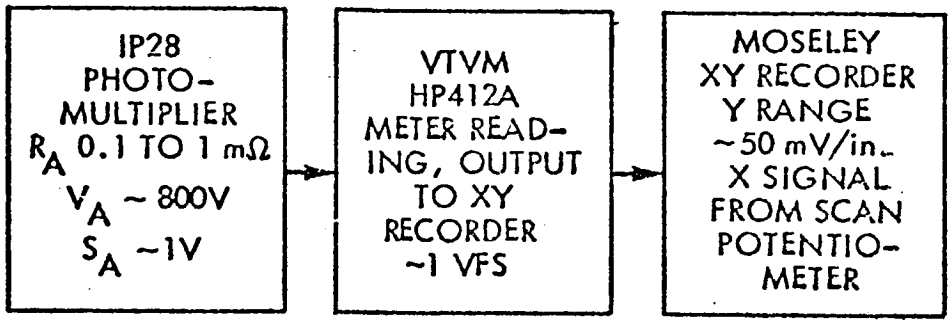

(b) MEASUREMENT OF $\bar{T}$

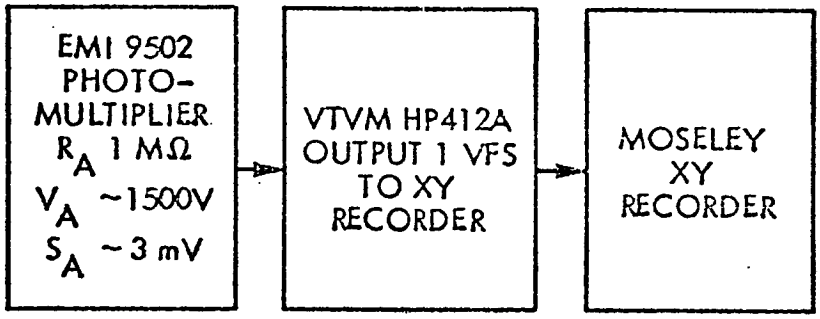

(c) MEASUREMENT OF ρ'

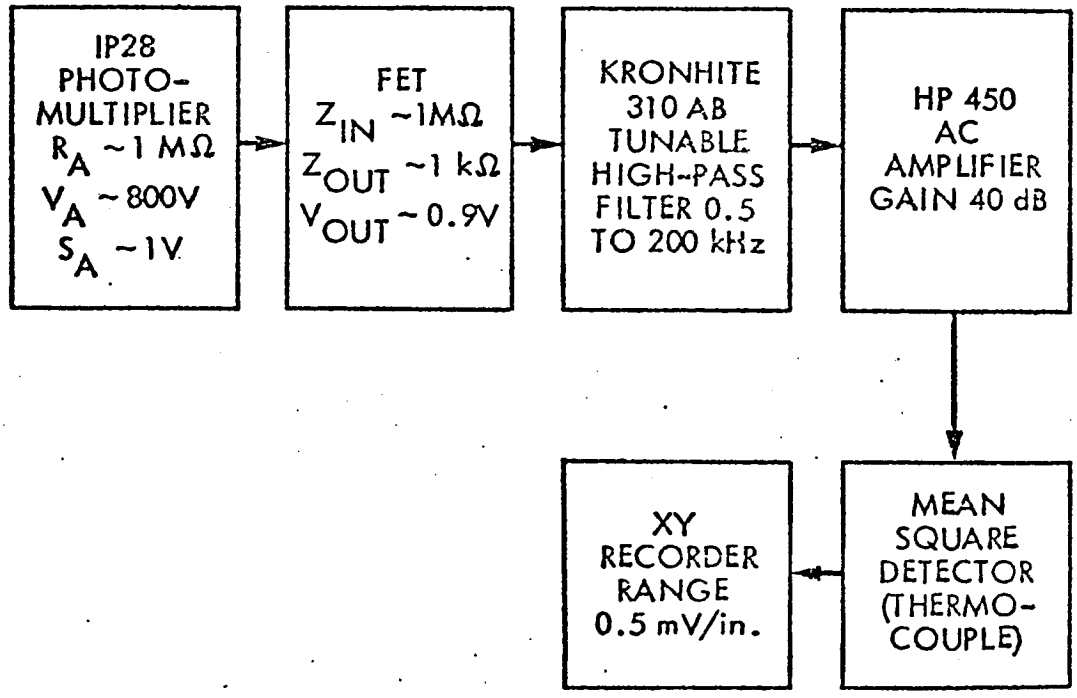

Fig. 11. Recording instrumentation

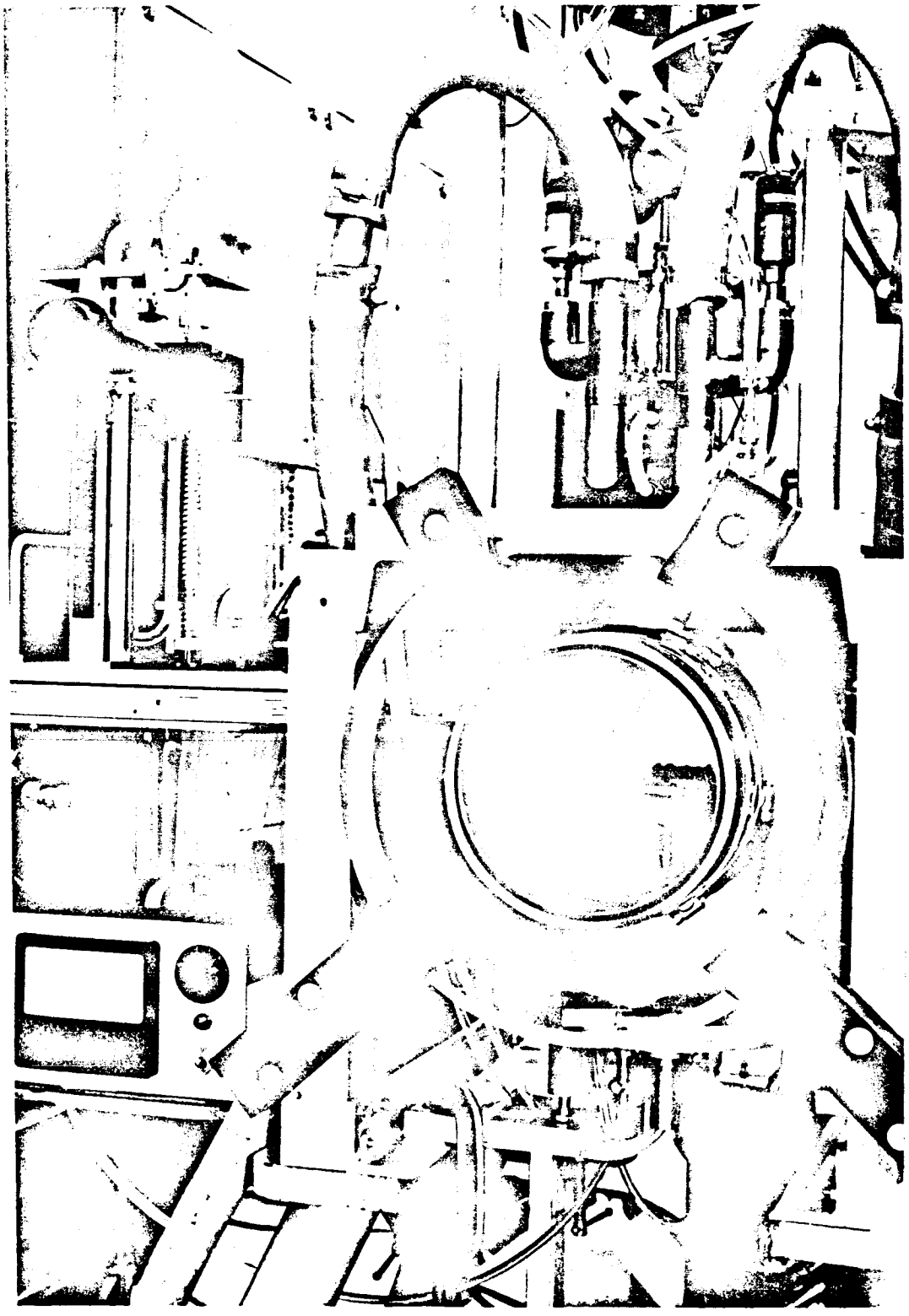

Fig. 12a. Still-air calibration tank

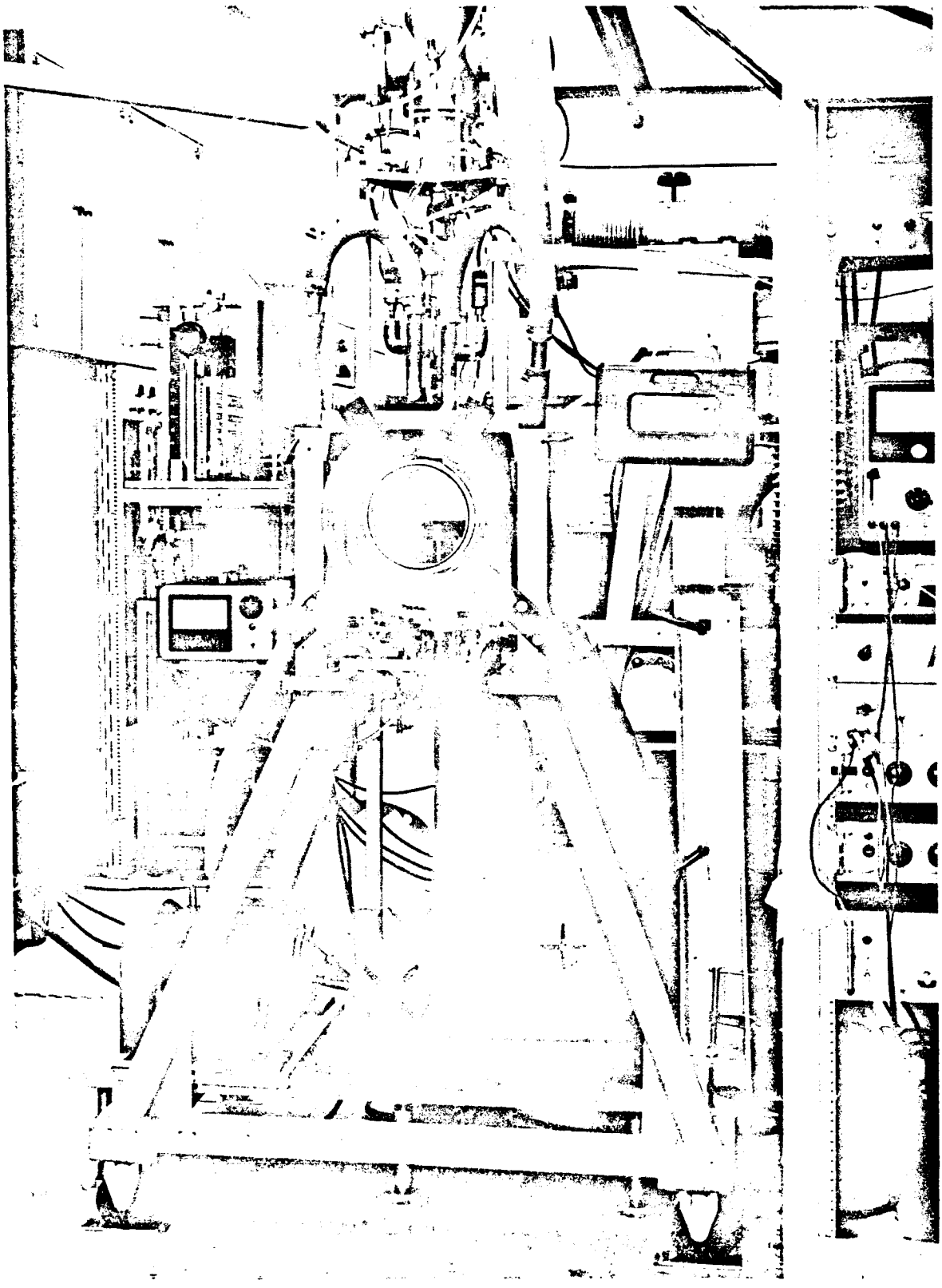

Fig. 12b. Still-air calibration tank on test stand

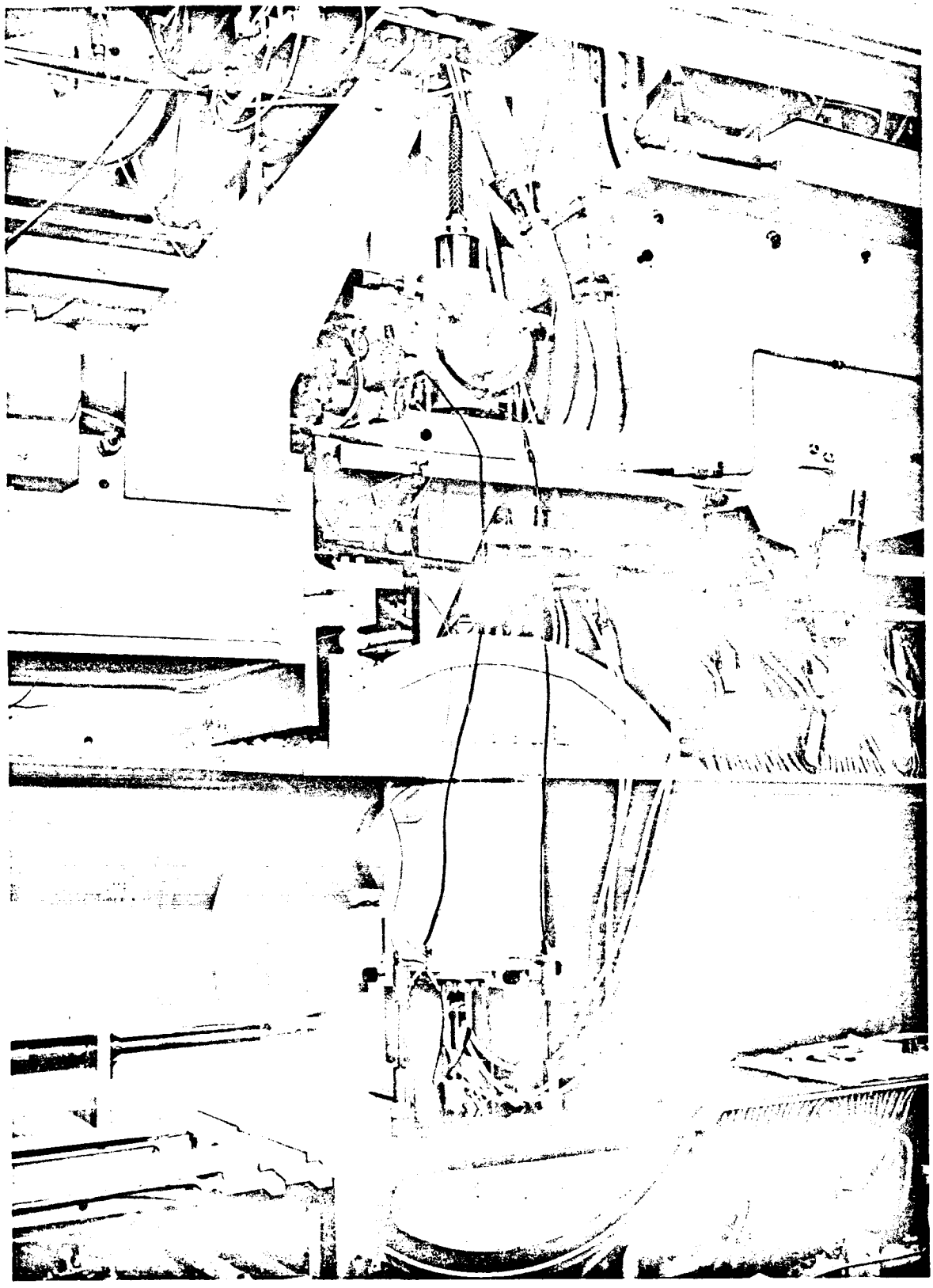

Fig. 12c. Still-air calibration tank in HWT working section

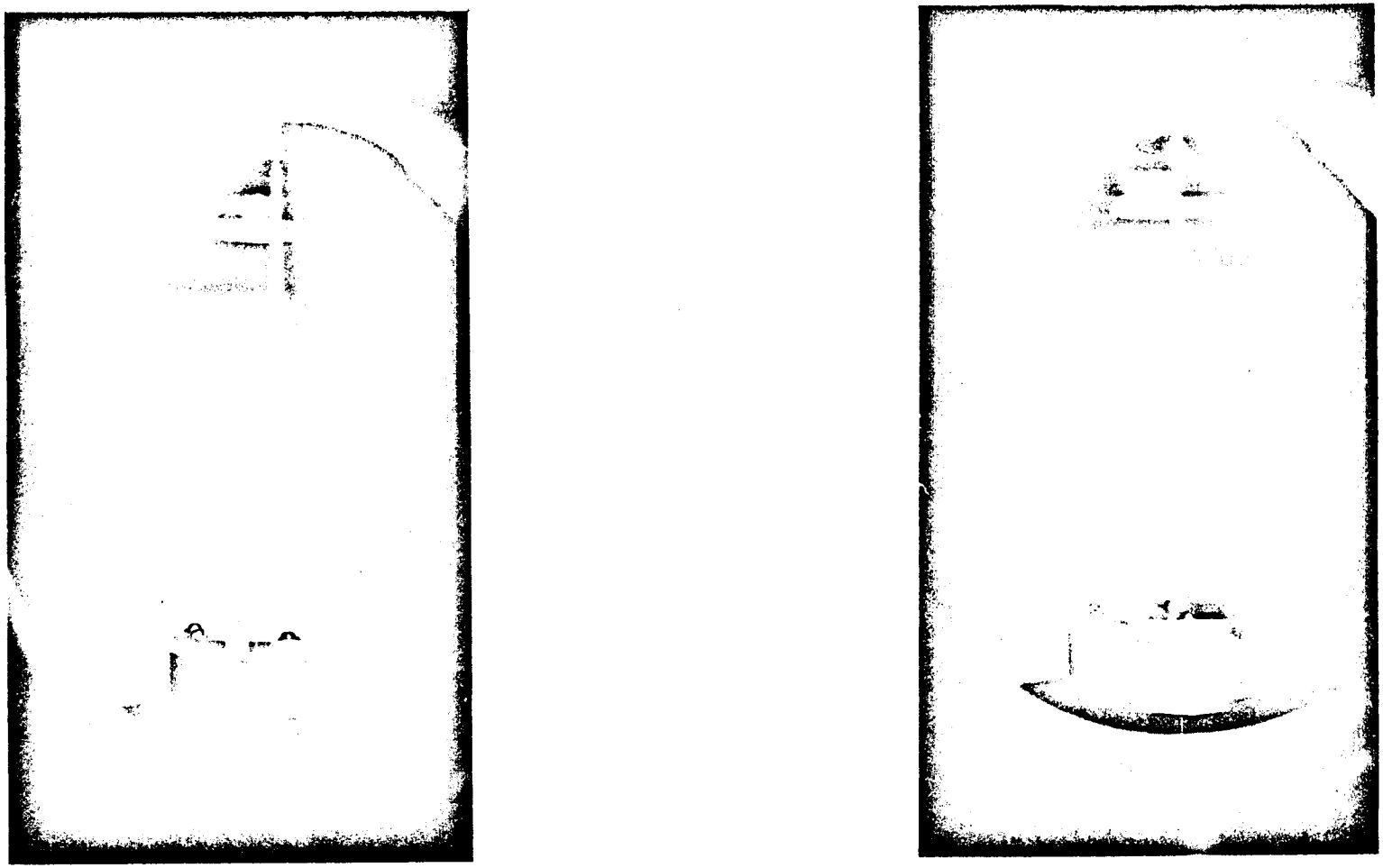

Fig. 12d. Electron beam in calibration tank

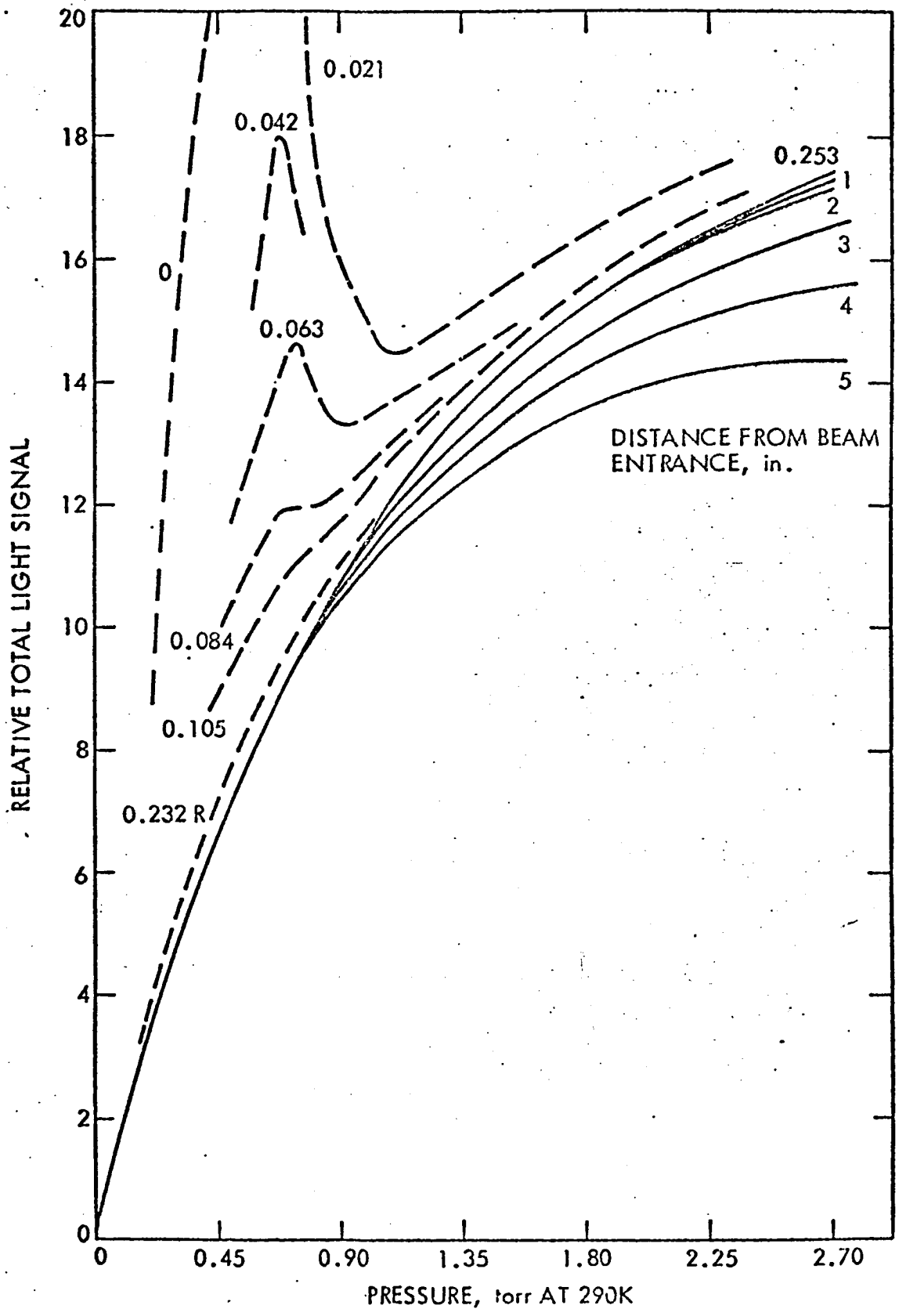

Fig. 13. Still-air light versus density calibration

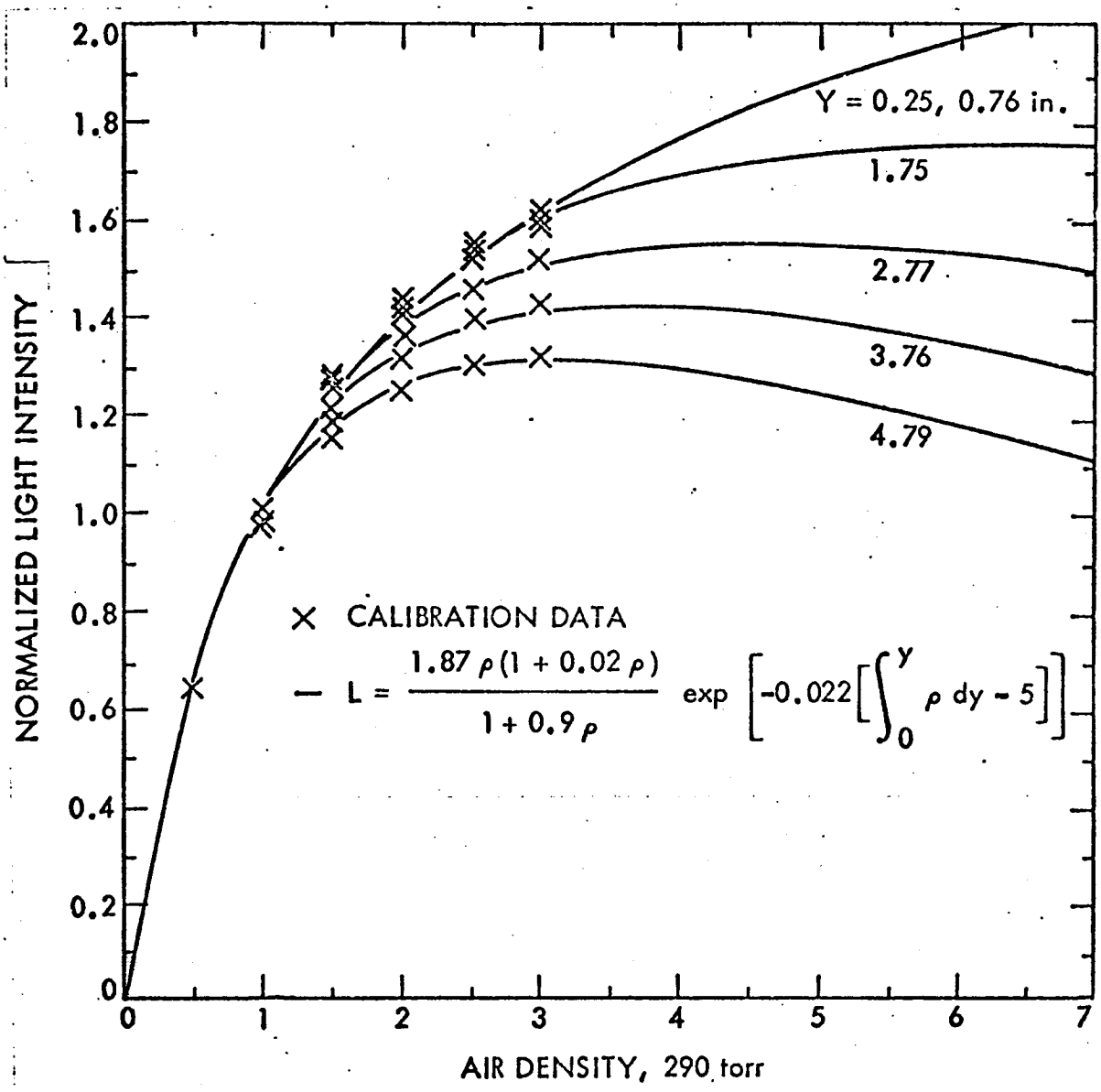

Fig. 14. Normalized Light Versus Density Calibration

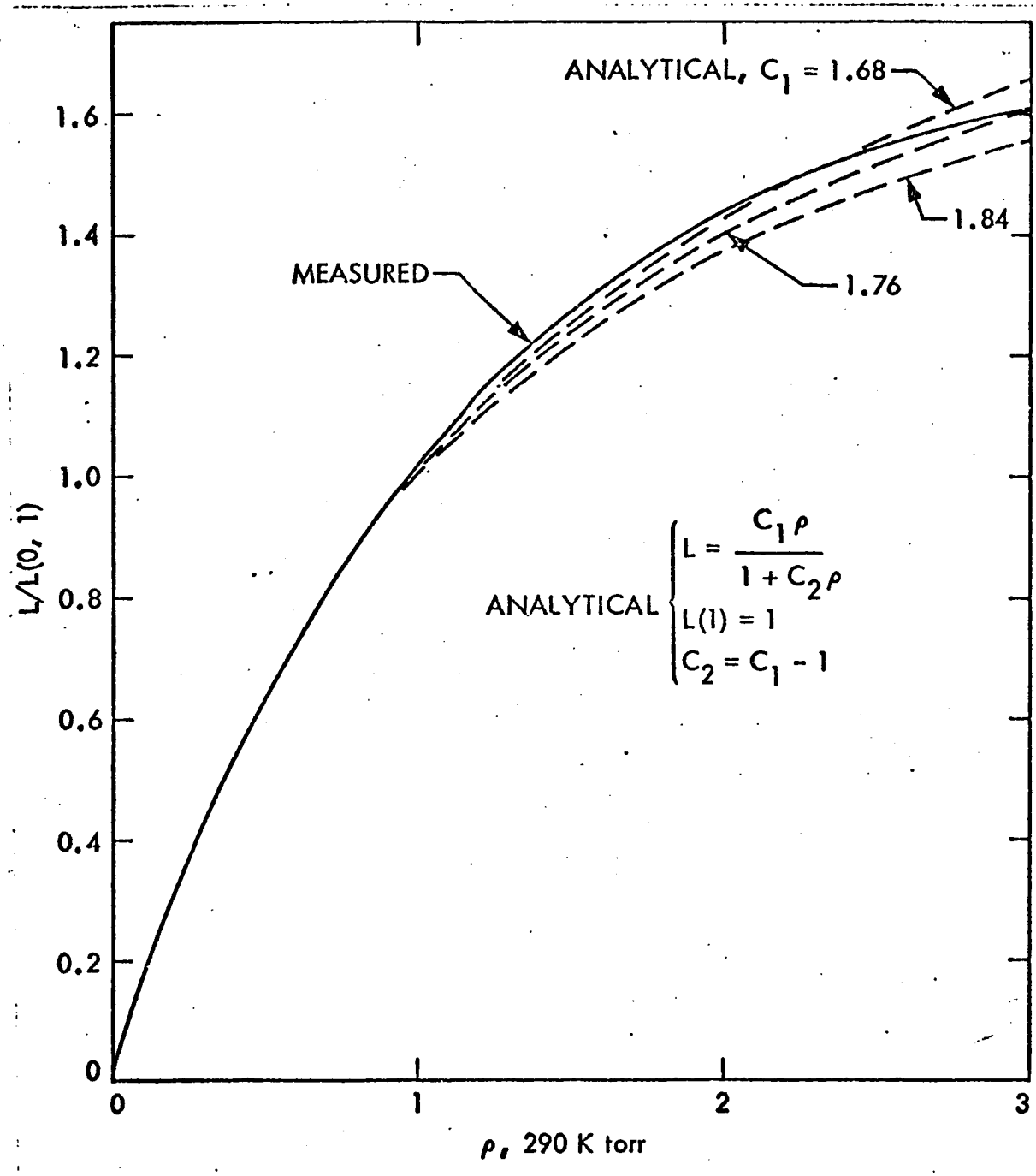

Fig. 14a. Effect of Quenching Pressure on Light Calibration

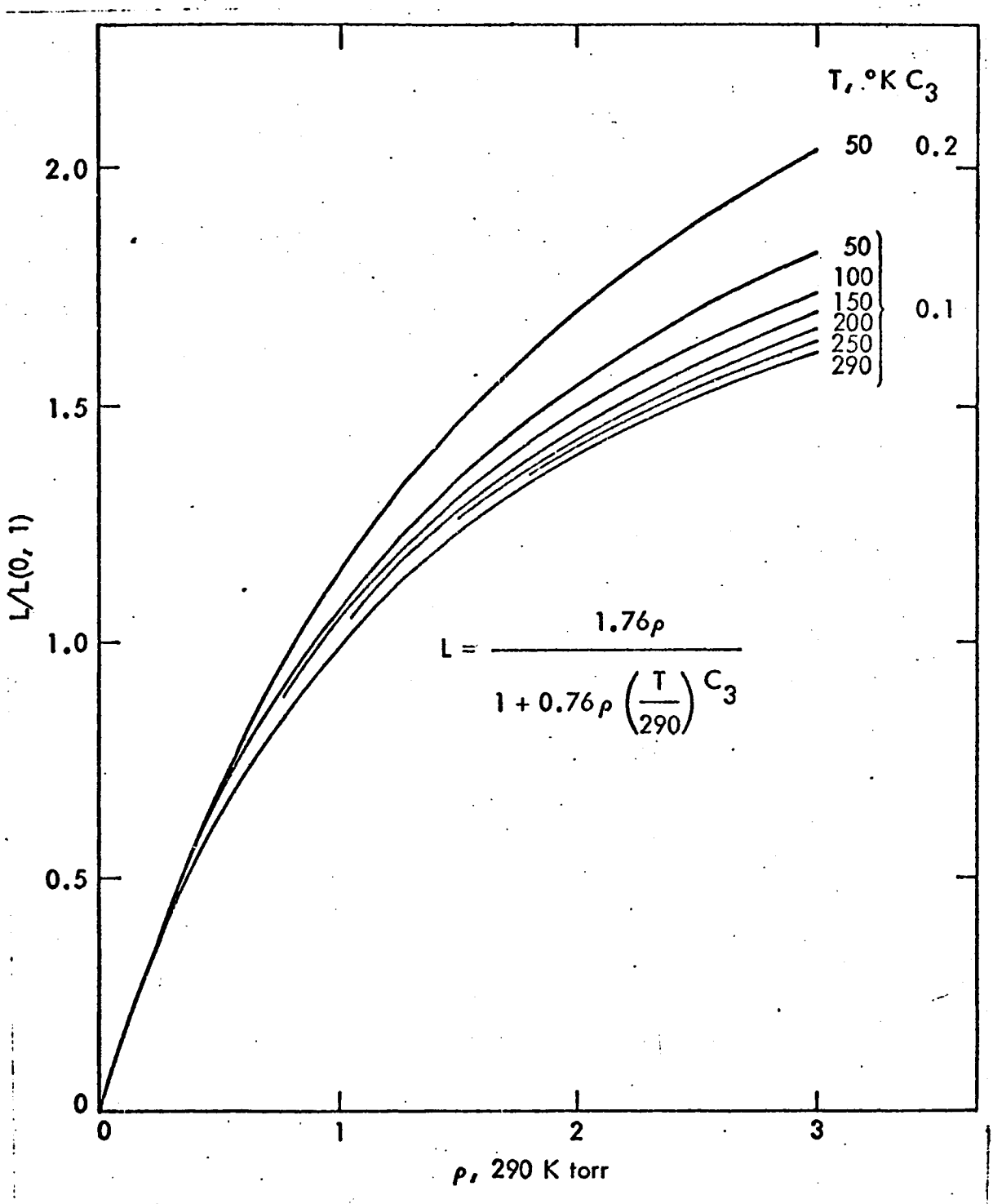

Fig. 14b. Effect of Temperature on Light Calibration

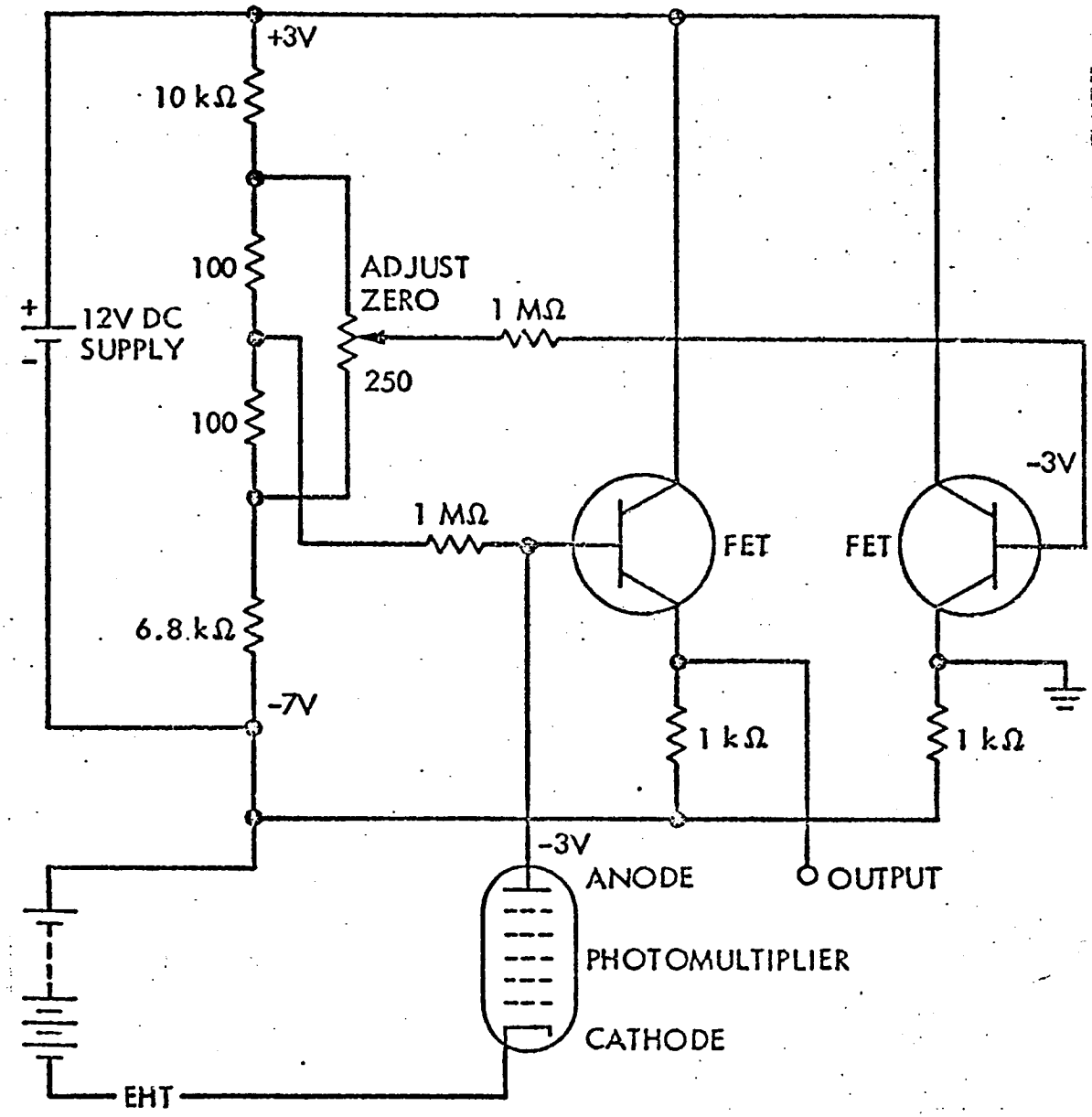

Fig. 15. Balanced circuit for the FET

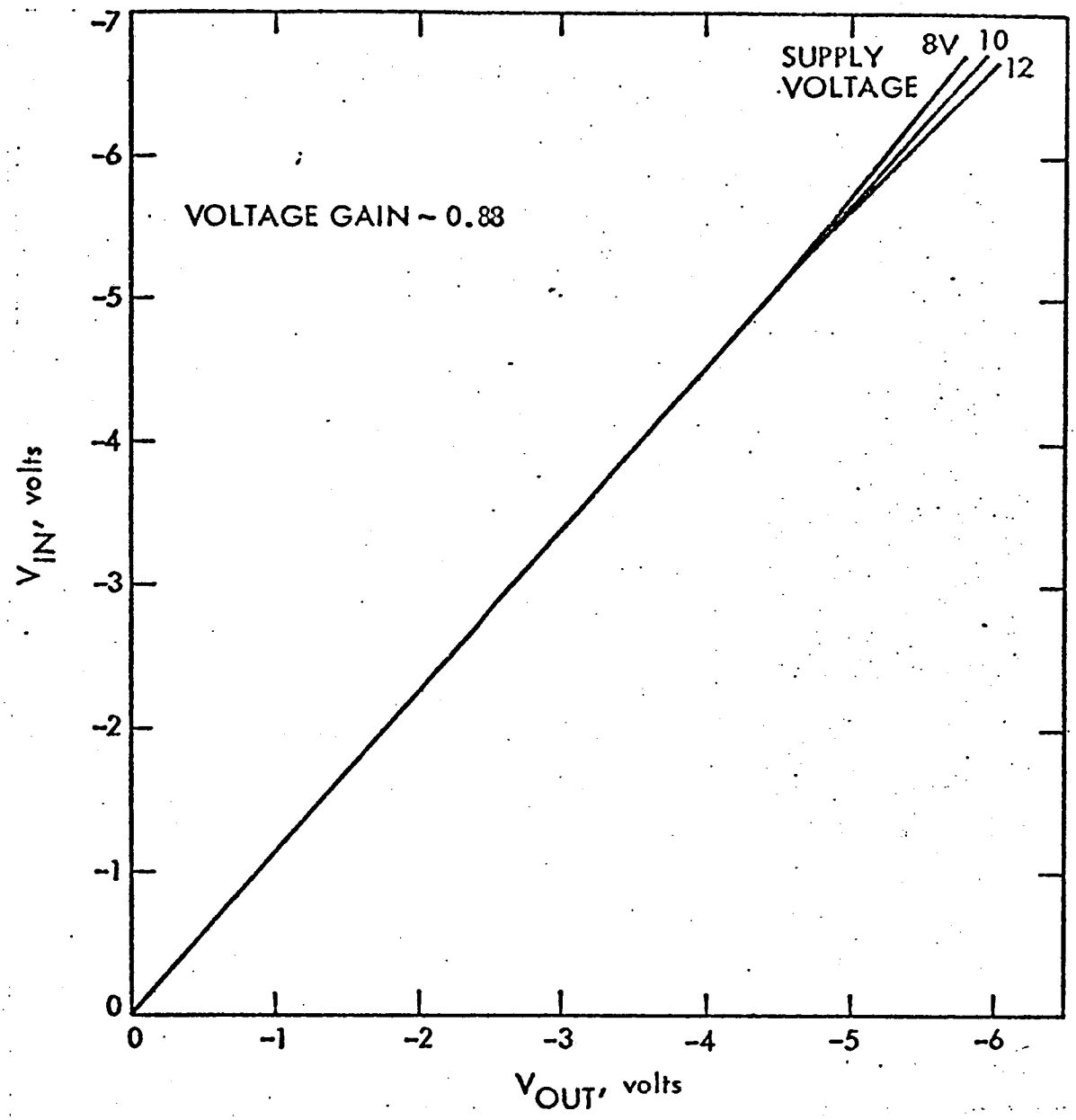

Fig. 15a. Input-output characteristic of FET stage

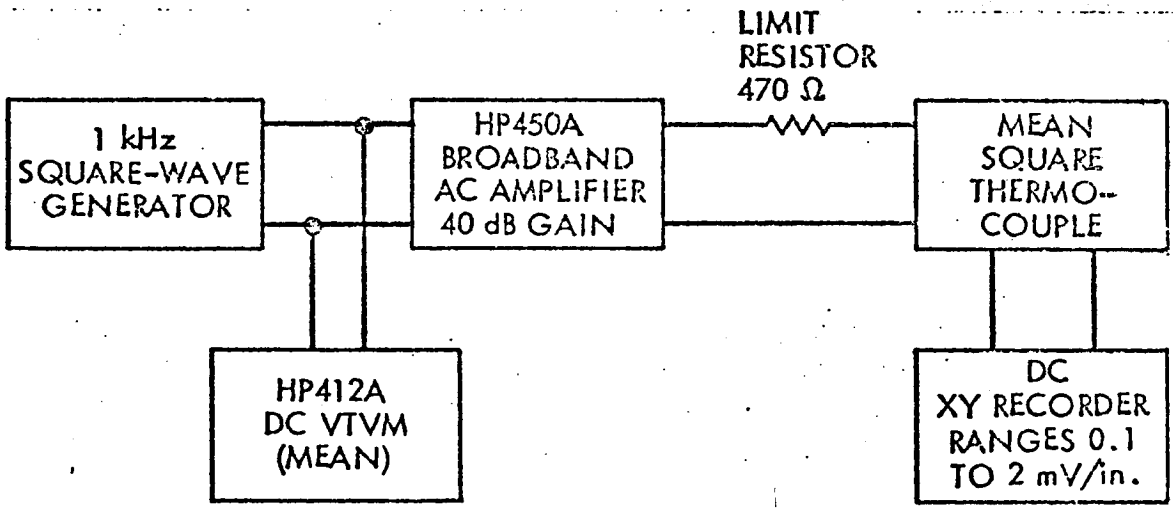

Fig. 16. Arrangement for voltage calibration of mean square thermocouple detector

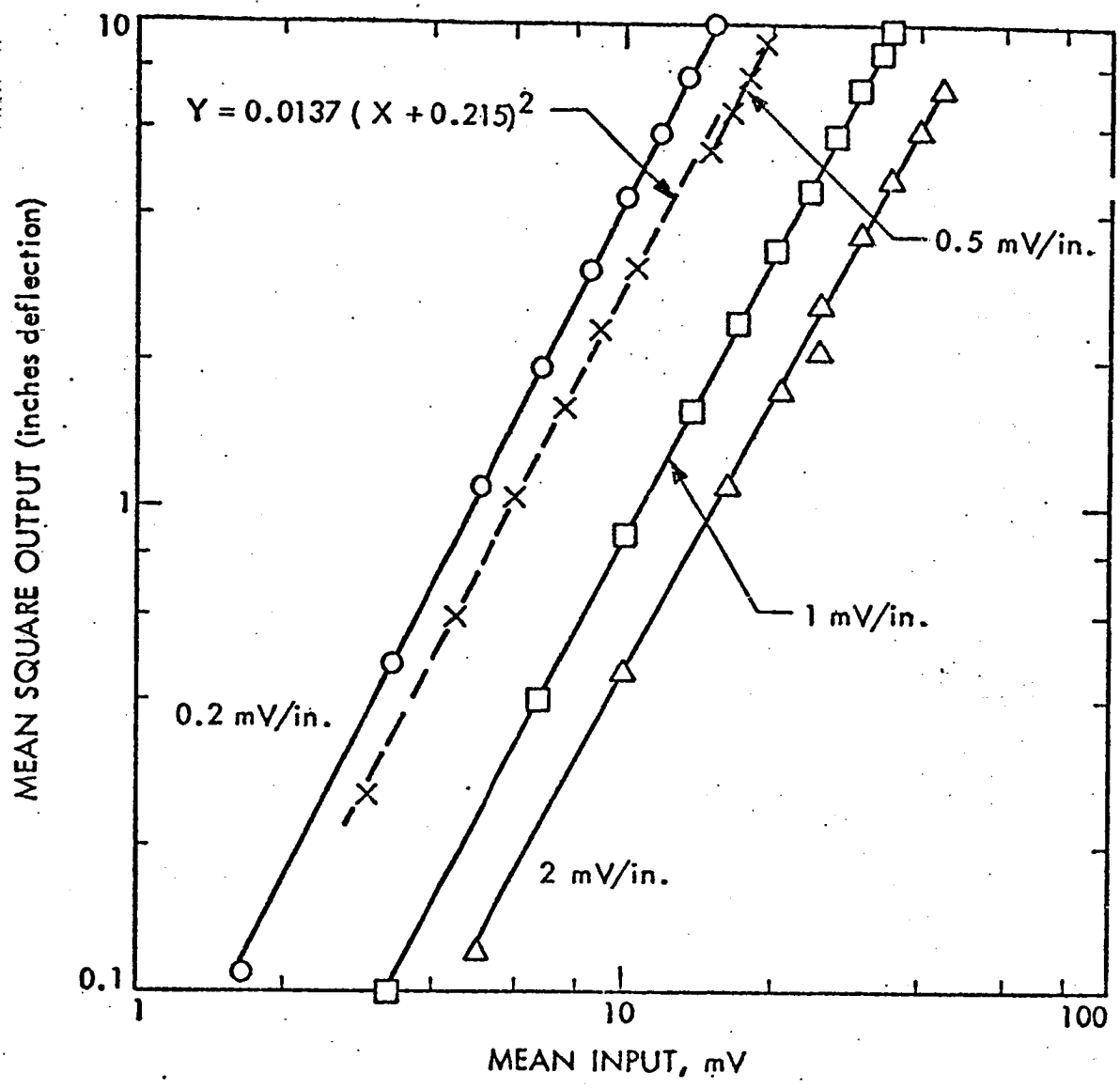

Fig. 16a. Input-output characteristic of mean square detector

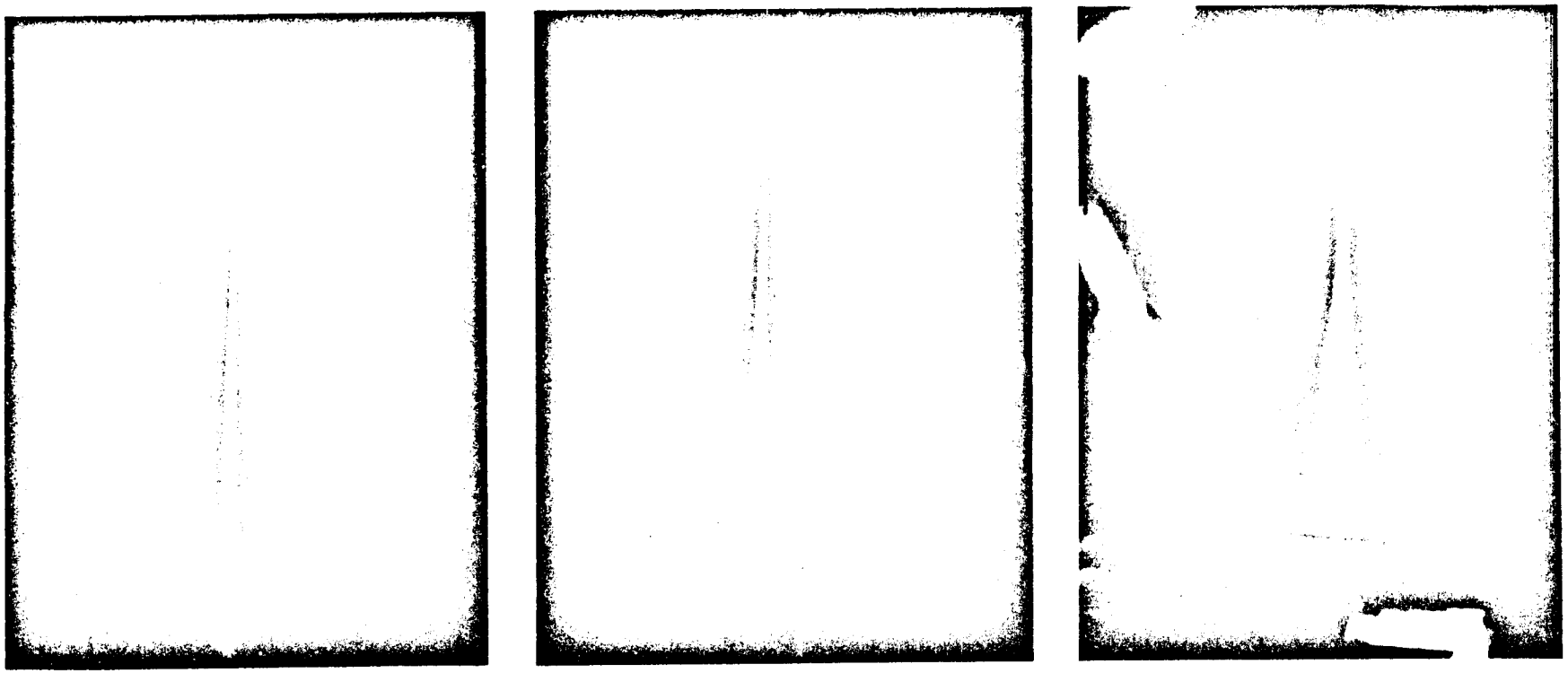

P_T = 500 cm Hg

P_T = 1700 cm Hg

P_T = 3200 cm Hg

Fig. 17. Photographs of electron beam in the HWT

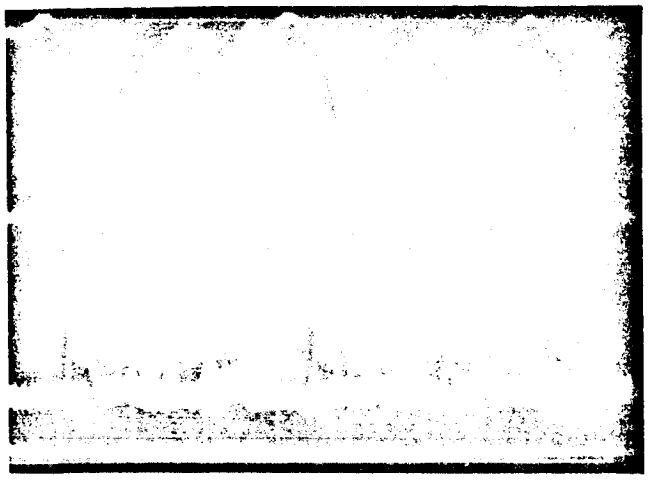

BEAM CURRENT

Y = 0" (AT WALL)

LIGHT SIGNAL

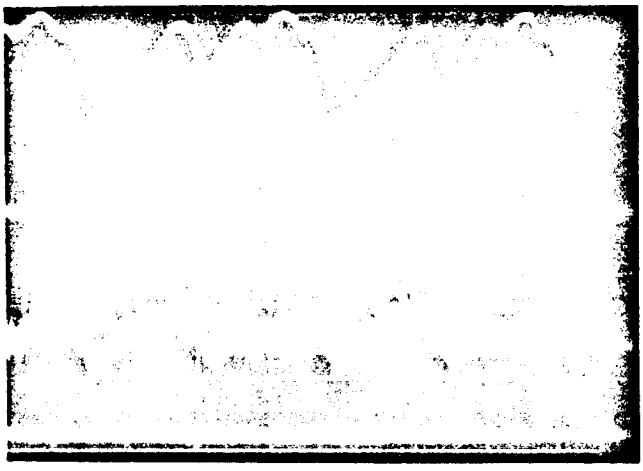

TIME BASE 5 msec/cm

Y = 2.7"
(NEAR PEAK TURBULENCE)

Y = 6.0"
(FREE STREAM)

Fig. 18. Beam current and light signal waveforms

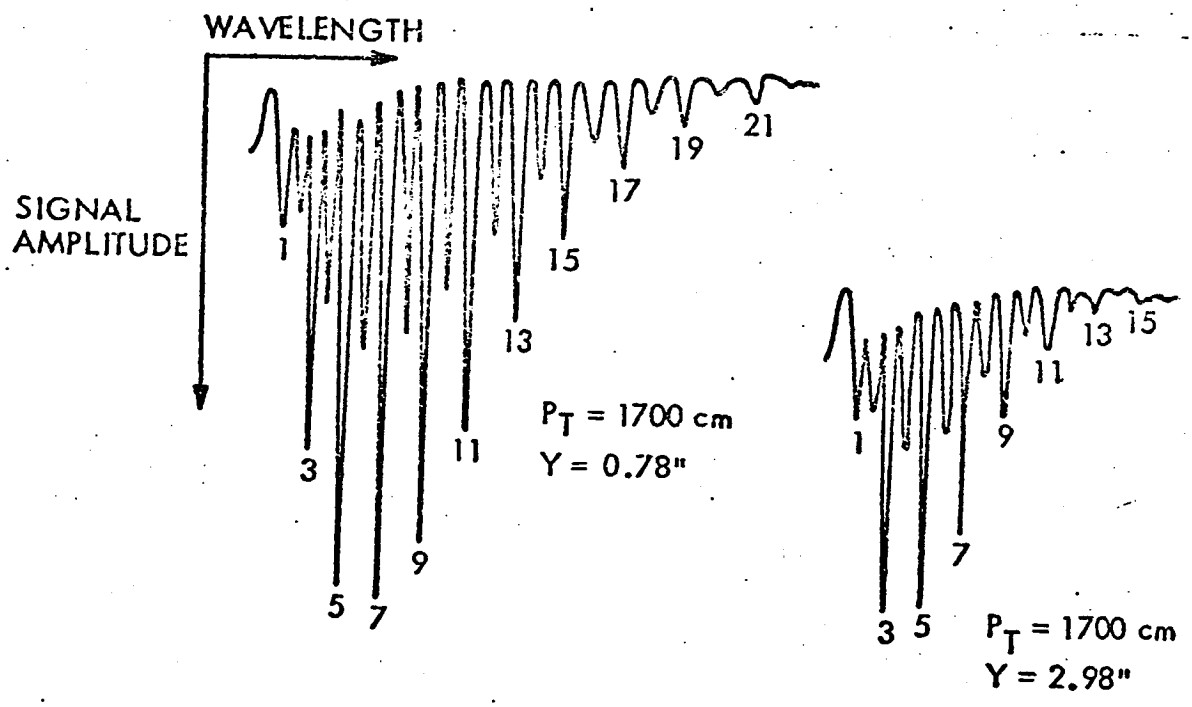

Fig. 19. Sample rotational temperature record

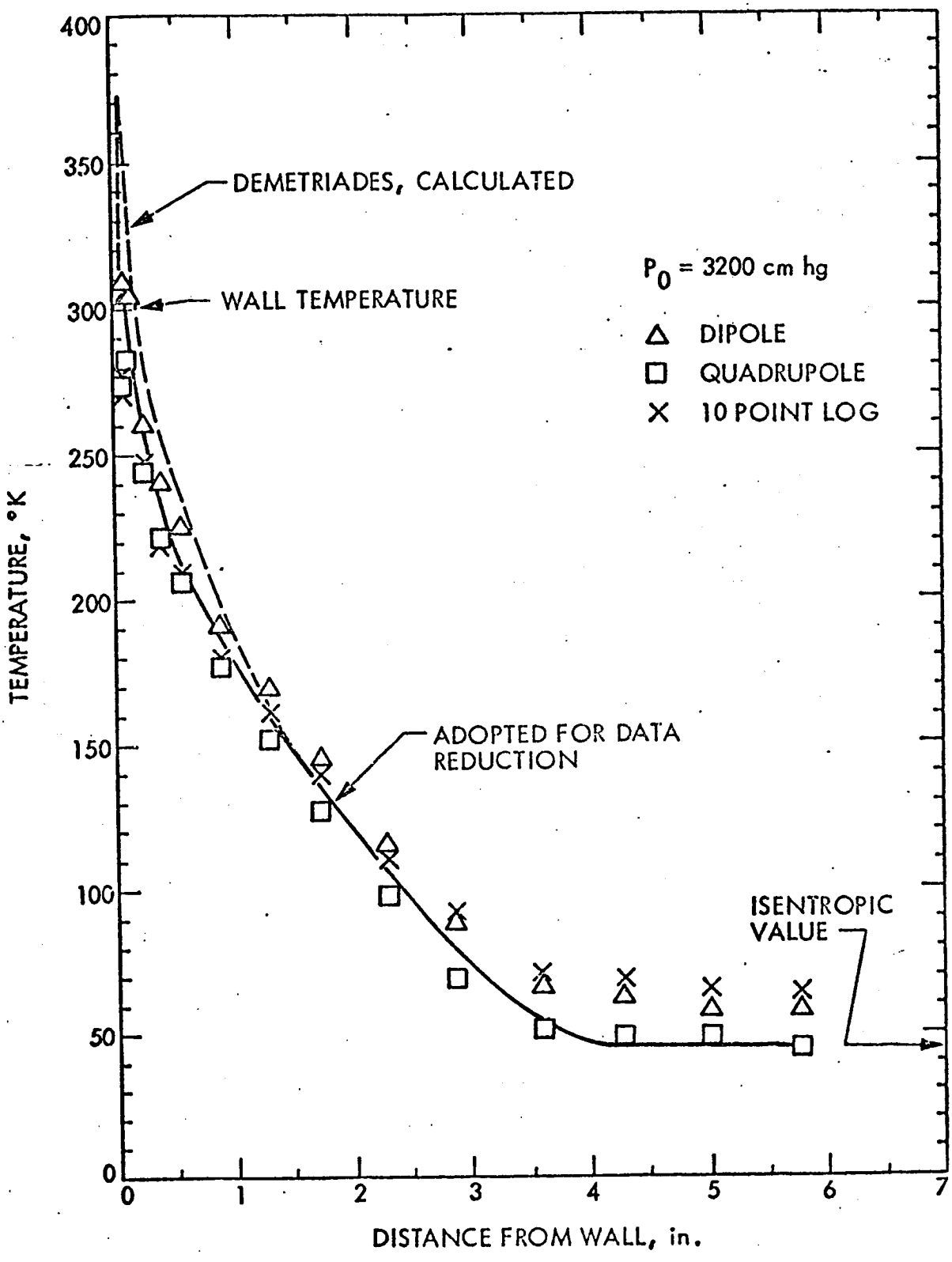

Fig. 20a. Rotational Temperature Profiles: P_0 = 3200 cm Hg

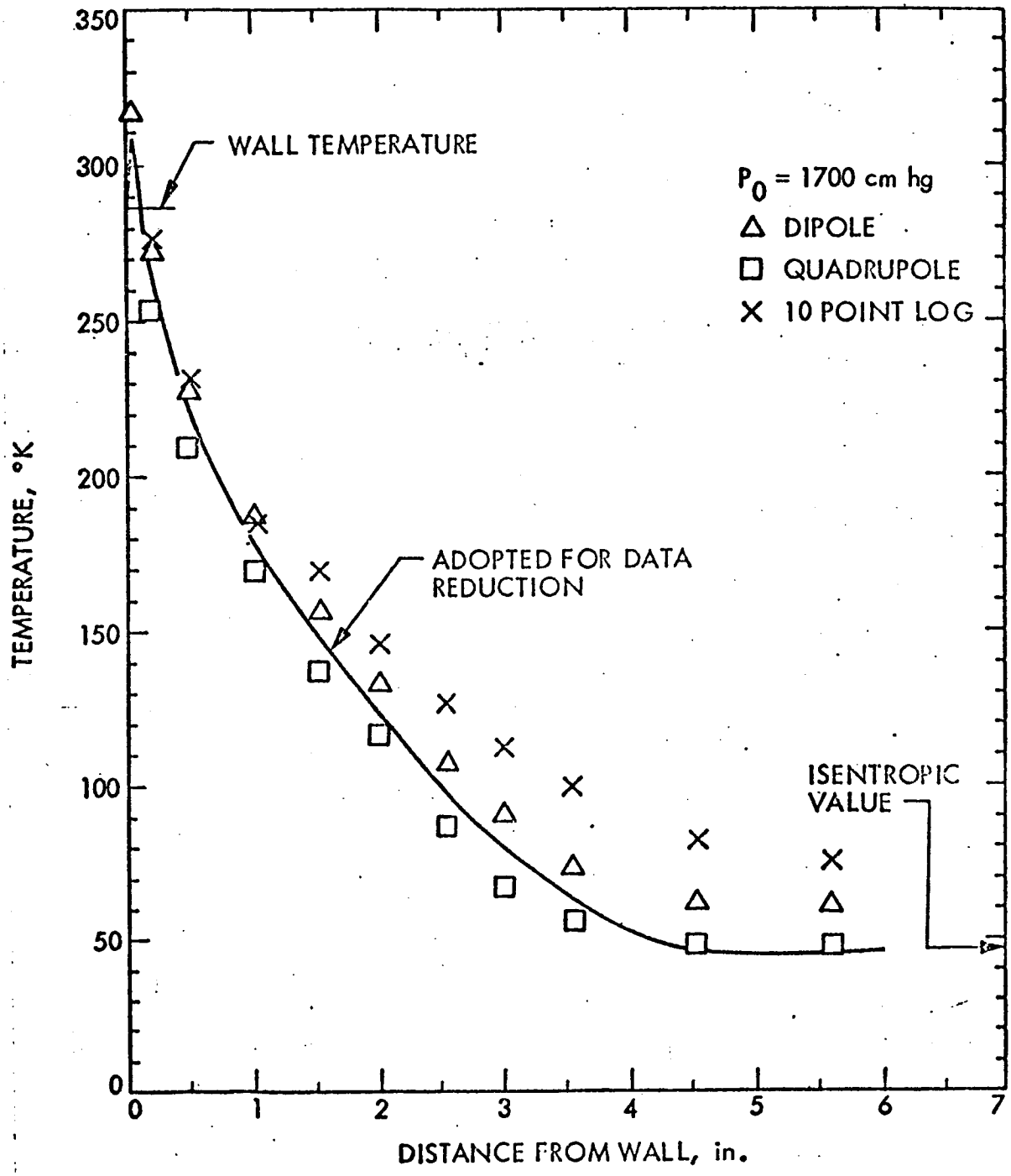

Fig. 20b. Rotational Temperature Profiles: P_0 = 1700 cm Hg

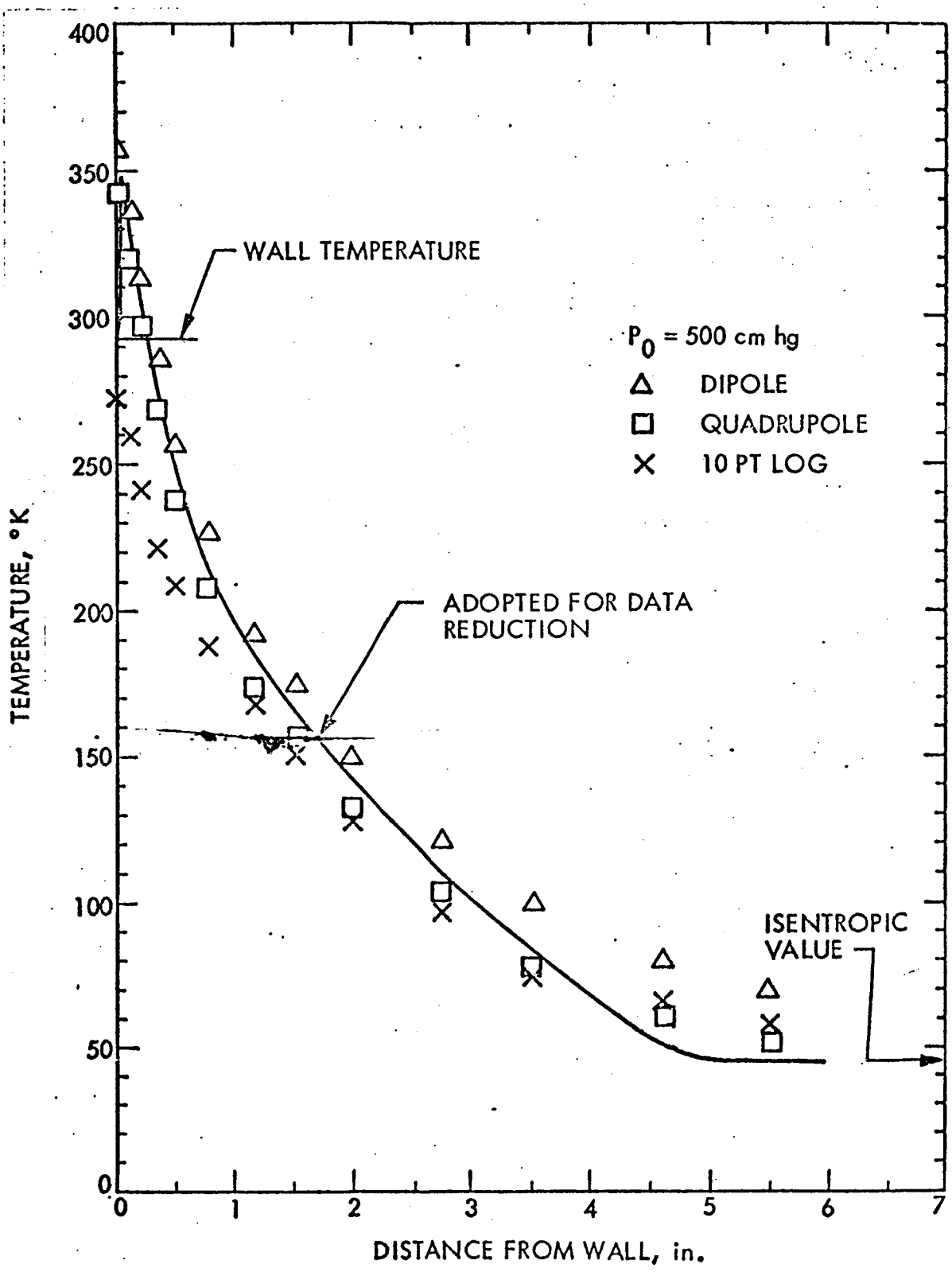

Fig. 20c. Rotational Temperature Profiles: P_0 = 500 cm Hg

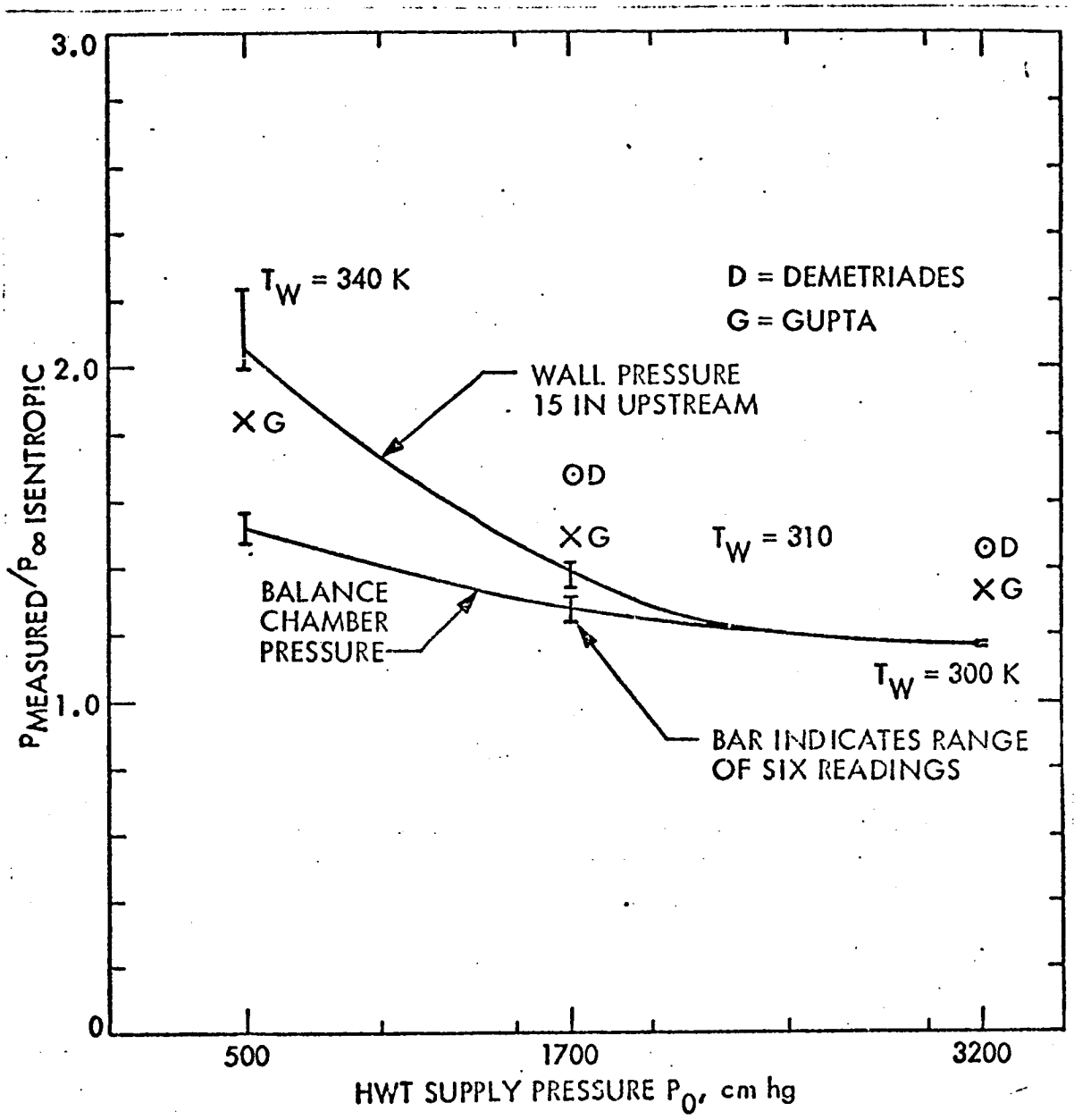

Fig. 21. Measured Wall and Balance-Chamber Pressures

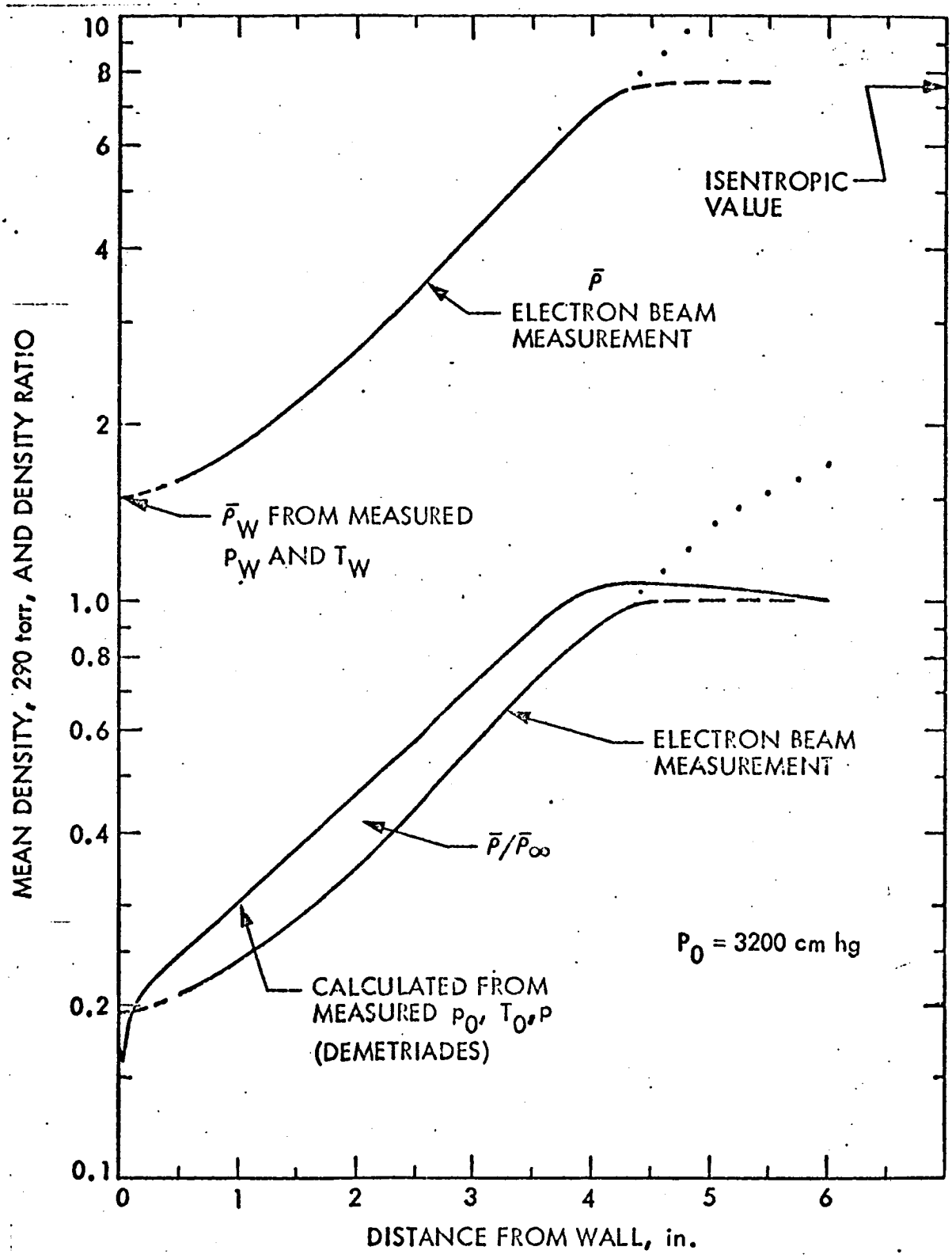

Fig. 22a. Mean Density Profile: P_0 = 3200 cm Hg

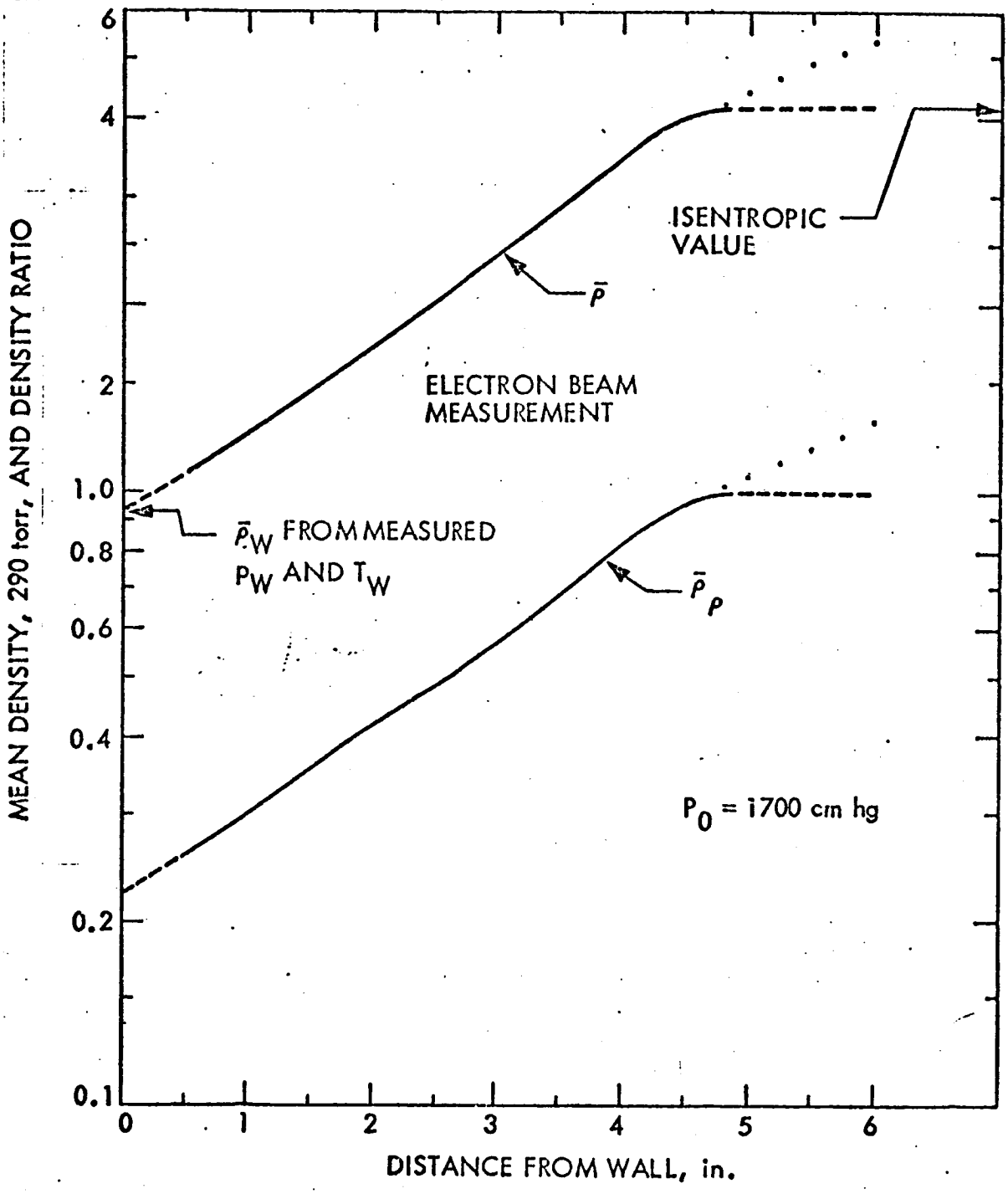

Fig. 22b. Mean Density Profile: P_0 = 1700 cm Hg

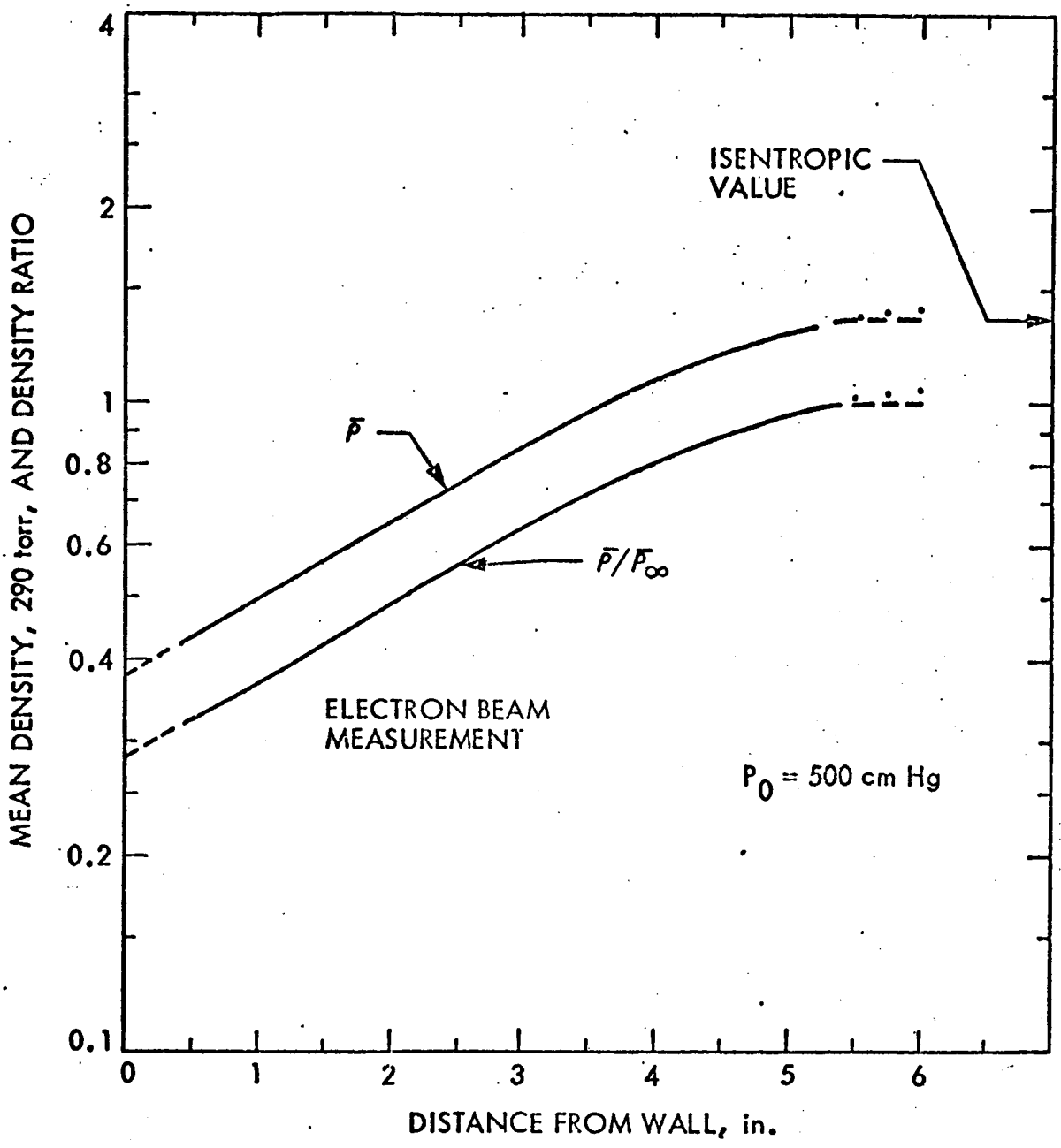

Fig. 22c. Mean Density Profile: P_0 = 500 cm Hg

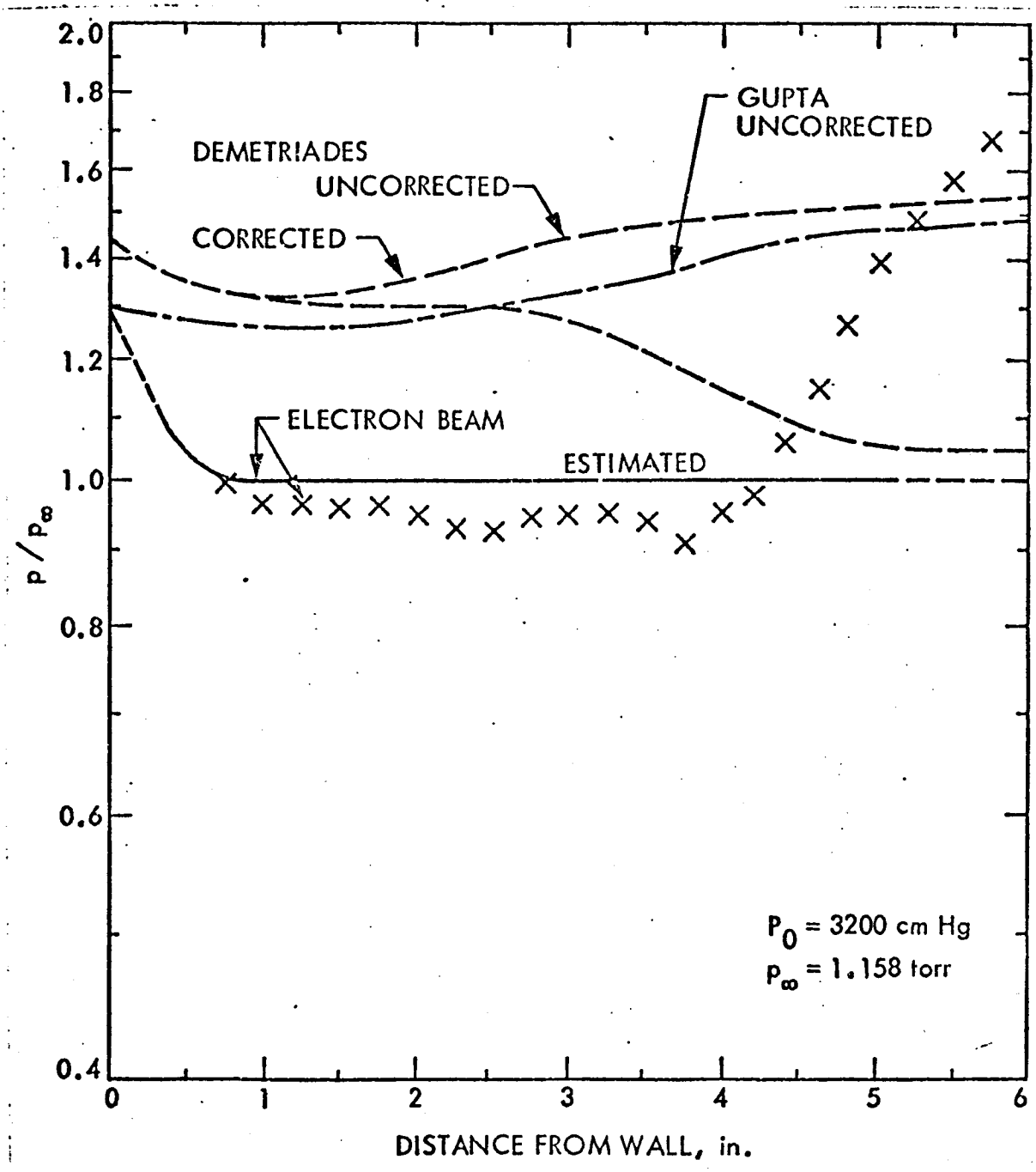

Fig. 23a. Profiles of Static Pressure from Density and Temperature: P_0 = 3200 cm Hg

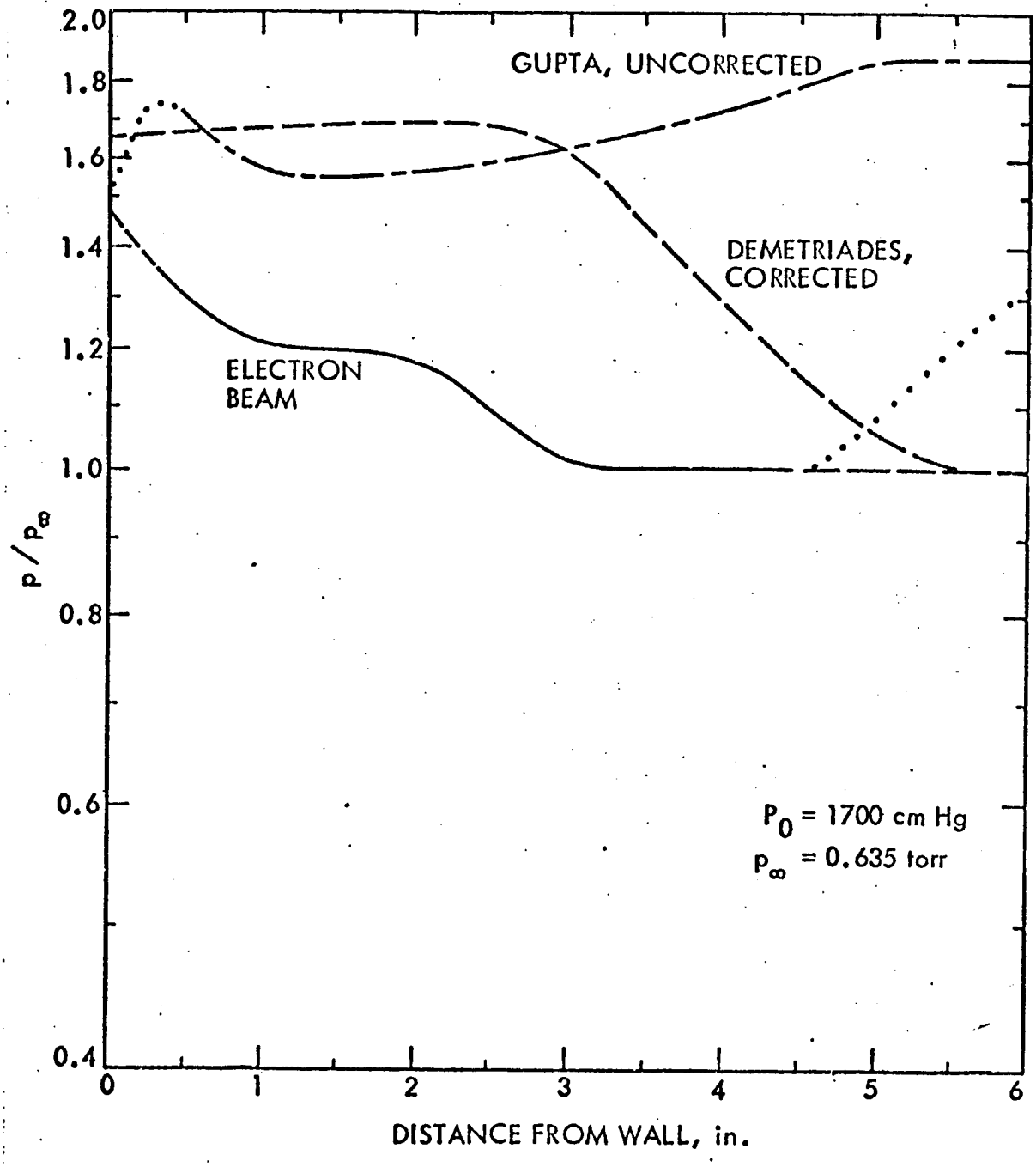

Fig. 23b. Profiles of Static Pressure from Density and Temperature: P_0 = 1700 cm Hg

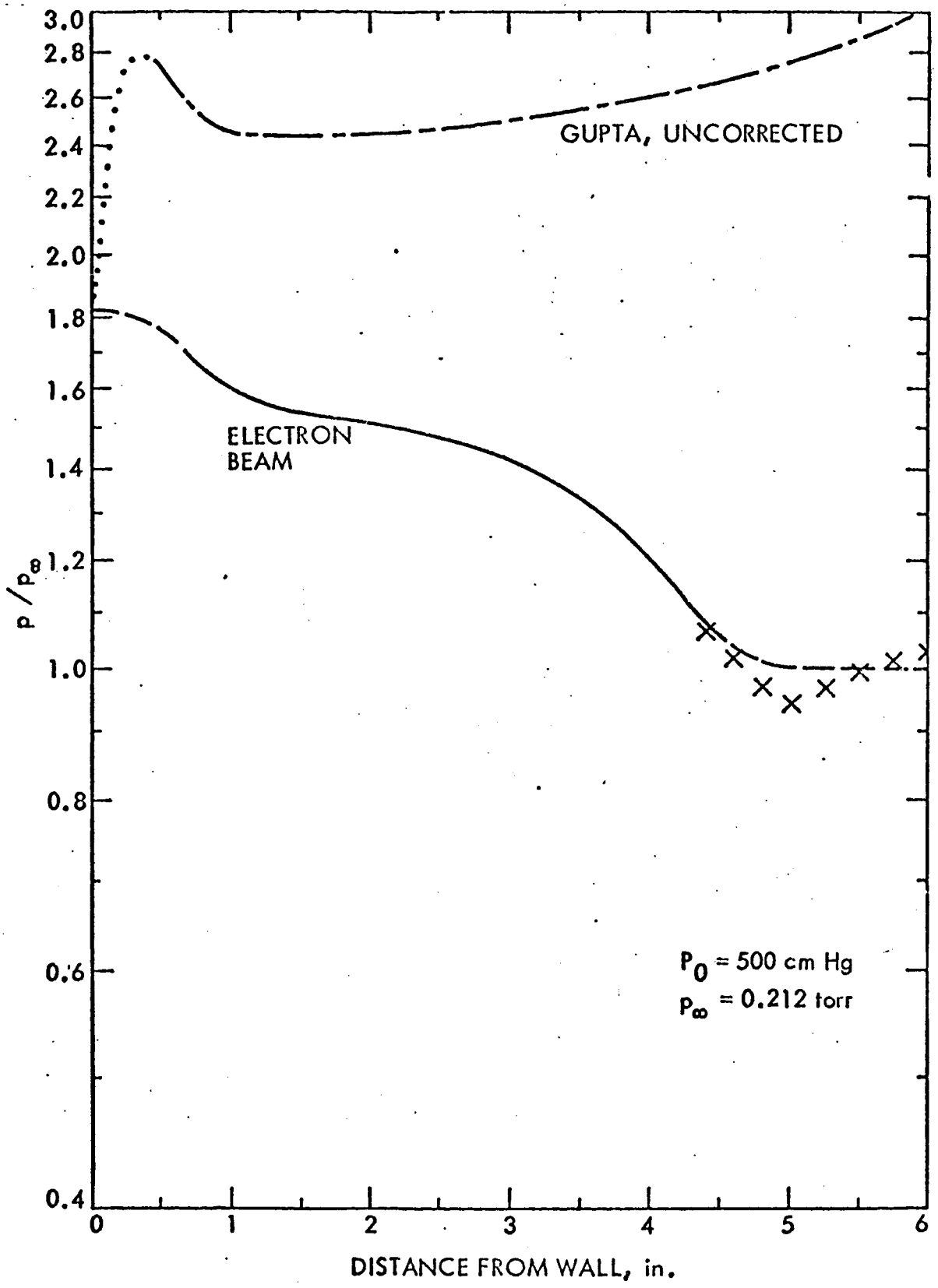

Fig. 23c. Profiles of Static Pressure from Density and Temperature: P_0 = 500 cm Hg

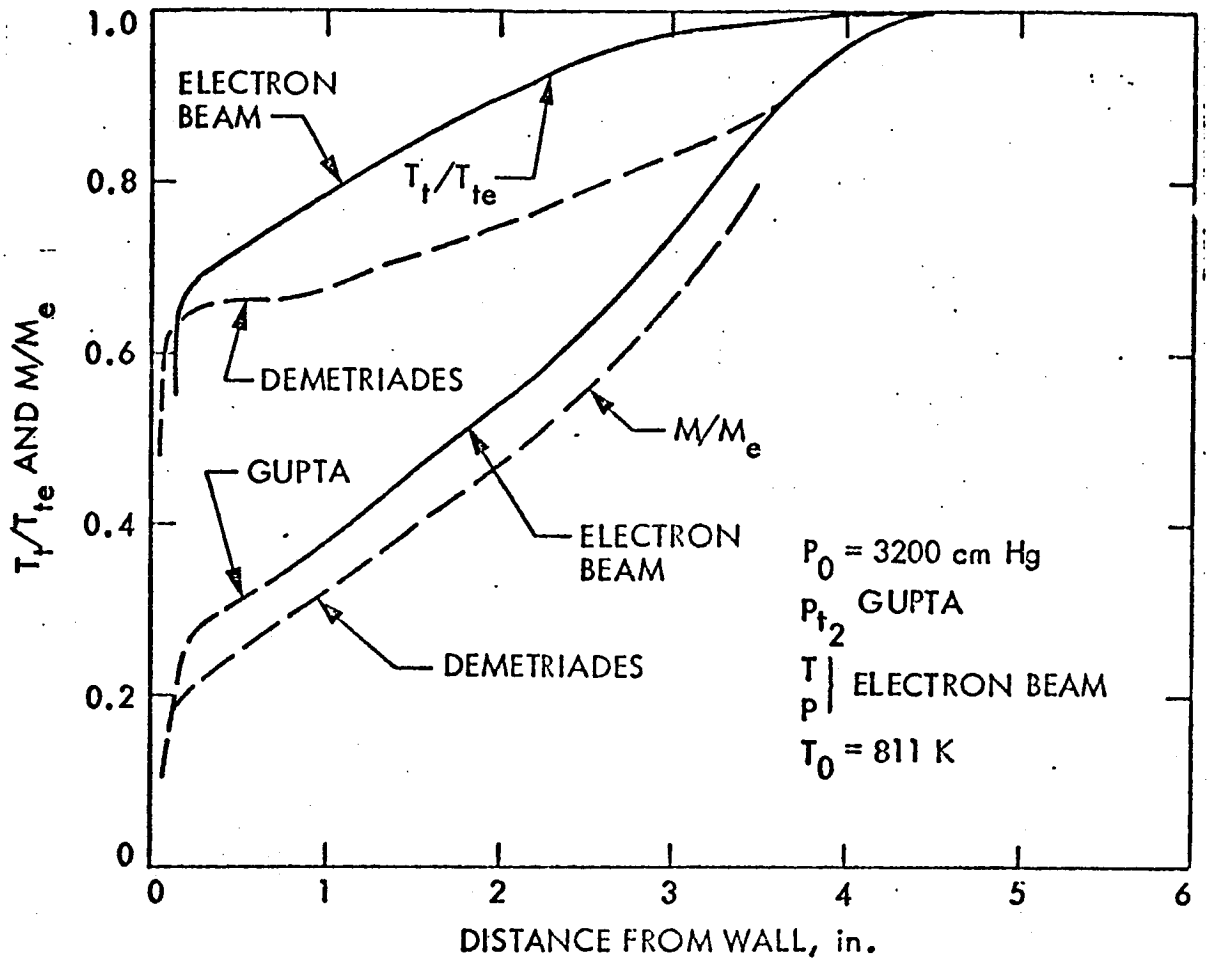

Fig. 24a. Profiles of Mach Number and Total Temperature: P_0 = 3200 cm Hg

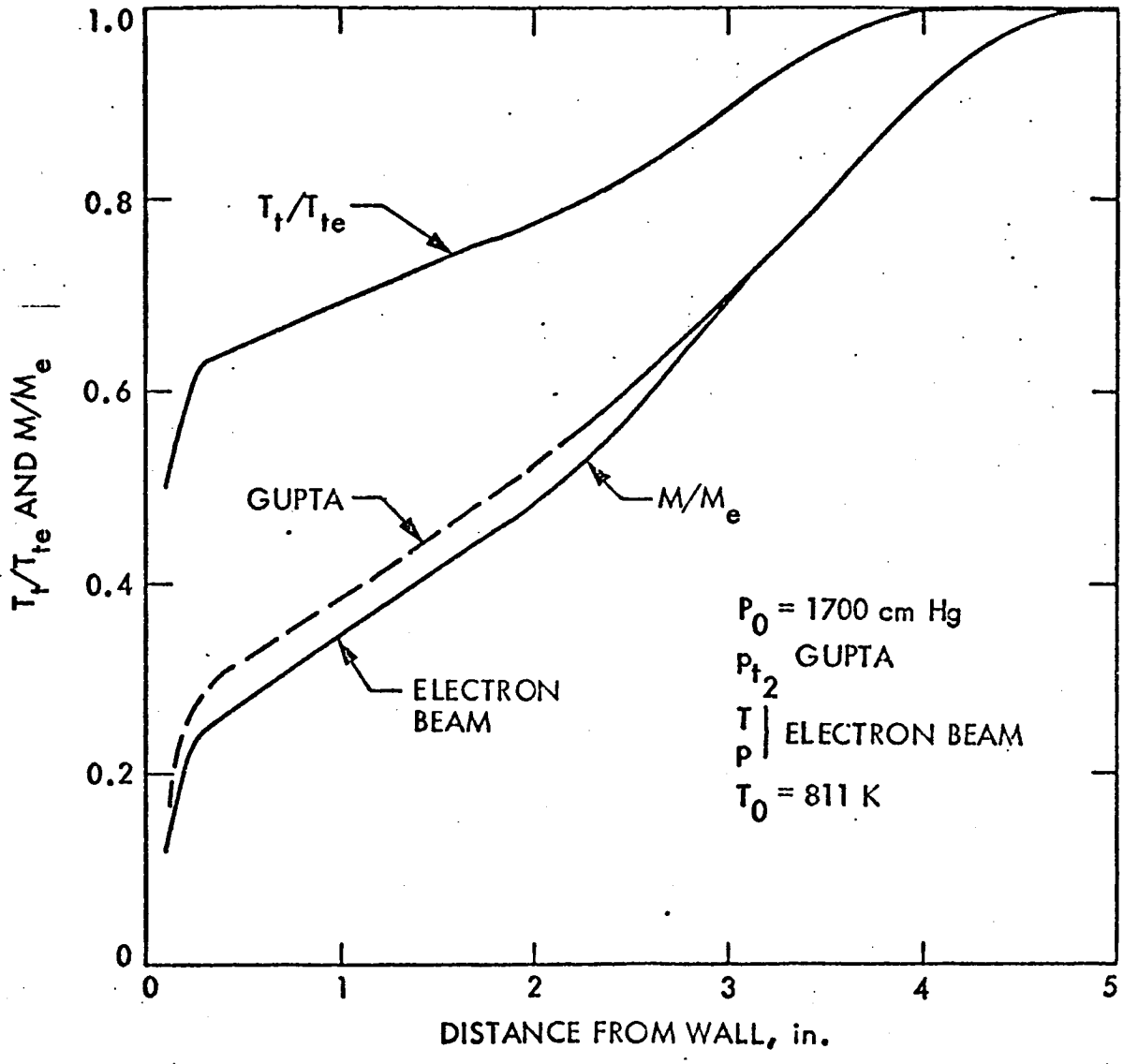

Fig. 24b. Profiles of Mach Number and Total Temperature: P_0 = 1700 cm Hg

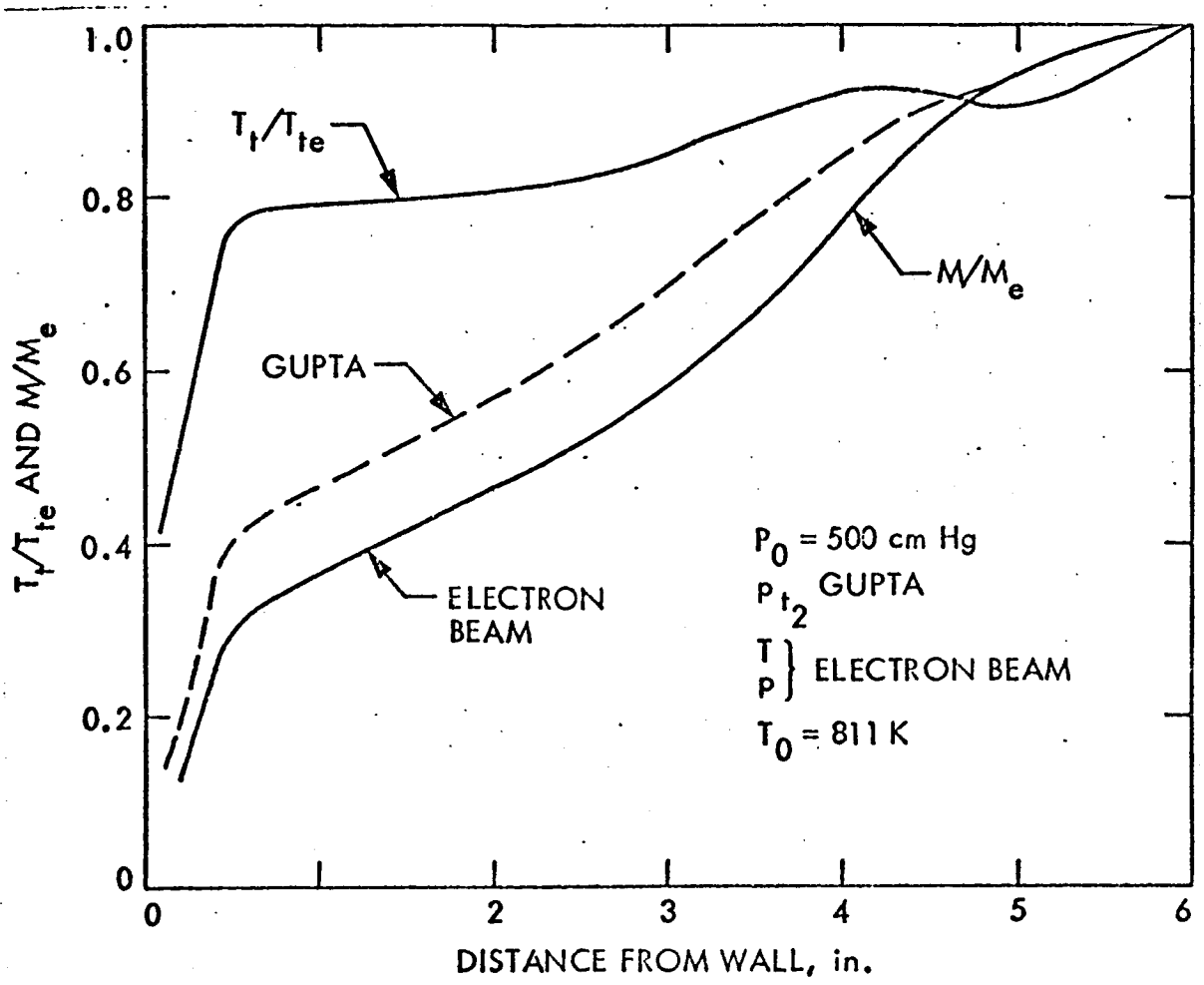

Fig. 24c. Profiles of Mach Number and Total Temperature: P_0 = 500 cm Hg

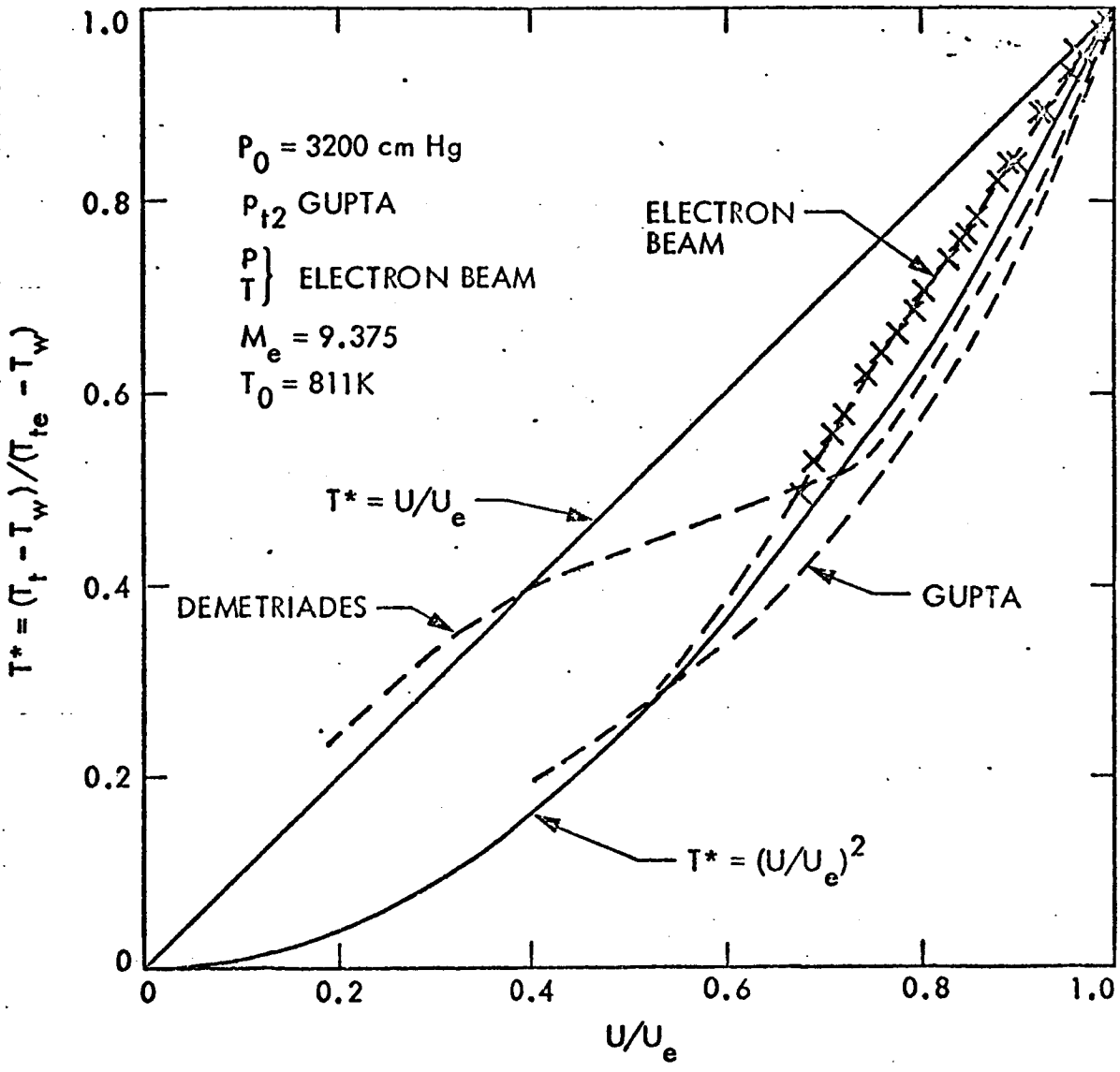

Fig. 25a. Total Temperature Versus Velocity: P_0 = 3200 cm Hg

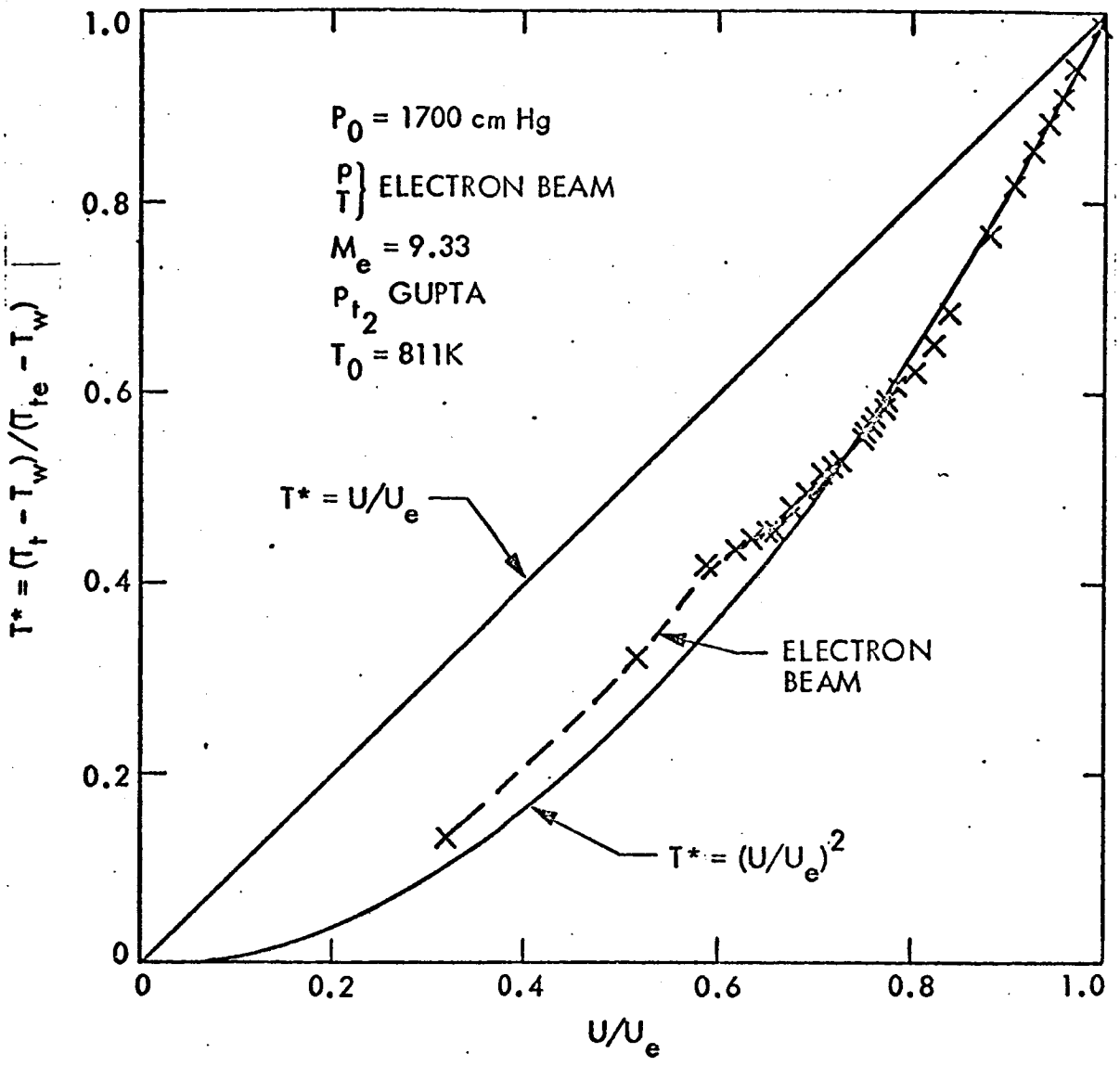

Fig. 25b. Total Temperature Versus Velocity: P_0 = 1700 cm Hg

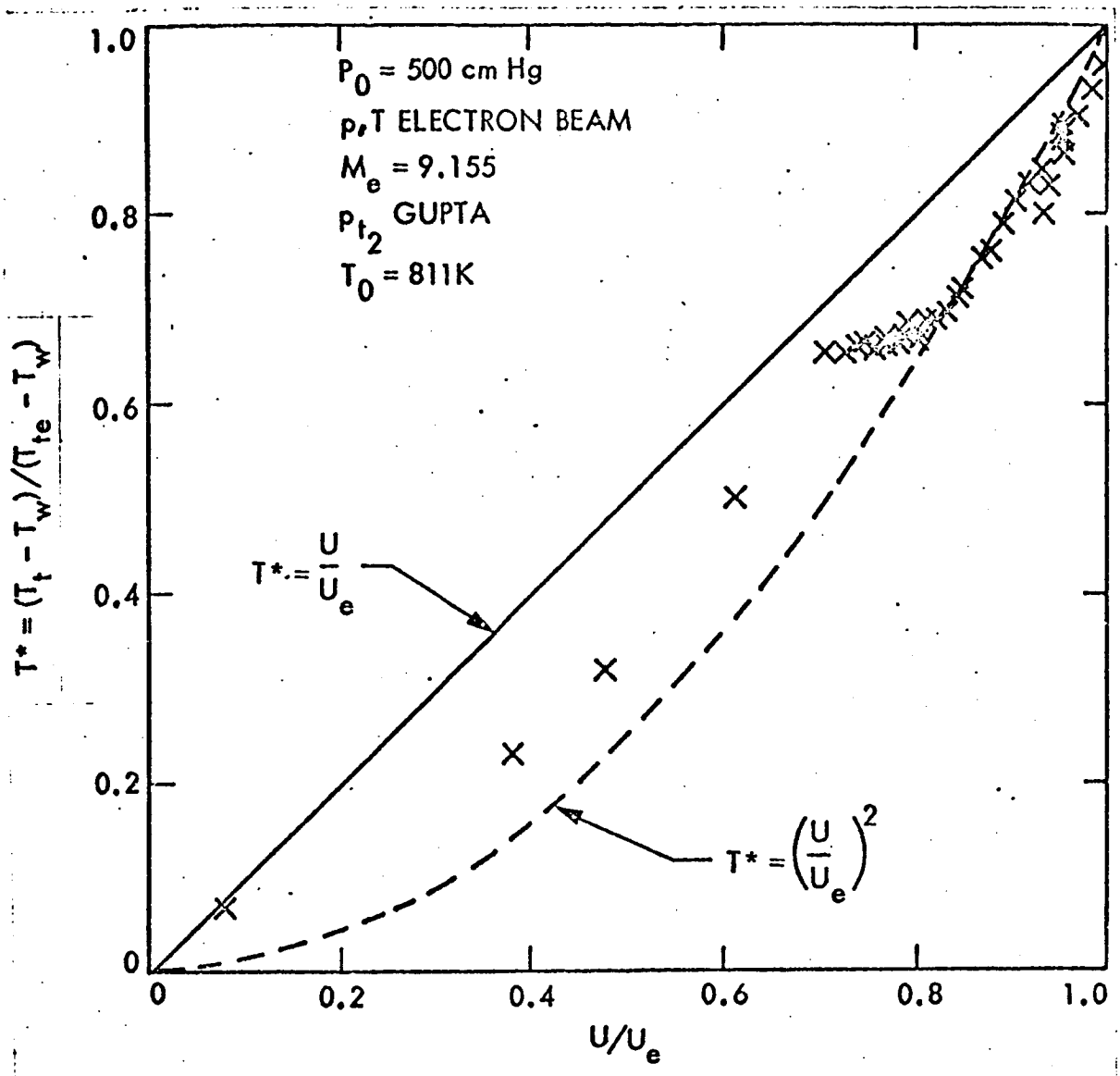

Fig. 25c. Total Temperature Versus Velocity: P_0 = 500 cm Hg